ASWING 5.99 Technical Description — Steady Formulation

Mark Drela

10 March 2015

Summary

ASWING is a program for the prediction of static and quasi-static loads and deformations of aircraft with flexible high aspect ratio surfaces and fuselage beams. The key features of the overall structural/aerodynamic model are sketched in Figure 1. A fully nonlinear Bernoulli-Euler beam representation is used for all the surface and fuselage structures, and an enhanced lifting-line representation is used to model the aerodynamic surface characteristics. The lifting-line model employs wind-aligned trailing vorticity, a Prandtl-Glauert compressibility transformation, and local-stall lift coefficient limiting to economically predict extreme flight situations with reasonable accuracy.

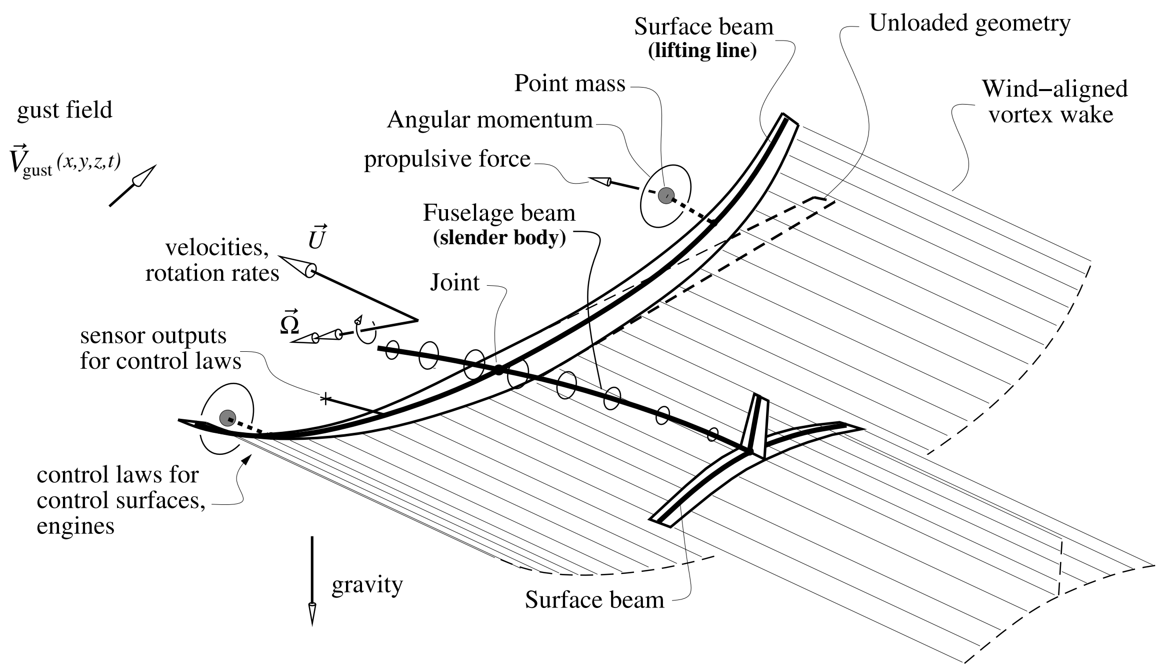

Figure 1: ASWING configuration representation

A primary intent of ASWING is to enable rapid and extensive exploration of the V-n flight envelope to identify potential failure scenarios. Divergence speeds, aileron reversal speeds, deformation effects on stability derivatives and control effectiveness, along with all the related stress distributions can be readily predicted. Effects of wing flexibility on induced drag can also be predicted. The full dynamic extension allows flutter predictions.

The interactive user interface allows on-the-spot redesign and resizing, thus permitting quick evaluation of structural and aerodynamic changes on the structural margins and aeroelastic behavior. Hence, ASWING is effective for preliminary structural design and sizing. It is also useful for obtaining initial estimates of the airloads on the deformed geometry, so that more realistic loads can be input into other more detailed structural analyses.

Contents

1 Coordinate Systems and Structural Equations **4**

1.1 Local coordinates and surface-beam transformation tensor 5

1.2 Fuselage-beam transformation tensor 6

1.3 Beam bending-moment and force resultants 6

1.4 Moment – beam-curvature relations 7

1.5 Section representation options 10

1.5.1 Representation 1 10

1.5.2 Representation 2 11

1.5.3 Representation 3 11

1.5.4 Axis relations 11

1.6 Force and moment equilibrium relations 12

2 Discrete Formulation **12**

2.1 Interior equations 12

2.2 Boundary conditions and interior constraints 14

3 Applied Loads **15**

3.1 Aerodynamic loads 15

3.2 Inertial and gravity loads 17

3.3 Point-mass loads 18

3.4 Engine loads and jet 20

3.4.1 Engine force and moment 20

3.4.2 Engine axes relations 20

3.4.3 Engine models 21

3.4.4 Propulsive jet 23

3.5 Strut loads 26

3.6 Joint loads 27

3.7 Ground-point loads 28

3.8 Beam Groups 29

4 Velocity Influence Coefficients **29**

4.1 Prandtl-Glauert Transformation 29

4.2 Vortex influence function 31

4.3 Volume influence functions 34

4.4 Point-mass influence functions 34

4.5 Ground effect 34
4.6 Linearization 36

5 Global Variables and Constraints **37**
5.1 Acceleration constraints 37
5.2 Lift-related constraints 37
5.3 Moment-related constraints 38
5.4 Beam joint constraints 39
5.5 Compliant beam joint constraints 39
5.6 Circulation coefficient constraints 40
5.7 Separation and stall modeling 40

6 Wing/Beam Description **42**
6.1 Point mass description 45
6.2 Engine description 45
6.3 Strut description 46
6.4 Ground point description 46
6.5 Beam joint description 47

7 Operating Parameters **47**
7.1 Constraint Well-Posedness 48

8 Computed Parameters **49**
8.1 Aerodynamic parameters 49
8.2 Structural parameters 50
8.3 Structural, aerodynamic stability and control derivatives 50
8.4 Interpretation of Stability Derivatives 51
8.5 Axis transformation 52
8.6 Force and moment derivatives 53
8.7 Real and Apparent Masses and Inertias 54
8.7.1 Real mass 55
8.7.2 Real-mass moment and mass centroid 55
8.7.3 Real-mass moment of inertia 56
8.7.4 Apparent mass 56
8.7.5 Apparent-mass moment 56
8.7.6 Apparent-mass inertia 57

1 Coordinate Systems and Structural Equations

The aircraft geometry, velocities, accelerations, and structural loads are expressed in a cartesian x, y, z body coordinate system sketched in Figure 2. The axis origin is grounded to the aircraft at some location. Hence this coordinate frame is not inertial, but instead has some linear acceleration $\vec{a}_o$, and also has angular velocity $\vec{\Omega}$ and angular acceleration $\vec{\alpha}_o$. The relative freestream velocity vector $\vec{V}_\infty$, also defined in the x, y, z system, is opposite to the aircraft velocity $\vec{U}$ and is related to the velocity magnitude V_∞ and angle of attack α and sideslip β as follows.

$$\vec{V}_\infty \;=\; V_\infty \left\{ \begin{array}{c} \cos\alpha\, \cos\beta \\ -\sin\beta \\ \sin\alpha\, \cos\beta \end{array} \right\} \;=\; -\vec{U} \tag{1}$$

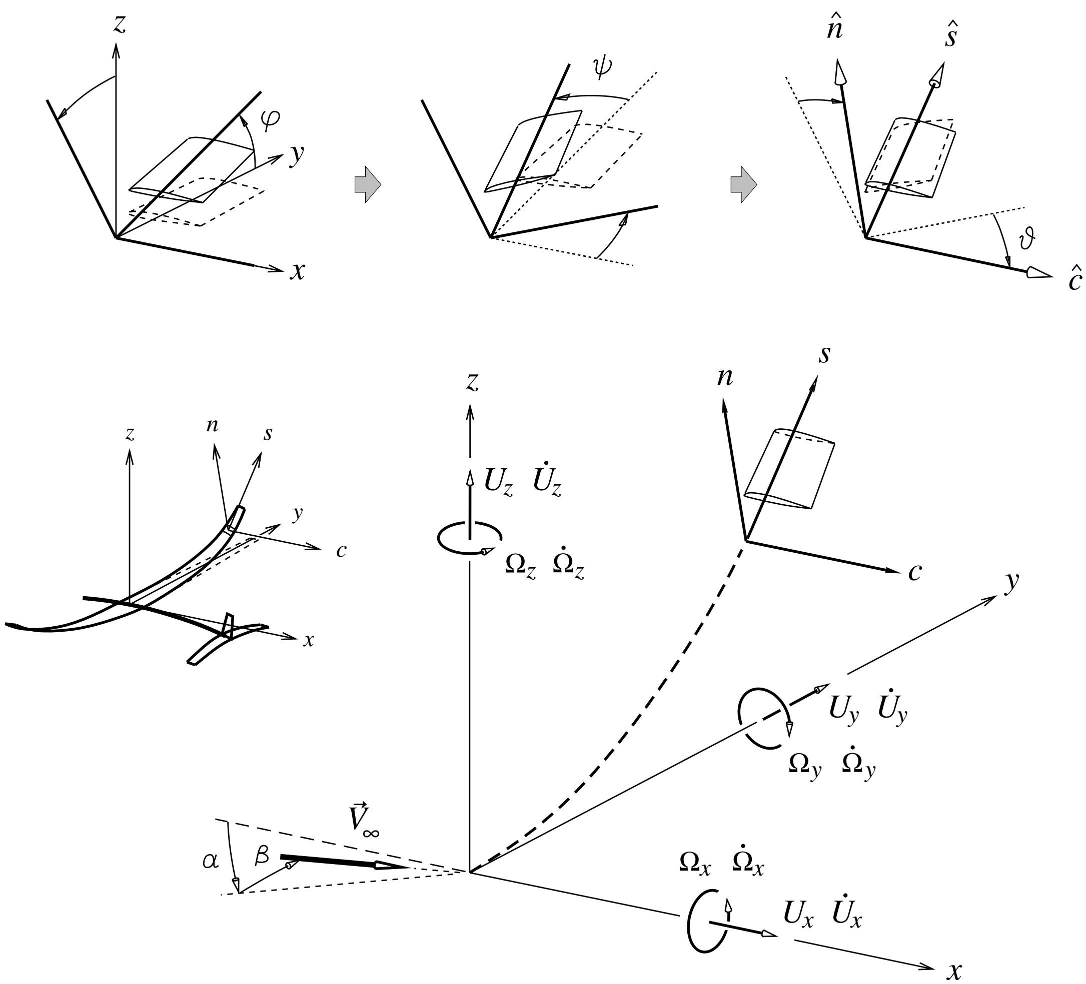

Figure 2: Coordinate systems, velocities, rotations, and accelerations.

1.1 Local coordinates and surface-beam transformation tensor

For the purpose of defining local stress/strain and aerodynamic force relations, a local beam-element c, s, n cartesian coordinate system is defined, with s nearly parallel with the tension axis. The transformation of any vector $\vec{A}$ from the x, y, z airplane body axes to the local c, s, n beam element axes is via the three Euler angles φ, ψ, ϑ, applied in that order for a surface beam.

$$\left\{ \begin{array}{c} A_c \\ A_s \\ A_n \end{array} \right\} = \left[\begin{array}{c} \\ \bar{\bar{T}} \\ \\ \end{array} \right] \left\{ \begin{array}{c} A_x \\ A_y \\ A_z \end{array} \right\} \tag{2}$$

$$\bar{\bar{T}} = \begin{bmatrix} \cos\vartheta & 0 & -\sin\vartheta \\ 0 & 1 & 0 \\ \sin\vartheta & 0 & \cos\vartheta \end{bmatrix} \begin{bmatrix} \cos\psi & \sin\psi & 0 \\ -\sin\psi & \cos\psi & 0 \\ 0 & 0 & 1 \end{bmatrix} \begin{bmatrix} 1 & 0 & 0 \\ 0 & \cos\varphi & \sin\varphi \\ 0 & -\sin\varphi & \cos\varphi \end{bmatrix} \qquad \text{(surface beam)} \tag{3}$$

$$\bar{\bar{T}} = \begin{bmatrix} \cos\vartheta\,\cos\psi & \cos\vartheta\,\sin\psi\,\cos\varphi + \sin\vartheta\,\sin\varphi & \cos\vartheta\,\sin\psi\,\sin\varphi - \sin\vartheta\,\cos\varphi \\ -\sin\psi & \cos\psi\,\cos\varphi & \cos\psi\,\sin\varphi \\ \sin\vartheta\,\cos\psi & \sin\vartheta\,\sin\psi\,\cos\varphi - \cos\vartheta\,\sin\varphi & \sin\vartheta\,\sin\psi\,\sin\varphi + \cos\vartheta\,\cos\varphi \end{bmatrix} \tag{4}$$

Figure 2 shows the transformation sequence. The beam curvature tensor $\bar{\bar{\kappa}}$ is related to the rate of change of the transformation tensor $\bar{\bar{T}}$ by

$$\frac{d\bar{\bar{T}}}{ds} = -\bar{\bar{\kappa}}\,\bar{\bar{T}} \qquad \longrightarrow \qquad \bar{\bar{\kappa}} \equiv \begin{bmatrix} 0 & -\kappa_n & \kappa_s \\ \kappa_n & 0 & -\kappa_c \\ -\kappa_s & \kappa_c & 0 \end{bmatrix} = -\frac{d\bar{\bar{T}}}{ds}\,\bar{\bar{T}}^T \tag{5}$$

or equivalently

$$\left\{ \begin{array}{c} \kappa_c \\ \kappa_s \\ \kappa_n \end{array} \right\} = \left[\begin{array}{c} \dfrac{d\bar{\bar{T}}}{ds} \end{array} \right] \times\cdot \left[\begin{array}{c} \bar{\bar{T}} \end{array} \right] \tag{6}$$

where the tensor cross-dot product $\times\cdot$ is defined as a generalization of the standard vector cross-product rule, with dot products replacing the usual scalar multiplications.

$$\begin{bmatrix} \cdots\ \vec{a}_1^T \cdots \\ \cdots\ \vec{b}_1^T \cdots \\ \cdots\ \vec{c}_1^T \cdots \end{bmatrix} \times\cdot \begin{bmatrix} \cdots\ \vec{a}_2^T \cdots \\ \cdots\ \vec{b}_2^T \cdots \\ \cdots\ \vec{c}_2^T \cdots \end{bmatrix} \equiv \det \begin{vmatrix} \hat{\imath} & \hat{\jmath} & \hat{k} \\ \vec{a}_1\cdot & \vec{b}_1\cdot & \vec{c}_1\cdot \\ \vec{a}_2 & \vec{b}_2 & \vec{c}_2 \end{vmatrix} = \left\{ \begin{array}{c} \vec{b}_1\cdot\vec{c}_2 - \vec{c}_1\cdot\vec{b}_2 \\ \vec{c}_1\cdot\vec{a}_2 - \vec{a}_1\cdot\vec{c}_2 \\ \vec{a}_1\cdot\vec{b}_2 - \vec{b}_1\cdot\vec{a}_2 \end{array} \right\} \tag{7}$$

Applying these operations to the $\bar{\bar{T}}$ components in (4) gives explicit expressions for the three curvature components (κ_s is actually a twist rate).

$$\left\{ \begin{array}{c} \kappa_c \\ \kappa_s \\ \kappa_n \end{array} \right\} = \left[\begin{array}{c} \\ \bar{\bar{K}} \\ \\ \end{array} \right] \left\{ \begin{array}{c} d\varphi/ds \\ d\vartheta/ds \\ d\psi/ds \end{array} \right\} \tag{8}$$

$$\bar{\bar{K}} = \begin{bmatrix} \cos\psi\,\cos\vartheta & 0 & -\sin\vartheta \\ -\sin\psi & 1 & 0 \\ \cos\psi\,\sin\vartheta & 0 & \cos\vartheta \end{bmatrix} \qquad \text{(surface beam)} \tag{9}$$

1.2 Fuselage-beam transformation tensor

The curvature-definition matrix $\bar{\bar{K}}$ as given by (9) for a surface beam is singular at a sweep angle of $\psi = \pm 90°$. Such a polar singularity always occurs in Euler-angle axis transformations, and will cause numerical solution failure if $\psi \simeq \pm 90°$ is encountered in a calculation. For surface beams, a 90° sweep angle is unlikely, but for a typical fuselage beam roughly parallel to the x axis it is inevitable. This problem is eliminated by defining an alternative rotation sequence ψ, φ, ϑ for fuselage beams, with the order of the φ and ψ rotations switched from the surface-beam case.

$$\bar{\bar{T}} = \begin{bmatrix} \cos\vartheta & 0 & -\sin\vartheta \\ 0 & 1 & 0 \\ \sin\vartheta & 0 & \cos\vartheta \end{bmatrix} \begin{bmatrix} 1 & 0 & 0 \\ 0 & \cos\varphi & \sin\varphi \\ 0 & -\sin\varphi & \cos\varphi \end{bmatrix} \begin{bmatrix} \cos\psi & \sin\psi & 0 \\ -\sin\psi & \cos\psi & 0 \\ 0 & 0 & 1 \end{bmatrix} \quad \text{(fuselage beam)} \tag{10}$$

$$\bar{\bar{T}} = \begin{bmatrix} \cos\vartheta\,\cos\psi - \sin\vartheta\,\sin\psi\,\sin\varphi & \cos\vartheta\,\sin\psi + \sin\vartheta\,\cos\psi\,\sin\varphi & -\sin\vartheta\,\cos\varphi \\ -\sin\psi\,\cos\varphi & \cos\psi\,\cos\varphi & \sin\varphi \\ \sin\vartheta\,\cos\psi + \cos\vartheta\,\sin\psi\,\sin\varphi & \sin\vartheta\,\sin\psi - \cos\vartheta\,\cos\psi\,\sin\varphi & \cos\vartheta\,\cos\varphi \end{bmatrix} \tag{11}$$

The beam curvatures are then given by the alternative curvature-definition matrix

$$\bar{\bar{K}} = \begin{bmatrix} \cos\vartheta & 0 & -\cos\varphi\,\sin\vartheta \\ 0 & 1 & \sin\varphi \\ \sin\vartheta & 0 & \cos\varphi\,\cos\vartheta \end{bmatrix} \qquad \text{(fuselage beam)} \tag{12}$$

which is now singular when the beam is vertical at $\varphi = \pm 90°$, which is unlikely for a fuselage. The subsequent derivations assume that the appropriate $\bar{\bar{T}}$ and $\bar{\bar{K}}$ definitions are used for each type of beam.

1.3 Beam bending-moment and force resultants

Standard beam force-resultant and moment-resultant vectors are defined in the local axes.

$$\begin{aligned} F_c &= \iint \tau_{cs}\, dc\, dn & \qquad M_c &= \iint -\sigma_{ss} n\, dc\, dn \\ F_s &= \iint \sigma_{ss}\, dc\, dn & \qquad M_s &= \iint (\tau_{cs} n - \tau_{ns} c)\, dc\, dn \\ F_n &= \iint \tau_{ns}\, dc\, dn & \qquad M_n &= \iint \sigma_{ss} c\, dc\, dn \end{aligned} \tag{13}$$

These resultants can be expressed in either the local c, s, n axes as above, or in the global x, y, z axes. These two representations are related by the transformation tensor appropriate for that type of beam.

$$\begin{Bmatrix} F_c \\ F_s \\ F_n \end{Bmatrix} = \begin{bmatrix} & & \\ & \bar{\bar{T}} & \\ & & \end{bmatrix} \begin{Bmatrix} F_x \\ F_y \\ F_z \end{Bmatrix} \quad , \quad \begin{Bmatrix} M_c \\ M_s \\ M_n \end{Bmatrix} = \begin{bmatrix} & & \\ & \bar{\bar{T}} & \\ & & \end{bmatrix} \begin{Bmatrix} M_x \\ M_y \\ M_z \end{Bmatrix} \tag{14}$$

Figure 3 shows the sign conventions for the c, s, n components. Analogous sign conventions are used in the global x, y, z axes. Note that M_s is a torsion load while M_c and M_n are bending moments. Likewise, F_s is an axial load, while F_c and F_n are shear loads. Such interpretation cannot be made for the x, y, z components.

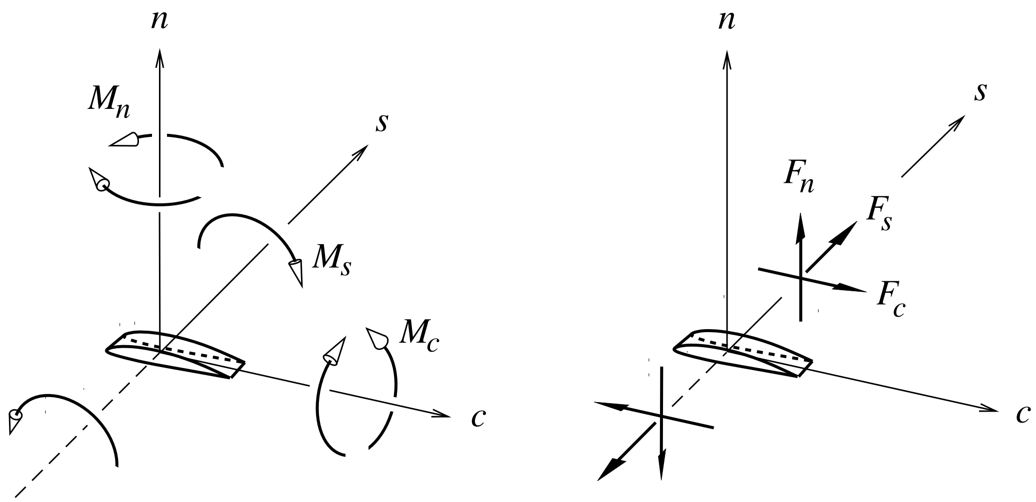

Figure 3: Load resultants on element of beam, in local axes.

1.4 Moment – beam-curvature relations

The beam section of a lifting surface is shown in Figure 4. The elastic and tension axes are offset from the arbitrary s axis by c_{ea},n_{ea} and c_{ta},n_{ta}. Assuming the section does not warp out of the c-n plane, the overall extensional strain at some location c, n is

$$\epsilon \;=\; \epsilon_s \;+\; c\,(\kappa_n - \kappa_{n0}) \;-\; n\,(\kappa_c - \kappa_{n0}) \tag{15}$$

where ϵ_s is the strain at the c,n origin, and κ_{c0}, κ_{n0} are the curvatures of the unloaded beam, calculated from the unloaded φ_0, ϑ_0, and ψ_0 distributions (i.e. the jig shape). The angle α_A of the zero lift line relative to the chosen c axis will be used later in the aerodynamic formulation.

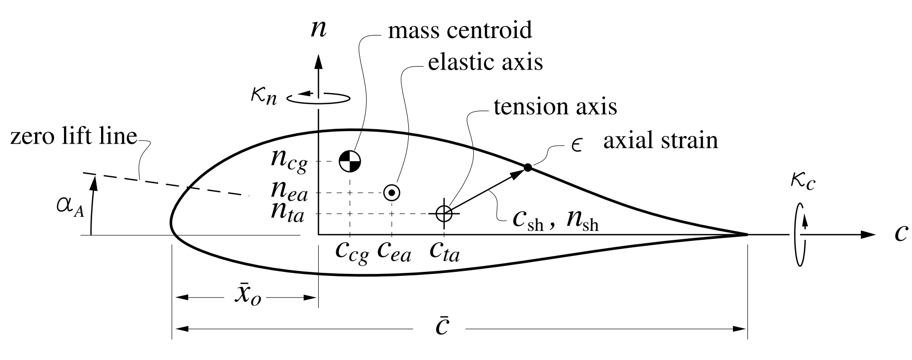

Figure 4: Beam section with curvatures and resulting strain.

Following Minguet [1], the force and moment vectors in the local axes are related to the beam strains and curvatures via the stiffness matrix (necessarily symmetric).

$$\left\{\begin{array}{c} F_c \\ F_s \\ F_n \\ \hline M_c \\ M_s \\ M_n \end{array}\right\} = \left[\begin{array}{ccc|ccc} \mathcal{E}_{11} & \mathcal{E}_{12} & \mathcal{E}_{13} & \mathcal{E}_{14} & \mathcal{E}_{15} & \mathcal{E}_{16} \\ . & \mathcal{E}_{22} & \mathcal{E}_{23} & \mathcal{E}_{24} & \mathcal{E}_{25} & \mathcal{E}_{26} \\ . & . & \mathcal{E}_{33} & \mathcal{E}_{34} & \mathcal{E}_{35} & \mathcal{E}_{36} \\ \hline . & . & . & \mathcal{E}_{44} & \mathcal{E}_{45} & \mathcal{E}_{46} \\ . & . & . & . & \mathcal{E}_{55} & \mathcal{E}_{56} \\ . & . & . & . & . & \mathcal{E}_{66} \end{array}\right] \left\{\begin{array}{l} \gamma_c \\ \epsilon_s \\ \gamma_n \\ \kappa_c - \kappa_{c0} \\ \kappa_s - \kappa_{s0} \\ \kappa_n - \kappa_{n0} \end{array}\right\} \tag{16}$$

It is not necessary to include the jig-shape strains such as ϵ_{s0} since these can be lumped into the jig shape x_0,y_0,z_0 itself. The stiffness matrix has 21 independent elements in general. For beam-bending applications, however, it is assumed that all but the lower right quadrant have a more restricted form as follows.

$$\left[\begin{array}{ccc|ccc} \mathcal{E}_{11} & \mathcal{E}_{12} & \mathcal{E}_{13} & \mathcal{E}_{14} & \mathcal{E}_{15} & \mathcal{E}_{16} \\ . & \mathcal{E}_{22} & \mathcal{E}_{23} & \mathcal{E}_{24} & \mathcal{E}_{25} & \mathcal{E}_{26} \\ . & . & \mathcal{E}_{33} & \mathcal{E}_{34} & \mathcal{E}_{35} & \mathcal{E}_{36} \\ \hline . & . & . & \mathcal{E}_{44} & \mathcal{E}_{45} & \mathcal{E}_{46} \\ . & . & . & . & \mathcal{E}_{55} & \mathcal{E}_{56} \\ . & . & . & . & . & \mathcal{E}_{66} \end{array}\right] \rightarrow \left[\begin{array}{ccc|ccc} GK_c & 0 & 0 & 0 & GK_c\, n_{ea} & 0 \\ . & EA & 0 & -EA\, n_{ta} & 0 & EA\, c_{ta} \\ . & . & GK_n & 0 & -GK_n\, c_{ea} & 0 \\ \hline . & . & . & \mathcal{E}_{44} & \mathcal{E}_{45} & \mathcal{E}_{46} \\ . & . & . & . & \mathcal{E}_{55} & \mathcal{E}_{56} \\ . & . & . & . & . & \mathcal{E}_{66} \end{array}\right] \tag{17}$$

It is convenient to first define a moment $\vec{M}'$ which is translated to the tension and elastic axes.

$$\left\{\begin{array}{c} M'_c \\ M'_s \\ M'_n \end{array}\right\} = \left\{\begin{array}{c} M_c \\ M_s \\ M_n \end{array}\right\} + \left[\begin{array}{ccc} 0 & n_{ta} & 0 \\ -n_{ea} & 0 & c_{ea} \\ 0 & -c_{ta} & 0 \end{array}\right] \left\{\begin{array}{c} F_c \\ F_s \\ F_n \end{array}\right\} \tag{18}$$

The elements of the *net* moment/curvature stiffness submatrix $\bar{\bar{E}}$ are defined as follows.

$$\left[\begin{array}{c} \\ \bar{\bar{E}} \\ \\ \end{array}\right] \equiv \left[\begin{array}{ccc} EI_{cc} & EI_{cs} & EI_{cn} \\ . & GJ & EI_{sn} \\ . & . & EI_{nn} \end{array}\right] = \left[\begin{array}{lll} \mathcal{E}_{44} - \mathcal{E}_{22} n_{ta}^2 & \mathcal{E}_{45} & \mathcal{E}_{46} + \mathcal{E}_{22} c_{ta} n_{ta} \\ . & \mathcal{E}_{55} - \mathcal{E}_{11} n_{ea}^2 - \mathcal{E}_{33} c_{ea}^2 & \mathcal{E}_{56} \\ . & . & \mathcal{E}_{66} - \mathcal{E}_{22} c_{ta}^2 \end{array}\right]$$

The system (16) can then be inverted into the following form.

$$\left\{\begin{array}{c} \gamma_c \\ \epsilon_s \\ \gamma_n \end{array}\right\} = \left\{\begin{array}{c} F_c/GK_c \\ F_s/EA \\ F_n/GK_n \end{array}\right\} + \left[\begin{array}{ccc} 0 & -n_{ea} & 0 \\ n_{ta} & 0 & -c_{ta} \\ 0 & c_{ea} & 0 \end{array}\right] \left[\begin{array}{c} \\ \bar{\bar{E}}^{-1} \\ \\ \end{array}\right] \left\{\begin{array}{c} M'_c \\ M'_s \\ M'_n \end{array}\right\} \tag{19}$$

$$\left\{\begin{array}{c} \kappa_c - \kappa_{c0} \\ \kappa_s - \kappa_{s0} \\ \kappa_n - \kappa_{n0} \end{array}\right\} = \left[\begin{array}{c} \\ \bar{\bar{E}}^{-1} \\ \\ \end{array}\right] \left\{\begin{array}{c} M'_c \\ M'_s \\ M'_n \end{array}\right\} \tag{20}$$

Normally the stiffnesses GK_c, EA, GK_n in (19) are sufficiently large so that F_c, F_s, F_n do not significantly contribute to the beam strains γ_c, ϵ_s, γ_n in the first force term in equation (19). The second moment term vanishes entirely if the tension and elastic axes coincide with the reference s axis, i.e. $c_{ta}, n_{ta}, c_{ea}, n_{ea} = 0$. These assumptions are characteristic of classical Bernoulli-Euler beam theory formulations. Here, the general form (20) will be retained to make the results independent of the rather arbitrary location of the reference s axis, and to give better accuracy for beams which may have significant extensional and shear compliance.

It is useful to note that for a beam with no twist/bending coupling, this net stiffness matrix takes the simpler form

$$\bar{\bar{E}} = \begin{bmatrix} EI_{cc} & 0 & EI_{cn} \\ . & GJ & 0 \\ . & . & EI_{nn} \end{bmatrix}$$

and if the c, n axes are aligned with the principal bending axes of the beam section, the off-diagonal elements EI_{cn} vanish.

For a rigid beam, the diagonal elements of the stiffness matrix in (16) are effectively infinite. In this limiting case, $1/GK$, $1/EA$, and $\bar{\bar{E}}^{-1}$ all vanish, automatically giving zero beam strains and load-induced curvatures in relations (19) and (20).

The extensional stiffness and tension axis locations are defined as

$$EA = \iint E \, dc \, dn \tag{21}$$

$$c_{ta} = \frac{1}{EA} \iint E \, c \, dc \, dn \tag{22}$$

$$n_{ta} = \frac{1}{EA} \iint E \, n \, dc \, dn \tag{23}$$

and the net bending stiffnesses are also defined in the usual manner.

$$EI_{cc} = \iint E \, (n - n_{ta})^2 \, dc \, dn \tag{24}$$

$$EI_{nn} = \iint E \, (c - c_{ta})^2 \, dc \, dn \tag{25}$$

$$EI_{cn} = \iint -E \, (c - c_{ta})(n - n_{ta}) \, dc \, dn \tag{26}$$

Computation of the shear center c_{ea}, n_{ea} and the stiffnesses GJ, EI_{cs}, EI_{sn} typically requires a shear-flow analysis. For a simple closed shell with enclosed area $A_{\rm sh}$, perimeter $S_{\rm sh}$, and uniform wall thickness $t_{\rm sh}$, the torsional stiffness is

$$GJ = 4G \, A_{\rm sh}^2 t_{\rm sh} / S_{\rm sh} . \tag{27}$$

The axial material strain at some location can be written as

$$\epsilon = c_{\rm sh} \left(\kappa_n - \kappa_{n0} \right) - n_{\rm sh} \left(\kappa_c - \kappa_{n0} \right) + F_s / EA \tag{28}$$

where

$$c_{\rm sh} = c - c_{ta} \quad , \qquad n_{\rm sh} = n - n_{ta}$$

are distances from the tension axis to a structural location as shown in Figure 4. The shear stress of a uniform hollow torsion shell is given by

$$\tau = \frac{M_s'}{2 \, A_{\rm sh} \, t_{\rm sh}} . \tag{29}$$

where M_s' is the torsion moment about the shear center, defined in equation (18).

1.5 Section representation options

It's useful to point out here that the geometric and structural parameters defined above are non-unique, in that any given wing section can be modeled by infinitely many alternative but equivalent representations. Three alternative representations are shown in Figure 5. The bottom sketch is the actual wing section to be modeled, specified by the local airfoil incidence α_{local}, the airfoil's zero-lift angle $\alpha_{L=0}$ (typically negative for cambered airfoils), and the principal-axis bend angle θ_{bend}. The latter may not be immediately available by inspection.

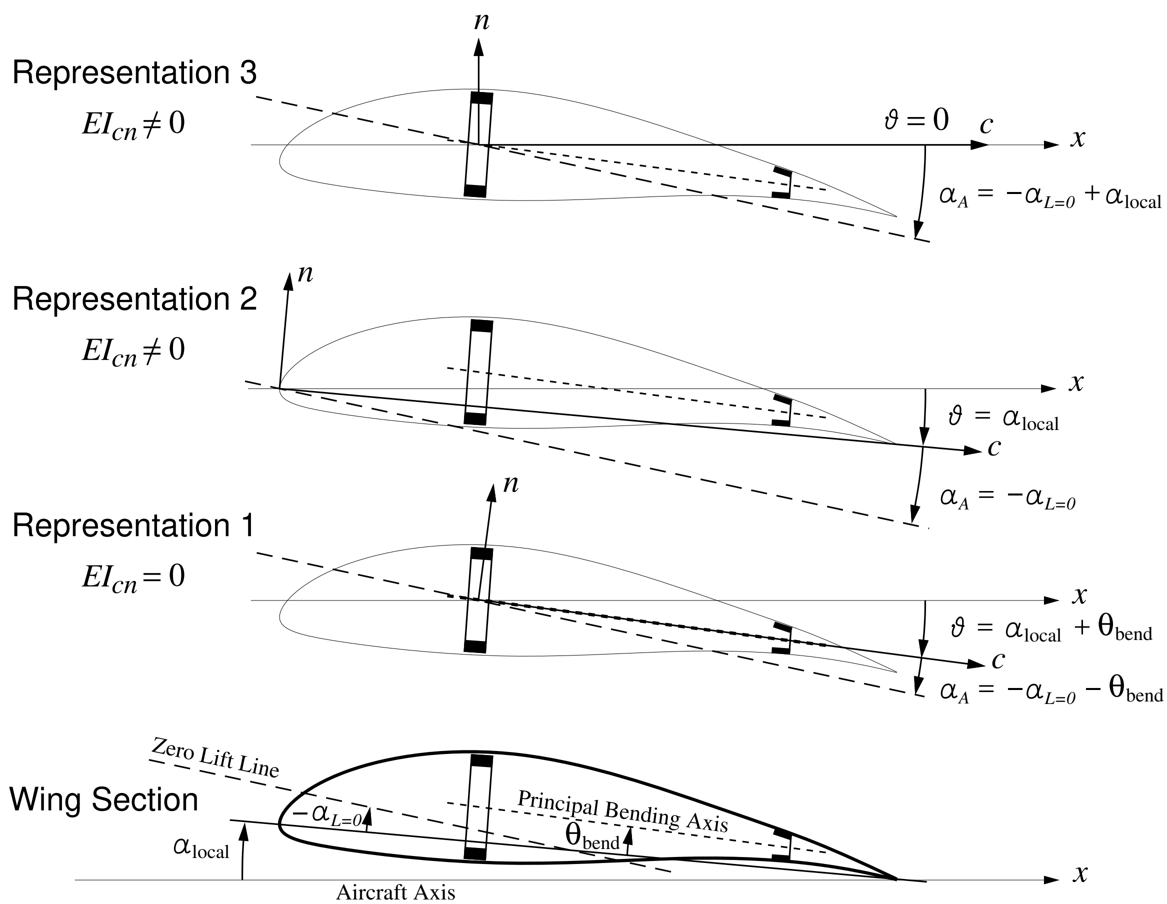

Figure 5: Three alternative but equivalent representations of a structural wing section. Represen-taion 1 is preferable if the principal axis is obvious by top/bottom structural symmetry.

1.5.1 Representation 1

This is usually the best choice if the principal bending axis angle θ_{bend} is known by inspection from symmetry. The c axis is chosen to lie along this principal bending axis, via the twist angle ϑ specifying its orientation relative to the airplane x axis. In terms of the section properties, the necessary defining relations are as follows.

$$\vartheta = \alpha_{\text{local}} + \theta_{\text{bend}} \tag{30}$$

$$\alpha_A = -\alpha_{L=0} - \theta_{\text{bend}} \tag{31}$$

$$
\begin{aligned}
n_{ta} &= 0 && (32)\\
EI_{cc} &= \iint E\, n^2 \, dc\, dn && (33)\\
EI_{nn} &= \iint E\, (c - c_{ta})^2 \, dc\, dn && (34)\\
EI_{cn} &= 0 && (35)
\end{aligned}
$$

The advantage here is the simplification of the bending stiffnesses, in particular $EI_{cn} = 0$ by definition.

1.5.2 Representation 2

This is usually the best choice if the principal axis is <u>not</u> obvious by inspection, so θ_{bend} is not immediately available. The c axis is then chosen to lie along the airfoil's chord line, giving the following defining relations.

$$
\begin{aligned}
\vartheta &= \alpha_{\text{local}} && (36)\\
\alpha_A &= -\alpha_{L=0} && (37)
\end{aligned}
$$

The bending stiffnesses $EI_{cc}, EI_{nn}, EI_{cn}$ do not simplify in this case, and must be computed along with EA, c_{ta}, n_{ta} directly from their full definitions (21)–(26) which are not restated here for brevity.

1.5.3 Representation 3

This choice may be the most convenient if all the section quantities are to be computed in the global aircraft axes xyz, e.g. if the section is defined in a CAD model. In this case the c axis is chosen to cooincide with the x axis, giving the following relations for the case of zero sweep and dihedral.

$$
\begin{aligned}
\vartheta &= 0 && (38)\\
\alpha_A &= -\alpha_{L=0} + \alpha_{\text{local}} && (39)\\
EI_{cc} &= EI_{xx} && (40)\\
EI_{nn} &= EI_{zz} && (41)\\
EI_{cn} &= EI_{xz} && (42)
\end{aligned}
$$

For nonzero sweep or dihedral, the xz stiffness-calculation plane would need to be rotated perpendicular to the spanwise axis.

1.5.4 Axis relations

If specifying θ_{bend} is more convenient than specifying EI_{cn} for some reason, standard Mohr's Circle relations can be used to switch from Representation 2 to 1.

$$
\begin{aligned}
\theta_{\text{bend}} &= \left[\frac{1}{2} \arctan \frac{-2\, EI_{cn}}{EI_{nn} - EI_{cc}} \right]_2 && (43)\\
(EI_{cc})_1 &= \left[\frac{1}{2} (EI_{nn} + EI_{cc}) - \sqrt{\frac{1}{4} (EI_{nn} - EI_{cc})^2 + EI_{cn}^2} \right]_2 && (44)\\
(EI_{nn})_1 &= \left[\frac{1}{2} (EI_{nn} + EI_{cc}) + \sqrt{\frac{1}{4} (EI_{nn} - EI_{cc})^2 + EI_{cn}^2} \right]_2 && (45)
\end{aligned}
$$

As written, these assume $EI_{nn} > EI_{cc}$, and are diagrammed in Figure 6.

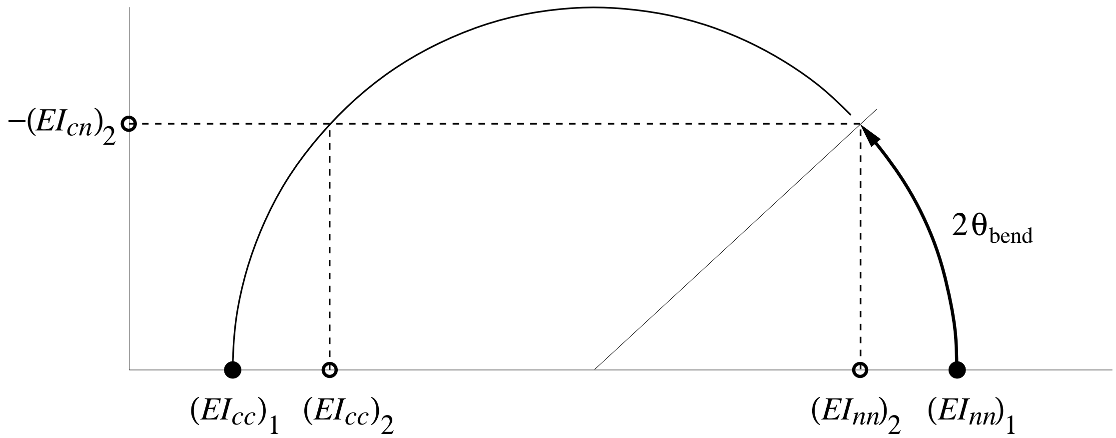

Figure 6: Mohr's circle relations between Representation 1 and 2 stiffnesses.

1.6 Force and moment equilibrium relations

The force and moment balance on a beam element of length ds is expressed in the x, y, z axes as

$$d\vec{F} \; + \; \vec{f}\, ds \; + \; \Delta\vec{F}\, d(1) \;\; = \;\; 0 \tag{46}$$

$$d\vec{M} \; + \; \vec{m}\, ds \; + \; \Delta\vec{M}\, d(1) \; + \; d\vec{r} \times \vec{F} \;\; = \;\; 0 \tag{47}$$

where $\vec{f}$ and $\vec{m}$ are the applied distributed force and moment, $\Delta\vec{F}$ and $\Delta\vec{M}$ are the applied concentrated force and moment, and $d(1)$ is the unit-impulse function.

2 Discrete Formulation

The discrete representation of the beam is given by the twelve nodal variables

$$\vec{r}_i \equiv \{x_i \;\; y_i \;\; z_i\}^T \qquad \vec{\theta}_i \equiv \{\varphi_i \;\; \vartheta_i \;\; \psi_i\}^T \qquad \vec{M}_i \equiv \{M_{xi} \;\; M_{y_i} \;\; M_{zi}\}^T \qquad \vec{F}_i \equiv \{F_{xi} \;\; F_{y_i} \;\; F_{zi}\}^T$$

where i is the node index along the beam at the prescribed s_i locations. This section describes the algebraic equations governing these variables.

2.1 Interior equations

The displacements and angles are related by three discrete compatibility relations

$$\begin{Bmatrix} \Delta x \\ \Delta y \\ \Delta z \end{Bmatrix} \;\; = \;\; \left[\quad \bar{\bar{T}}_a^T \quad \right] \begin{Bmatrix} \gamma_c \\ 1 + \epsilon_s \\ \gamma_n \end{Bmatrix}_a \Delta s_0 \tag{48}$$

where s_0 is the unloaded-beam arc length, and $\Delta(\;)$ is a difference and $(\;)_a$ is a simple average between the i and $i+1$ stations, e.g.

$$\Delta x \;\; = \;\; x_{i+1} - x_i \tag{49}$$

$$\bar{\bar{T}}_a \;\; = \;\; \frac{1}{2} \left(\bar{\bar{T}}_{i+1} + \bar{\bar{T}}_i \right) \tag{50}$$

The strains γ_c, ϵ_s,γ_n in the three relations (48) are negligible in most applications. However, if more than one kinematic constraint is applied to the beam, a nonzero ϵ_s (i.e. a finite EA) must be allowed to give the necessary extensional compliance to give a well-posed problem. The shear strains γ_c, γ_n in (48) compensate for the case where the s-axis does not cooincide with the elastic axis, i.e. if $c_{ea}, n_{ea} \neq 0, 0$.

The average strains $(\gamma_c, \epsilon_s, \gamma_n)_a$ in (48) are defined from relation (19). This in turn requires defining the average force and moment vectors in the local csn axes.

$$\begin{Bmatrix} F_c \\ F_s \\ F_n \end{Bmatrix}_a = \begin{bmatrix} & & \\ & \bar{\bar{T}}_a & \\ & & \end{bmatrix} \begin{Bmatrix} F_x \\ F_y \\ F_z \end{Bmatrix}_a \quad , \quad \begin{Bmatrix} M_c \\ M_s \\ M_n \end{Bmatrix}_a = \begin{bmatrix} & & \\ & \bar{\bar{T}}_a & \\ & & \end{bmatrix} \begin{Bmatrix} M_x \\ M_y \\ M_z \end{Bmatrix}_a \tag{51}$$

The translated average moment $(\vec{M}'_{csn})_a$ is then defined using relation (18).

Discretization of the beam curvature equation (16) first requires a discrete form of the beam curvatures. These can be defined via either the discrete form of the defining relation (6),

$$\begin{Bmatrix} \kappa_c \\ \kappa_s \\ \kappa_n \end{Bmatrix} \Delta s = \begin{bmatrix} & & \\ & \Delta\bar{\bar{T}} & \\ & & \end{bmatrix} \times\cdot \begin{bmatrix} & & \\ & \bar{\bar{T}}_a & \\ & & \end{bmatrix} \tag{52}$$

or via the discrete form of the analytically equivalent relation (8).

$$\begin{Bmatrix} \kappa_c \\ \kappa_s \\ \kappa_n \end{Bmatrix} \Delta s = \begin{bmatrix} & & \\ & \bar{\bar{K}}_a & \\ & & \end{bmatrix} \begin{Bmatrix} \Delta\varphi \\ \Delta\vartheta \\ \Delta\psi \end{Bmatrix} \tag{53}$$

These two discrete forms are equivalent to second order in $\Delta s, \Delta\varphi, \Delta\vartheta, \Delta\psi$, but (52) becomes singular if the Euler angle changes $\Delta\varphi, \Delta\vartheta, \Delta\psi$ approach $\pi/2$, as in a winglet junction, for example. The second form (53) remains well-conditioned and so is preferable, but care must be taken to initialize the angles so that the differences do not cross a $\pm\pi$ angle branch cut.

The curvature/moment relation is discretized as follows.

$$\begin{bmatrix} & & \\ & \bar{\bar{K}}_a & \\ & & \end{bmatrix} \begin{Bmatrix} \Delta\varphi \\ \Delta\vartheta \\ \Delta\psi \end{Bmatrix} - \begin{bmatrix} & & \\ & \bar{\bar{K}}_{a0} & \\ & & \end{bmatrix} \begin{Bmatrix} \Delta\varphi_0 \\ \Delta\vartheta_0 \\ \Delta\psi_0 \end{Bmatrix} = \begin{bmatrix} & & \\ & \bar{\bar{E}}_a^{-1} & \\ & & \end{bmatrix} \begin{Bmatrix} M'_c \\ M'_s \\ M'_n \end{Bmatrix}_a \Delta s \tag{54}$$

After discretization, equation (54) above has been multiplied through by the inverse of the discrete stiffness matrix to make the Jacobian's diagonal elements $\mathcal{O}(1)$ like the other equations.

The force and moment balance equations (46,47) are easily discretized as follows.

$$\vec{M}_{i+1} - \vec{M}_i + \vec{m}_a \Delta s + \Delta\vec{M} + \Delta\vec{r} \times \vec{F}_a = 0 \tag{55}$$

$$\vec{F}_{i+1} - \vec{F}_i + \vec{f}_a \Delta s + \Delta\vec{F} = 0 \tag{56}$$

The applied loads $\vec{f}$, $\vec{m}$, $\Delta\vec{F}$, and $\Delta\vec{M}$ are arbitrary for now, and will be derived in subsequent sections.

The discrete equations (55) and (56) have the attractive property of being strongly conservative, with no net force or moment being "lost" due to discretization errors. The wing root force $\vec{F}$, for example, is exactly equal to the net integrated loads $\vec{f}$ and $\Delta\vec{F}$ along the wing, even for very coarse grid node spacings.

A perfectly-rigid beam can be easily represented by setting the inverse of the stiffness matrix to zero in equation (54). Equations (55) and (56) will then still properly predict $\vec{M}$ and $\vec{F}$ despite the zero deformation. Of course, a rigid beam is not permissible if a kinematic constraint for any degree of freedom is imposed at more than one location.

Another attractive property of the entire discrete equation system is its ability to admit a zero-length structural interval where $\Delta\vec{r} = 0$, $\Delta s = 0$, for which case the system reduces to simple solution-continuity or solution-jump relations.

$$\begin{aligned}
\vec{r}_{i+1} - \vec{r}_i &= \vec{r}_{0_{i+1}} - \vec{r}_{0_i} \\
\vec{\theta}_{i+1} - \vec{\theta}_i &= \vec{\theta}_{0_{i+1}} - \vec{\theta}_{0_i} \\
\vec{M}_{i+1} - \vec{M}_i &= -\Delta\vec{M} \\
\vec{F}_{i+1} - \vec{F}_i &= -\Delta\vec{F}
\end{aligned}$$

Normally, $\vec{r}$ would be continuous at such an interval, but $\vec{\theta}$ might jump as in a dihedral break. Any concentrated load ΔM or ΔF applied at a zero-length interval is therefore captured as a perfect discontinuity in the solution with no artificial numerical "smearing", as shown in Figure 7. For maximum accuracy, it is advantageous to intentionally place such zero-length intervals at all concentrated load locations.

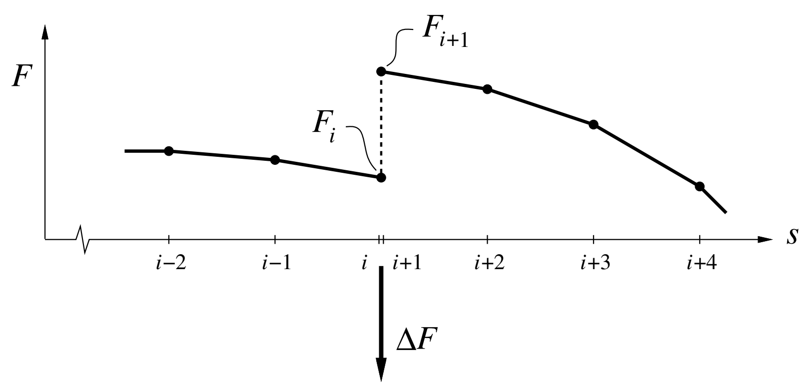

Figure 7: Concentrated load on zero-length $i \ldots i+1$ structural interval captured as perfect discontinuity in discrete solution.

2.2 Boundary conditions and interior constraints

The twelve discrete equations (48,54,55,56) for $i = 1 \ldots I-1$ require twelve appropriate boundary conditions to form a closed system for the $12I$ discrete variables. At each of the two free wing tips it is appropriate to impose six zero-load conditions.

$$\vec{M} = 0 \quad , \quad \vec{F} = 0 \tag{57}$$

These might be specified as nonzero if tip loads are applied by tip stores, joints, etc.

In addition to the twelve load boundary conditions, each beam must have at least six kinematic conditions — three on position $\vec{r}_i$ and three on angle $\vec{\theta}_i$ — to properly constrain the beam's rigid-body translation and rotation modes. Such a kinematic constraint location is either a *ground* or a *joint*, both described later. The constraint equations are effectively imposed within the discrete interval $i \ldots i+1$, and replace the moment-balance and force-balance equations (55,56) on that interval. Because its equilibrium equations are thus displaced, the interval will now admit jumps in the moment and force resultants, which represent the loads applied by the constraining object. If the grounding constraint is non-physical (e.g. the x, y, z axis origin attachment point) these loads will end up being computed to be zero within machine precision, since all real external forces, moments, plus inertial-reaction loads must sum up to zero.

3 Applied Loads

The total distributed applied loads consist of lift, drag, acceleration, and apparent-mass forces.

$$\vec{f} = \vec{f}_{\mathrm{lift}} + \vec{f}_{\mathrm{drag}} + \vec{f}_{\mathrm{acc}} + \vec{f}_{\mathrm{am}} \tag{58}$$

$$\vec{m} = \vec{m}_{\mathrm{lift}} + \vec{m}_{\mathrm{drag}} + \vec{m}_{\mathrm{acc}} + \vec{m}_{\mathrm{am}} \tag{59}$$

The concentrated applied loads are due to point masses responding to gravity, acceleration, and aero drag, due to engine forces, due to external elastic struts or bracing wires, and due to beam joints.

$$\Delta\vec{F} = \Delta\vec{F}_{\mathrm{pmass}} + \Delta\vec{F}_{\mathrm{eng}} + \Delta\vec{F}_{\mathrm{strut}} + \Delta\vec{F}_{\mathrm{joint}} \tag{60}$$

$$\Delta\vec{M} = \Delta\vec{M}_{\mathrm{pmass}} + \Delta\vec{M}_{\mathrm{eng}} + \Delta\vec{M}_{\mathrm{strut}} + \Delta\vec{M}_{\mathrm{joint}} \tag{61}$$

Expressions for all these loads are derived in the following sections.

3.1 Aerodynamic loads

The circulation distribution $\Gamma(s)$ for each lifting surface is defined either pointwise at each structural interval or as a Fourier series in the Glauert angle $\theta(s)$,

$$\Gamma(s_i) = A_i \tag{62}$$

$$\text{or} \qquad \Gamma(s) = \sum_{k=1}^{K} A_k \sin(k\theta) \quad , \qquad \theta = \arccos\left(\frac{s}{s_{\mathrm{max}}}\right) \tag{63}$$

where s_{max} is the structural semispan, and s has the range $-s_{\mathrm{max}} \leq s \leq s_{\mathrm{max}}$. The number of Fourier modes needed for good accuracy is typically smaller than the necessary number of structural intervals, so the Fourier representation is considerably more efficient. The differences are only in the implementation details, however, and the circulation variables can be either A_i or A_k depending on which approach is chosen. The Fourier approach will be used in the subsequent development.

The local velocity relative to the beam section at location $\vec{r}$ is

$$\vec{V}(\vec{r}) = \vec{V}_{\infty} - \vec{\Omega} \times \vec{r} + \vec{V}_{\mathrm{ind}}(\vec{r}) + \vec{V}_{\mathrm{gust}}(\vec{r}) \tag{64}$$

$$\vec{V}_{\mathrm{ind}}(\vec{r}) = \sum_{k=1}^{K} \vec{v}_k(\vec{r})\, A_k + \vec{w}_{\mathrm{vol}}(\vec{r})\, V_{\infty} \tag{65}$$

where A_k are Fourier mode coefficients for the bound circulation and $\vec{v}_k$ are their aerodynamic influence functions. The induced velocity due to beam volumes is given via the $\vec{w}_{\rm vol}$ influence function. Their contributions to the overall induced velocity $\vec{V}_{\rm ind}$ will be treated in a later section. The nonuniform gust perturbation velocity field $\vec{V}_{\rm gust}$, which is prescribed explicitly in subroutine VGUSTE, is included for completeness. Unlike $\vec{V}_\infty$, the gust velocity can have a spatial variation and so can represent tight thermal cores, sharp gusts, etc., which can have significant variations over the extent of a large aircraft.

For calculating the various aerodynamic loads, it is useful to define unit vectors giving the directions of the local c, s, n unit vectors in airplane axes. These are simply the rows of the transformation tensor.

$$\begin{bmatrix} - & \hat{c}^T & - \\ - & \hat{s}^T & - \\ - & \hat{n}^T & - \end{bmatrix} = \begin{bmatrix} & & \\ & \bar{\bar{T}} & \\ & & \end{bmatrix} \tag{66}$$

The aerodynamic lift vector then follows from the vector form of the Kutta-Joukowsky theorem,

$$\vec{f}_{\rm lift} \;=\; \rho\,\Gamma\,\vec{V} \times \hat{s} \qquad \text{(surface beam)} \tag{67}$$

where $\vec{V}$ is evaluated using (64) at the bound vortex location $\vec{r}_{h.v.}$, defined later. The local circulation Γ will be determined via a lifting-line formulation which employs the Prandtl-Glauert transformation, so that this lift force accounts for compressibility. For a fuselage beam with local radius R, the lift force is determined from slender-body theory using the beam-normal velocity $\vec{V}_\perp$.

$$\vec{f}_{\rm lift} \;=\; \rho\,\vec{V}_\perp\,(\vec{V}\cdot\hat{s})\,2\pi R\frac{dR}{ds} \qquad \text{(fuselage beam)} \tag{68}$$

$$\vec{V}_\perp \;=\; \vec{V} \,-\, (\vec{V}\cdot\hat{s})\,\hat{s} \tag{69}$$

In this case $\vec{V}$ is evaluated at $\vec{r}_a$ at the center of the cylindrical beam. The profile drag force is resolved into a friction-drag contribution acting along the local net velocity, and a pressure-drag contribution acting perpendicular to the beam's spanwise axis.

$$\vec{f}_{\rm drag} \;=\; \frac{1}{2}\rho\,|\vec{V}|\,\vec{V}\;\bar{c}\;c_{d_f} \;+\; \frac{1}{2}\rho\,|\vec{V}_\perp|\,\vec{V}_\perp\;\bar{c}\;c_{d_p} \;+\; 2\,\rho\,\frac{\vec{V}_\perp}{|\vec{V}_\perp|}\left(\vec{V}\cdot\hat{n}\right)^2_{c.p.}\bar{c} \qquad \text{(surface beam)} \tag{70}$$

$$\vec{f}_{\rm drag} \;=\; \frac{1}{2}\rho\,|\vec{V}|\,\vec{V}\,2R\,c_{d_f} \;+\; \frac{1}{2}\rho\,|\vec{V}_\perp|\,\vec{V}_\perp\,2R\,c_{d_p} \qquad \text{(fuselage beam)} \tag{71}$$

where $\bar{c}$ is the local chord. For an unswept wing, the sum $c_{d_f} + c_{d_p}$ constitutes the usual airfoil-section profile drag. For a fuselage, c_{d_f} is comparable to the skin friction coefficient C_f, and c_{d_p} is the drag coefficient of a circular cylinder, typically 1.2 for subcritical flow, and 0.4 for supercritical flow. The third term in the surface-beam drag force enters in only when the flow-tangency velocity $\vec{V}\cdot\hat{n}$ is nonzero, which occurs when the local c_ℓ exceeds the stall limits. This constitutes a simple post-stall model, and gives $f_{\rm drag} \simeq \rho V_\perp^2 \bar{c}$ when the local incidence angle approaches 90°.

Excluding the deep-stall condition, the drag forces controlled by c_{d_f} and c_{d_p} usually contribute very little to structural loads, but are included here since they do not impact the calculation cost significantly, and can give overall aircraft drag estimates. The fuselage lift forces can have significant impact on the overall aircraft pitching moment.

The aerodynamic profile moment vector is approximated by assuming that it is influenced only by the velocity component $\vec{V}_\perp$ perpendicular to the wing's spanwise axis.

$$\vec{m}_{\rm lift} \;=\; (\bar{c}/4 - \bar{x}_o)\,\hat{c}\times\vec{f}_{\rm lift} \;+\; \frac{1}{2}\rho\,|\vec{V}_\perp|^2\,\bar{c}^2\,c_m\,\hat{s} \qquad \text{(surface beam)} \tag{72}$$

The first term is simply the contribution of the lift force acting at the quarter-chord point, with $\bar{x}_o$ being the chordwise location of the c, s, n origin, as shown in Figure 16. The second term involves the 2-D section pitching moment coefficient c_m, which is defined as a constant part, plus contributions from control surface or flap deflections δ_F. Unsteady Theodorsen-type terms will be included in the apparent-mass contributions.

$$c_m \;=\; \left(c_{m\,o} \,+\, \frac{dc_m}{d\delta_{F_1}}\,\delta_{F_1} \,+\, \frac{dc_m}{d\delta_{F_2}}\,\delta_{F_2} \ldots \right) \frac{1}{\sqrt{1 - M_\perp^2}} \tag{73}$$

The Prandtl-Glauert factor uses the local perpendicular Mach number $M_\perp = |\vec{V}_\perp|/V_{\text{sound}}$, which is consistent with lifting line theory. The contribution of the flap-deflection moment derivative $dc_m/d\delta_F$ is very important in most applications, since it is the aerodynamic quantity directly responsible for aileron reversal, and often significantly reduces aileron response in normal flight conditions.

The distributed profile moment force due to friction forces is in general negligible:

$$\vec{m}_{\text{drag}} \;=\; 0 \tag{74}$$

3.2 Inertial and gravity loads

Absolute accelerations relative to an inertial frame are defined on the beam axis at $\vec{r}_i$, and at some nearby offset location $\vec{r}_p = \vec{r}_i + \Delta\vec{r}_p$.

$$\vec{a}_i \;=\; \vec{a}_o \,+\, \vec{\alpha}_o \times \vec{r}_i \,+\, \vec{\Omega} \times \left(\vec{\Omega} \times \vec{r}_i \right) \tag{75}$$

$$\vec{a}_p \;=\; \vec{a}_i \,+\, \vec{\alpha}_o \times \Delta\vec{r}_p \,+\, \vec{\Omega} \times \left(\vec{\Omega} \times \Delta\vec{r}_p \right) \tag{76}$$

The coordinate-system origin acceleration $\vec{a}_o$ can be prescribed arbitrarily, or can be related to the overall external force on the configuration. Both cases will be treated later. It must be stressed that the assumption of rigid-body rotations and accelerations made in (75,76) may not be realistic with large flexible aircraft, since structural dynamics and/or unsteady aerodynamics are being neglected. Nevertheless, the computed results for such cases represent the low-frequency limit, and hence still give useful information. The full dynamic formulation will be treated as a separate extension.

The local gravitational and inertial-reaction load acts at the local mass centroid offset from the beam axis by

$$\Delta\vec{r}_{cg} \;=\; c_{cg}\,\hat{c} \,+\, n_{cg}\,\hat{n} \tag{77}$$

where c_{cg}, n_{cg} is the location of the mass centroid of the beam cross-section as shown in Figure 4. This $\Delta\vec{r}_{cg}$ then defines the local acceleration $\vec{a}_{cg}$ via relations (75,76). The corresponding loads are

$$\vec{f}_{\text{acc}} \;=\; \mu\,(\vec{g} - \vec{a}_{cg}) \tag{78}$$

$$\vec{m}_{\text{acc}} \;=\; \Delta\vec{r}_{cg} \times \vec{f}_{\text{acc}} \;-\; \bar{\bar{T}}^T\,\bar{\bar{\iota}}\,\bar{\bar{T}}\,\vec{\alpha}_o \;-\; \vec{\Omega} \times \left\{ \bar{\bar{T}}^T\,\bar{\bar{\iota}}\,\bar{\bar{T}}\,\vec{\Omega} \right\} \tag{79}$$

where μ is the mass/length density of the beam, $\bar{\bar{\iota}}$ is the section inertia/length tensor. This tensor is defined to have the form

$$\bar{\bar{\iota}} \;\equiv\; \begin{bmatrix} \iota_{cc} & 0 & 0 \\ 0 & \iota_{ss} & 0 \\ 0 & 0 & \iota_{nn} \end{bmatrix} \,+\, \frac{\Delta s^2}{12} \begin{bmatrix} \mu & 0 & 0 \\ 0 & 0 & 0 \\ 0 & 0 & \mu \end{bmatrix} \tag{80}$$

$$\iota_{cc} = \int (n - n_{cg})^2 \, d\mu \tag{81}$$

$$\iota_{nn} = \int (c - c_{cg})^2 \, d\mu \tag{82}$$

$$\iota_{ss} = \int [(c - c_{cg})^2 + (n - n_{cg})^2] \, d\mu \;=\; \iota_{nn} + \iota_{cc} \tag{83}$$

which reasonably assumes that the tensor's principal axes are aligned with the local c, n axes. The second term in (80) is formally $\mathcal{O}(\Delta s^2)$ and normally negligible, but is retained to improve accuracy for very coarse discretizations.

The surface apparent-mass force contribution depends only on the normal component of the local accelerations, and the resulting pressure forces can act only normal to the surface. Hence the apparent-mass force is along $\hat{n}$ and the apparent-mass moment is along $\hat{s}$.

$$\vec{f}_{\mathrm{am}} = \frac{\pi}{4} \rho \, \bar{c}^2 \left(\vec{V} \times \vec{\Omega} \cdot \hat{n} \;-\; \vec{a}_{c/2} \cdot \hat{n} \right) \hat{n} \qquad \text{(surface beam)} \tag{84}$$

$$\vec{m}_{\mathrm{am}} = -\frac{\pi}{4} \rho \, \bar{c}^2 \, \frac{\bar{c}}{4} \left(\vec{V} \times \vec{\Omega} \cdot \hat{n} \;+\; \frac{\bar{c}}{8} \vec{\alpha}_o \cdot \hat{s} \right) \hat{s} \;+\; \Delta\vec{r}_{c/2} \times \vec{f}_{\mathrm{am}} \tag{85}$$

The midchord acceleration $\vec{a}_{c/2}$ is evaluated at

$$\Delta\vec{r}_{c/2} = (\bar{c}/2 - \bar{x}_o)\hat{c}$$

using relations (75,76). All the apparent-mass terms above correspond to the "instantaneous" (non-lag) forces and moments from Theodorsen's theory. The various vector projections are necessary to reproduce the theory's results in the perpendicular c-n airfoil plane. The net velocity $\vec{V}$ in the Coriolis-like term above is evaluated on the beam itself at $\vec{r}_i$.

For a fuselage beam, the apparent-mass force is obtained from slender-body theory as follows.

$$\vec{f}_{\mathrm{am}} = -2\pi \, \rho \, R^2 \left(\vec{a}_i - (\vec{a}_i \cdot \hat{s}) \, \hat{s} \right) \qquad \text{(fuselage beam)} \tag{86}$$

3.3 Point-mass loads

In addition to the continuous mass/span distribution μ, it is useful to also consider point masses m_p which are cantilevered from the beam's structural axis by a rigid pylon with geometric dimensions c_p, s_p, n_p in the local wing-section coordinates, as shown in Figure 8. These pylon dimensions are determined via the transformation tensor.

$$\{ \, c_p \; s_p \; n_p \, \}^T \;=\; \bar{\bar{T}}_0 \; \{\Delta\vec{r}_p\}_0 \tag{87}$$

The $(\;)_0$ subscript denotes values for the undeformed state which is known a priori, so that c_p, s_p, n_p are in effect fixed constants. Similarly, the undeformed-state angular momentum vector $\vec{H}_{p_0}$ defines its corresponding fixed c, s, n components.

$$\{ \, H_{c_p} \; H_{s_p} \; H_{n_p} \, \}^T \;=\; \bar{\bar{T}}_0 \left\{ \vec{H}_p \right\}_0 \tag{88}$$

The point mass can represent a nacelle, external store, rotor, etc, mounted to the beam. It must be noted that the assumption that the pylon is rigid does not eliminate the ability to represent a mass which is mounted on an elastic pylon. In this case, the elastic pylon would be represented by a fuselage-type beam, and the point mass would be attached to this flexible beam.

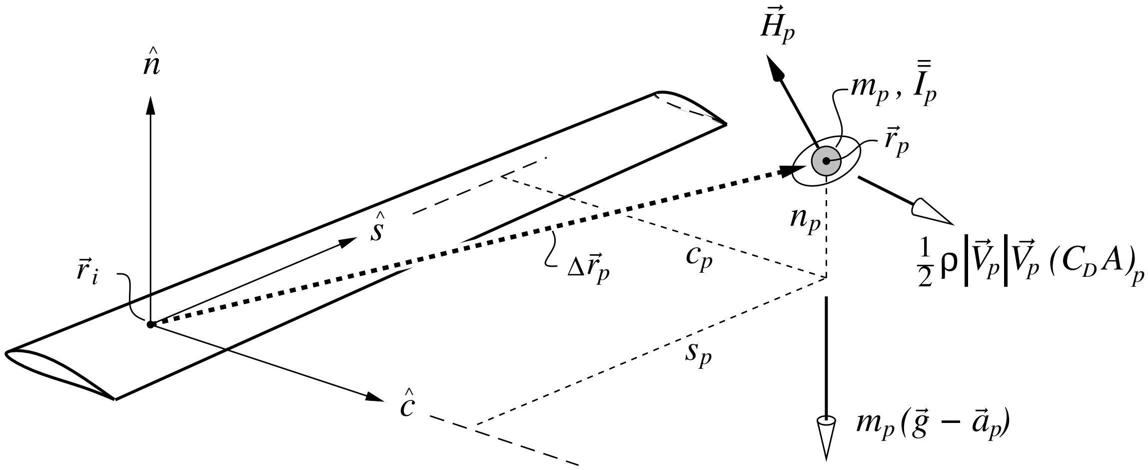

Figure 8: Point mass m_p with inertia $\bar{\bar{I}}_p$ and angular momentum $\vec{H}_p$, cantilevered from wing by rigid pylon, with various applied loads shown. Pylon endpoint $\vec{r}_p$ is defined by the anchor point $\vec{r}_i$, the anchor's point orientation ($\bar{\bar{T}}$), and the pylon's fixed c_p, s_p, n_p components.

The location $\vec{r}_p$ of the point mass in airplane axes is given by

$$\Delta\vec{r}_p \;=\; \bar{\bar{T}}^T \left\{ c_p \; s_p \; n_p \right\}^T \;=\; \bar{\bar{T}}^T \, \bar{\bar{T}}_0 \, \Delta\vec{r}_{p0} \tag{89}$$

$$\vec{r}_p \;=\; \vec{r}_i \,+\, \Delta\vec{r}_p \tag{90}$$

where $\bar{\bar{T}}$ is the transformation tensor at the pylon-attachment location $\vec{r}_i$ on the wing/beam at the local c, s, n origin. Although c_p, s_p, n_p are fixed, both $\vec{r}_i$ and $\bar{\bar{T}}$ change as the beam deforms, so that the point mass at $\vec{r}_p$ is "waved around" appropriately in space along with the beam. The angular momentum vector and inertia tensor are rotated in the same manner.

$$\vec{H}_p \;=\; \bar{\bar{T}}^T \left\{ H_{c_p} \; H_{s_p} \; H_{n_p} \right\}^T \;=\; \bar{\bar{T}}^T \, \bar{\bar{T}}_0 \, \vec{H}_{p0} \tag{91}$$

$$\bar{\bar{I}}_p \;=\; \bar{\bar{T}}^T \, \bar{\bar{T}}_0 \, \bar{\bar{I}}_{p0} \, \bar{\bar{T}}_0^T \, \bar{\bar{T}} \tag{92}$$

The local relative air velocity at the point mass and the mass's acceleration follow from relations (64) and (75,76).

$$\vec{V}_p \;=\; \vec{V}_\infty \,-\, \vec{\Omega} \times \vec{r}_p \,+\, \vec{V}_{\rm ind}(\vec{r}_p) \,+\, \vec{V}_{\rm gust}(\vec{r}_p) \tag{93}$$

$$\vec{a}_p \;=\; \vec{a}_i \,+\, \vec{\alpha}_o \times \Delta\vec{r}_p \,+\, \vec{\Omega} \times \left(\vec{\Omega} \times \Delta\vec{r}_p \right) \tag{94}$$

The gravitational, inertial-reaction, and aerodynamic drag loads applied to the beam by the point mass are

$$\Delta\vec{F}_{\rm pmass} \;=\; m_p \left(\vec{g} - \vec{a}_p \right) \,+\, \frac{1}{2} \rho \, |\vec{V}_p| \, \vec{V}_p \, (C_D A)_p \tag{95}$$

$$\Delta\vec{M}_{\rm pmass} \;=\; \Delta\vec{r}_p \times \Delta\vec{F}_{\rm pmass} \,-\, \vec{\Omega} \times \vec{H}_p \,-\, \bar{\bar{I}}_p \vec{\alpha}_o \,-\, \vec{\Omega} \times \left(\bar{\bar{I}}_p \, \vec{\Omega} \right) \tag{96}$$

with the mass m_p, undeformed-state angular momentum $\vec{H}_{p0}$, and the net drag area $(C_D A)_p$ of the point mass being specified.

3.4 Engine loads and jet

3.4.1 Engine force and moment

An "Engine" entity is treated very much like a point mass. As shown in Figure 9, it is mounted on a rigid pylon, and has a force $\vec{F}_{\rm eng}$ and moment $\vec{M}_{\rm eng}$ acting on it. The loads applied to the beam at the pylon attachment point are

$$\Delta\vec{F}_{\rm eng} = \vec{F}_{\rm eng} \tag{97}$$

$$\Delta\vec{M}_{\rm eng} = \vec{M}_{\rm eng} + \Delta\vec{r}_p \times \Delta\vec{F}_{\rm eng} \tag{98}$$

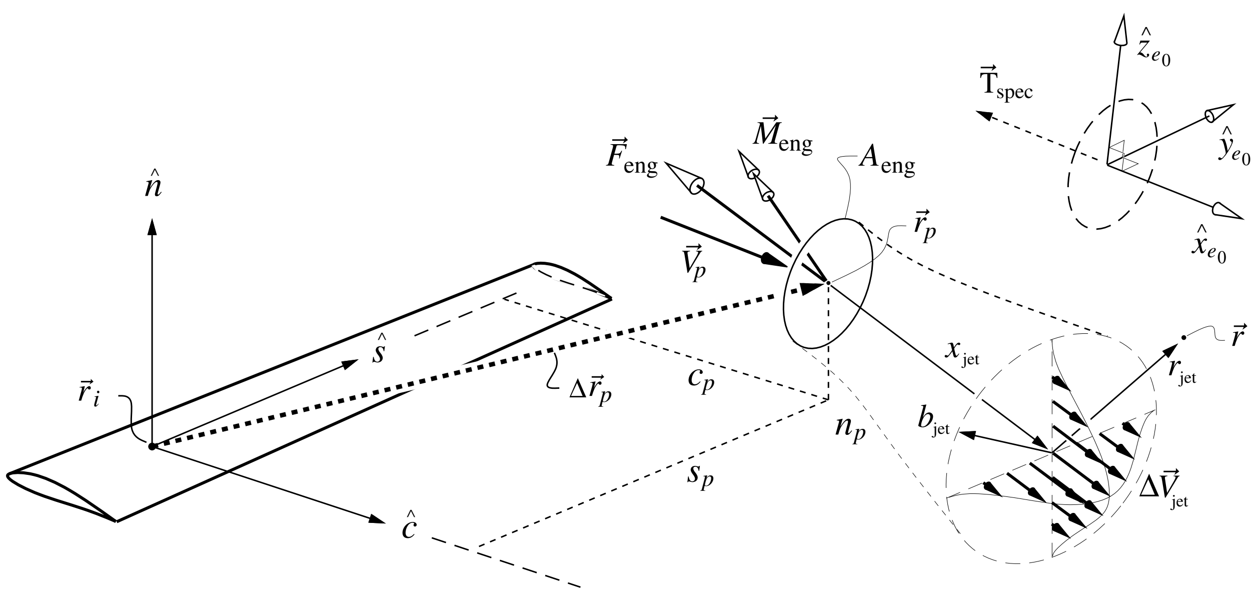

Figure 9: Engine cantilevered from wing by rigid pylon, with thrust force and moment. Propulsive jet velocity $\Delta\vec{V}_{\rm jet}$ affects downstream surfaces on which it impinges.

3.4.2 Engine axes relations

The engine force and moment $\vec{F}_{\rm eng}$ and $\vec{M}_{\rm eng}$ in equations (97) and (98) are obtained from an engine "black box" subroutine (treated later), which performs its computations in the engine axes x_e,y_e,z_e. The transformation from x,y,z to x_e,y_e,z_e and vice-versa is performed outside the engine black-box routine. The engine axis directions are specified via the "thrust vector" $\vec{\rm T}_{\rm spec}$ shown in Figure 9, which will normally correspond to the prop shaft axis for the undeformed geometry. This defines the undeformed-state engine axis unit vectors as follows.

$$\hat{x}_{e_0} = -\vec{\rm T}_{\rm spec} / \left|\vec{\rm T}_{\rm spec}\right|$$

$$\hat{y}_{e_0} = \hat{k} \times \hat{x}_{e_0} / \left|\hat{k} \times \hat{x}_{e_0}\right|$$

$$\hat{z}_{e_0} = \hat{x}_{e_0} \times \hat{y}_{e_0}$$

It is assumed that the engine force is unaffected by the rotating the whole powerplant around the $\hat{x}_{e0}$ axis. This justifies the arbitrary placement of the $\hat{y}_{e0}$ axis perpendicular to the $\hat{k}$-$\hat{x}_{e0}$ plane.

The rotation of the attachment point and pylon will give the engine axes a new orientation.

$$\begin{aligned}
\hat{x}_e &= \bar{\bar{T}}^T \bar{\bar{T}}_0 \, \hat{x}_{e0} \\
\hat{y}_e &= \bar{\bar{T}}^T \bar{\bar{T}}_0 \, \hat{y}_{e0} \\
\hat{z}_e &= \bar{\bar{T}}^T \bar{\bar{T}}_0 \, \hat{z}_{e0}
\end{aligned}$$

These three deformed-state unit vectors define a convenient engine-axis transformation tensor,

$$\bar{\bar{T}}_e \equiv \begin{bmatrix} - & \hat{x}_e & - \\ - & \hat{y}_e & - \\ - & \hat{z}_e & - \end{bmatrix} = \begin{bmatrix} - & \hat{x}_{e0} & - \\ - & \hat{y}_{e0} & - \\ - & \hat{z}_{e0} & - \end{bmatrix} \begin{bmatrix} & & \\ & \bar{\bar{T}}^T \bar{\bar{T}}_0 & \\ & & \end{bmatrix}^T \tag{99}$$

which depends on the specified $\vec{\mathrm{T}}_{\mathrm{spec}}$, and also on the local beam Euler angles φ_i, ϑ_i, and ψ_i for the deformed and undeformed geometry.

An alternative "fixed" engine-axis definition is to simply define

$$\hat{x}_e = \hat{x}_{e0} \tag{100}$$

$$\hat{y}_e = \hat{y}_{e0} \tag{101}$$

$$\hat{z}_e = \hat{z}_{e0} \tag{102}$$

so that the axes are held fixed to their specified orientations, although this would be difficult to physically implement on a real flexible aircraft. In any case, in the program this type of fixed engine is specified by simply attaching it at the ground point. The engine location $\vec{r}_p$ will then stay at its initial location $\vec{r}_{p_0}$.

The engine black-box routine receives the relative velocity $\vec{V}_e$ in the engine axes. This is computed from the body-axes relative velocity $\vec{V}_p$ defined by equation (93), together with the transformation tensor.

$$\vec{V}_e = \bar{\bar{T}}_e \vec{V}_p \tag{103}$$

The resulting computed engine force and moment $\vec{F}_e$, $\vec{M}_e$ are then transormed back to the body axes, again using the transformation tensor.

$$\vec{F}_{\mathrm{eng}} = \bar{\bar{T}}_e^T \vec{F}_e \tag{104}$$

$$\vec{M}_{\mathrm{eng}} = \bar{\bar{T}}_e^T \vec{M}_e \tag{105}$$

These are then used in (97) and (98) to determine the applied beam loads.

3.4.3 Engine models

Proportional engine model

The simplest engine model assumes the thrust and moment are directly proportional to the engine power parameter Δ_e, with specified unit-power force and moment coefficients F_{e_1} and M_{e_1}. The thrust and moment are assumed to be in the $-\hat{x}_e$ direction (i.e. $\vec{\mathrm{T}}_{\mathrm{spec}}$ direction tilted by structural deformation).

$$\vec{F}_e \;=\; -\Delta_e\, F_{e_1}\, \hat{x}_e \qquad\qquad \vec{M}_e \;=\; -\Delta_e\, M_{e_1}\, \hat{x}_e \tag{106}$$

Actuator disk engine model

A more realistic engine model uses actuator disk theory, which can represent effects such as thrust lapse with density and air velocity, e.g. $\vec{F}_e(\Delta_e, \rho, \vec{V}_e)$, $\vec{M}_e(\Delta_e, \rho, \vec{V}_e)$. We assume that Δ_e represents the engine shaft power:

$$P_{\mathrm{eng}} \;=\; \Delta_e \tag{107}$$

For constructing the propeller model, we need to define V_{eng}, which is the axial component of the relative onset flow at the propeller.

$$V_{\mathrm{eng}} \;=\; V_{x_e} \;=\; \vec{V}_p \cdot \hat{x}_e \tag{108}$$

A reasonable estimate for viscous power loss due to profile drag is

$$\begin{aligned} P_{\mathrm{v}} &= B \int_0^{R_{\mathrm{eng}}} \frac{1}{2}\rho \left(V_{\mathrm{eng}}^2 + \Omega_{\mathrm{eng}}^2 r^2\right)^{3/2} c_d\, c\, dr \\ P_{\mathrm{v}} &\simeq \frac{1}{8}\,\rho \left(V_{\mathrm{eng}}^2 + \Omega_{\mathrm{eng}}^2 R_{\mathrm{eng}}^2\right)^{1/2} \left(V_{\mathrm{eng}}^2 + 3\Omega_{\mathrm{eng}}^2 R_{\mathrm{eng}}^2\right)\; (C_D A)_{\mathrm{eng}} && (109) \\ (C_D A)_{\mathrm{eng}} &= B R_{\mathrm{eng}} \bar{c}\, \bar{c}_d && (110) \end{aligned}$$

where $(C_D A)_{\mathrm{eng}}$ is the total effective blade drag area, defined in terms of the number of blades B, the effective blade chord $\bar{c}$, and the blade airfoil drag coefficient $\bar{c}_d$. Both $\bar{c}$ and $\bar{c}_d$ are best taken from the blade radius $r \simeq 0.8R_{\mathrm{eng}}$ where the viscous-power integrand is typically close to maximum. Extended actuator disk theory then gives

$$\begin{aligned} F_{\mathrm{eng}} &= \rho A_{\mathrm{eng}} \left(V_{\mathrm{eng}} + \frac{1}{2}\Delta V_{\mathrm{eng}}\right) \Delta V_{\mathrm{eng}} && (111) \\ P_{\mathrm{eng}} - P_{\mathrm{v}} &= \left[V_{\mathrm{eng}} \;+\; \left(1 + 5\lambda^2\right) \frac{\Delta V_{\mathrm{eng}}}{2}\right] F_{\mathrm{eng}} && (112) \\ P_{\mathrm{eng}} - P_{\mathrm{v}} &= \rho A_{\mathrm{eng}} \left[V_{\mathrm{eng}} \;+\; \left(1 + 5\lambda^2\right) \frac{\Delta V_{\mathrm{eng}}}{2}\right] \left(V_{\mathrm{eng}} + \frac{1}{2}\Delta V_{\mathrm{eng}}\right) \Delta V_{\mathrm{eng}} && (113) \\ \lambda &= V_{\mathrm{eng}} / \Omega_{\mathrm{eng}} R_{\mathrm{eng}} && (114) \end{aligned}$$

where the empirical factor of $1 + 5\lambda^2$ accounts for induced swirl losses, which become significant when the advance ratio λ becomes large.

If the shaft power P_{eng} is specified, and the viscous power P_{v} is computed using the approximation (109), equation (113) becomes a solvable cubic equation for ΔV_{eng}. In lieu of using cubic equation formulas, it is simplest to solve equation (113) using Newton iteration. Several precautions must be made for the windmill case where the net inviscid power $P_{\mathrm{i}} \equiv P_{\mathrm{eng}} - P_{\mathrm{v}}$ is negative, which is easily encountered in the power-off case if $P_{\mathrm{eng}} = 0$ and P_{v} is finite. For a given airspeed V_{eng}, the minimum P_{i} corresponds to the Betz limit,

$$(P_{\mathrm{i}})_{\mathrm{min}} \;=\; -\frac{8}{27}\, \rho V_{\mathrm{eng}}^3 A_{\mathrm{eng}} \tag{115}$$

which occurs when

$$\Delta V_{\mathrm{eng}} \;=\; -\frac{2}{3} V_{\mathrm{eng}} \qquad\qquad \text{(at Betz limit)} \tag{116}$$

Any specified $P_{\rm i}$ below $(P_{\rm i})_{\rm min}$ must be clipped at $(P_{\rm i})_{\rm min}$, else there will be no physical $\Delta V_{\rm eng}$ root to the cubic equation (113), possibly resulting in an arithmetic fault.

After $\Delta V_{\rm eng}$ is computed from (113), the thrust force is obtained immediately via (111). The shaft moment is given simply by a power balance requirement, with $\Omega_{\rm eng}$ defined positive about $\vec{\rm T}_{\rm spec}$. The functional dependencies have the following forms.

$$F_{\rm eng} = F_{\rm eng}(P_{\rm eng}, \rho, V_{\rm eng}) \tag{117}$$

$$M_{\rm eng} = M_{\rm eng}(P_{\rm eng}, \Omega_{\rm eng}) = -P_{\rm eng}/\Omega_{\rm eng} \tag{118}$$

These are assumed to act along the engine axis direction $-\hat{x}_e$, so that the components of the engine force and moment vectors $\vec{F}_e$ and $\vec{M}_e$ are then given as follows:

$$\vec{F}_e = \{-F_{\rm eng}\,,\,0\,,\,0\}^T \tag{119}$$

$$\vec{M}_e = \{-M_{\rm eng}\,,\,0\,,\,0\}^T \tag{120}$$

Off-axial forces and moments could be incorporated here using P-factor relations.

If the thrust is specified rather than the power, then $\Delta V_{\rm eng}$ does not get involved in the calculations. Since it is still needed for the propulsive jet model developed next, it is in this case computed directly from the quadratic thrust relation (111).

$$\Delta V_{\rm eng} = \sqrt{V_{\rm eng}^2 + \frac{2F_{\rm eng}}{\rho A_{\rm eng}}} - V_{\rm eng} \tag{121}$$

3.4.4 Propulsive jet

Engine force will be accompanied by a propulsive jet with velocity increment field $\Delta\vec{V}_{\rm jet}$. The jet is assumed to lie along some unit direction vector $\hat{\xi}$, which is also the direction of the trailing vortex legs in the vortex-lattice system (described in a later section). The spatial variation of this jet velocity field is constructed using a combination of actuator disk theory together with jet and wake mixing theory. These will be applied in terms of the lateral distance $r_{\rm jet}$ from the thrust line and the distance $x_{\rm jet}$ behind the engine, defined by the following vector operations.

$$x_{\rm jet} = \hat{\xi}\cdot(\vec{r}-\vec{r}_p) \tag{122}$$

$$\vec{r}_{\rm jet} = (\vec{r}-\vec{r}_p) - \hat{\xi}\,x_{\rm jet} \tag{123}$$

$$r_{\rm jet} = |\vec{r}_{\rm jet}| \tag{124}$$

As shown in Figure 10, there will be an initial induced velocity increment $\Delta V_{\rm eng}$ a short distance behind the engine disk, once ambient pressure is reached. The self-induced velocity increment at the disk itself will be only $\Delta V_{\rm eng}/2$, so that the jet will have a fast initial contraction from engine disk radius $R_{\rm eng}$, to $R'_{\rm eng}$ as given by the mass continuity requirement.

$$R_{\rm eng} = \sqrt{\frac{A_{\rm eng}}{\pi}} \tag{125}$$

$$R'_{\rm eng} = R_{\rm eng}\sqrt{\frac{V_{\rm eng}+\Delta V_{\rm eng}/2}{V_{\rm eng}+\Delta V_{\rm eng}}} \tag{126}$$

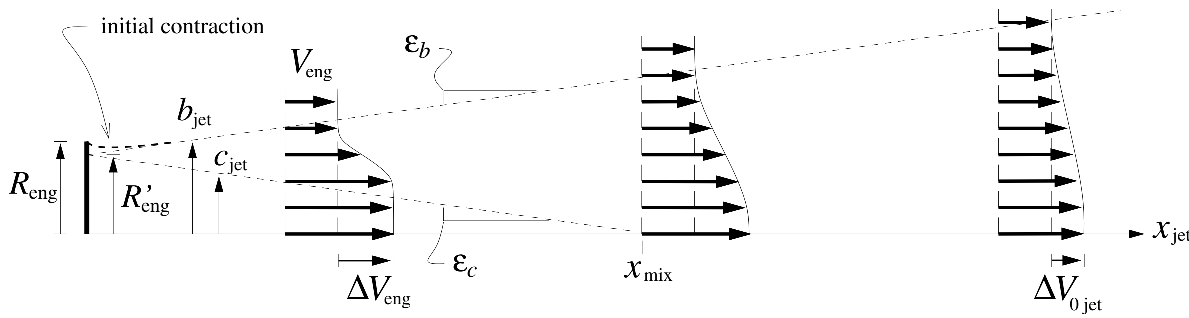

Figure 10: Evolution of jet radius and jet profile behind an engine.

Jet spreading and jet velocity profile

As shown in Figure 10, the boundary of the jet will spread laterally due to turbulent mixing at a half-angle of $\arctan(\varepsilon)$. Mixing-layer theory, as described by White [2], assumes the lateral growth rate scales with the lateral turbulent velocity fluctuations.

$$\begin{aligned} \frac{Db}{Dt} &\sim v' \\ \frac{db}{dx} &= K_\varepsilon \frac{\Delta V}{V_{\text{convective}}} \end{aligned}$$

Applying this concept to the inner and outer shear layer boundaries gives

$$\varepsilon_c = K_\varepsilon \frac{|\Delta V_{\text{eng}}|}{V_{\text{eng}} + 1.0\,\Delta V_{\text{eng}}} \tag{127}$$

$$\varepsilon_b = K_\varepsilon \frac{|\Delta V_{\text{eng}}|}{V_{\text{eng}} + 0.5\,\Delta V_{\text{eng}}} \tag{128}$$

$$K_\varepsilon = 0.11 \tag{129}$$

The constants 1.0 and 0.5 for the effective convective speeds in the denominators are calibrated to give a nearly constant momentum flux in the resulting jet profile, as will be seen later. The $K_\varepsilon = 0.11$ value approximately matches observed experimental shear layer spreading rates. For very light disk loadings, $\Delta V_{\text{eng}} \ll V_{\text{eng}}$, and the spreading angle is close to zero. For very large disk loadings, $\Delta V_{\text{eng}} \gg V_{\text{eng}}$, the outer spreading angle approaches $\arctan(K_\varepsilon/0.5) \simeq 12°$. The inner spreading angle defines a "mixing distance" x_{mix} where the inner mixing layer boundaries merge at the centerline, and it also defines the inner and outer mixing layer boundaries c_{jet} and b_{jet}, as shown in Figure 10.

$$x_{\text{mix}} = R'_{\text{eng}}/\varepsilon_c \tag{130}$$

$$b_{\text{jet}} = R'_{\text{eng}} + \varepsilon_b\, x_{\text{jet}} \tag{131}$$

$$c_{\text{jet}} = \begin{cases} R'_{\text{eng}} - \varepsilon_c\, x_{\text{jet}} & , \quad x_{\text{jet}} < x_{\text{mix}} \\ 0 & , \quad x_{\text{jet}} > x_{\text{mix}} \end{cases} \tag{132}$$

The velocity profile over the mixing layer is closely approximated by Schlichting's asymptotic wake profile as given by White [2].

$$\Delta V_{\text{jet}} = \begin{cases} 0 & , \quad x_{\text{jet}} < 0 \quad \text{or} \quad r_{\text{jet}} > b_{\text{jet}} \\ \Delta V_{0\,\text{jet}} \left\{ 1 - \left[(r_{\text{jet}} - c_{\text{jet}})/(b_{\text{jet}} - c_{\text{jet}}) \right]^{3/2} \right\}^2 & , \quad x_{\text{jet}} > 0 \quad \text{and} \quad b_{\text{jet}} > r_{\text{jet}} > c_{\text{jet}} \\ \Delta V_{0\,\text{jet}} & , \quad x_{\text{jet}} > 0 \quad \text{and} \quad c_{\text{jet}} > r_{\text{jet}} \end{cases} \tag{133}$$

The jet centerline velocity increment $\Delta V_{0\,\mathrm{jet}}$ used in (133) is obtained by the physical requirement that the jet's momentum excess must always be equal to the engine thrust.

$$
\begin{aligned}
F_{\mathrm{eng}} &= \iint \rho \Delta V_{\mathrm{jet}} \left(V_{\mathrm{eng}} + \Delta V_{\mathrm{jet}}\right) \, dA & (134)\\
&= 2\pi \int_0^b \rho \Delta V_{\mathrm{jet}} \left(V_{\mathrm{eng}} + \Delta V_{\mathrm{jet}}\right) \, r_{\mathrm{jet}} \, dr_{\mathrm{jet}} \\
&= \pi \, \rho \left(k_1 \, V_{\mathrm{eng}} \, \Delta V_{0\,\mathrm{jet}} \; + \; k_2 \, \Delta V_{0\,\mathrm{jet}}^2\right) \\
k_1 &= c^2 \; + \; \frac{9}{10} c(b-c) \; + \; \frac{9}{35}(b-c)^2 \\
k_2 &= c^2 \; + \frac{243}{385} c(b-c) \; + \frac{243}{1820}(b-c)^2 \\
\Delta V_{0\,\mathrm{jet}} &= \sqrt{\frac{1}{4}\frac{k_1^2}{k_2^2} V_{\mathrm{eng}}^2 \; + \; \frac{F_{\mathrm{eng}}}{\rho \pi k_2}} \; - \; \frac{1}{2}\frac{k_1}{k_2} V_{\mathrm{eng}} & (135)
\end{aligned}
$$

Figure 11 shows the predicted jet spreading for two different disk loadings, characterized by the initial jet velocity ΔV_{eng} relative to V_{eng}. Also shown are the predicted velocity profiles, and centerline velocities $\Delta V_{0\,\mathrm{jet}}$. The latter are approximately equal to ΔV_{eng} until the inner mixing layer edge reaches the centerline, after which $\Delta V_{0\,\mathrm{jet}}$ gradually decreases. The total jet momentum excess defined by (134) is exactly equal to F_{eng} for all x_{jet} locations.

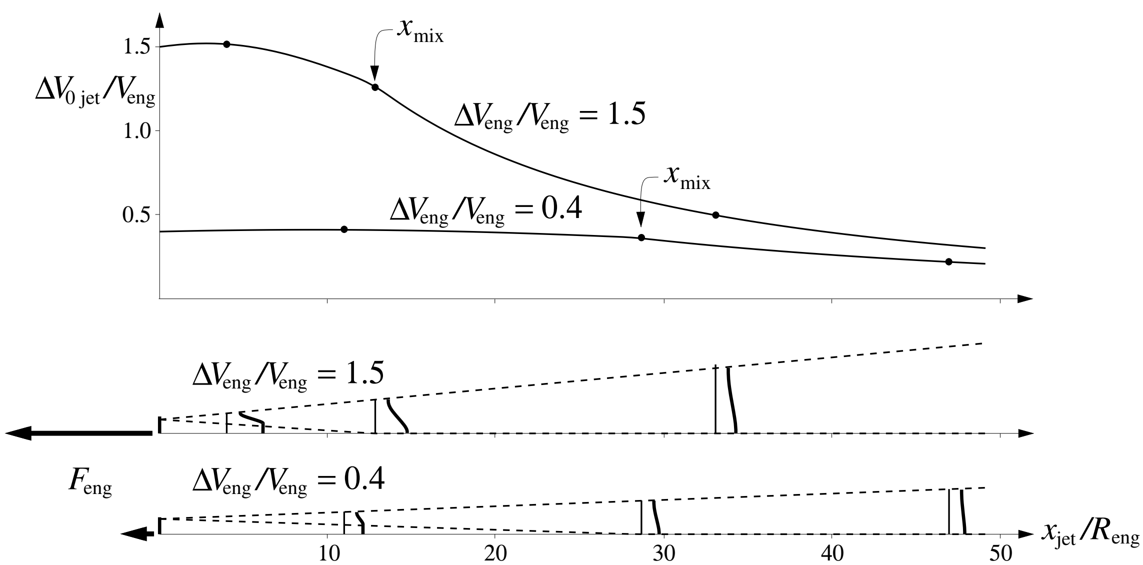

Figure 11: Predicted jet spreading and centerline jet velocities for moderate disk loading and high disk loading.

Jet swirl

In general, there will also be a swirl velocity ΔW_{jet} in the prop jet (not shown in the figures). It is assumed that this has the same profile shape as the axial jet velocity.

$$
\Delta W_{\mathrm{jet}} = \begin{cases} 0 & , \quad x_{\mathrm{jet}} < 0 \quad \text{or} \quad r_{\mathrm{jet}} > b_{\mathrm{jet}} \\ \Delta W_{0\,\mathrm{jet}} \left\{1 - \left[(r_{\mathrm{jet}} - c_{\mathrm{jet}})/(b_{\mathrm{jet}} - c_{\mathrm{jet}})\right]^{3/2}\right\}^2 & , \quad x_{\mathrm{jet}} > 0 \quad \text{and} \quad b_{\mathrm{jet}} > r_{\mathrm{jet}} > c_{\mathrm{jet}} \\ \Delta W_{0\,\mathrm{jet}} & , \quad x_{\mathrm{jet}} > 0 \quad \text{and} \quad c_{\mathrm{jet}} > r_{\mathrm{jet}} \end{cases} \qquad (136)
$$

The jet centerline velocity increment $\Delta W_{0\,\mathrm{jet}}$ used in (136) is obtained by the physical requirement that the jet's angular momentum must always be equal and opposite to the propeller torque.

$$
\begin{aligned}
-M_{\mathrm{eng}} &= \iint \rho\ (V_{\mathrm{eng}} + \Delta V_{\mathrm{jet}})\ \Delta W_{\mathrm{jet}}\, r\ dA && (137)\\
&= 2\pi \int_0^b \rho\ (V_{\mathrm{eng}} + \Delta V_{\mathrm{jet}})\ \Delta W_{\mathrm{jet}}\, r_{\mathrm{jet}}^2\, dr_{\mathrm{jet}} \\
&= \pi\rho\ (k_3\, V_{\mathrm{eng}}\ +\ k_4\, \Delta V_{0\,\mathrm{jet}})\ \Delta W_{0\,\mathrm{jet}} \\
k_3 &= \frac{2}{3}c^3\ +\ \frac{9}{10}c^2(b-c)\ +\ \frac{9}{35}c(b-c)^2\ +\ \frac{1}{9}(b-c)^3 \\
k_4 &= \frac{2}{3}c^3\ +\frac{243}{385}c^2(b-c)\ +\frac{243}{1820}c(b-c)^2\ +\ \frac{2}{45}(b-c)^3 \\
\Delta W_{0\,\mathrm{jet}} &= \frac{-M_{\mathrm{eng}}}{\pi\rho}\ \frac{1}{k_3 V_{\mathrm{eng}} + k_4 \Delta V_{0\,\mathrm{jet}}} && (138)
\end{aligned}
$$

Jet velocity vector

The jet axial velocity is assumed to be oriented along the thrust axis direction $\hat{x}_e$, and the swirl is perpendicular to the radial vector.

$$\Delta\vec{V}_{\mathrm{jet}}\ =\ \hat{x}_e\ \Delta V_{\mathrm{jet}}\ +\ \left(\frac{\vec{r}_{\mathrm{jet}}}{r_{\mathrm{jet}}} \times \hat{x}_e\right) \Delta W_{\mathrm{jet}} \qquad (139)$$

3.5 Strut loads

A strut or bracing wire represents another type of load applied to the end of the rigid pylon cantilevered from the beam. One end of the strut is attached to the pylon end at $\vec{r}_p$, while the other end is grounded (fixed in x, y, z axes) at location $\vec{r}_w$ as indicated in Figure 12. The pylon mount for the strut end at $\vec{r}_p$ allows modeling of a typical strut attachment point to a spar flange, in which case the length of the pylon $\Delta\vec{r}_p$ from the tension axis to the spar flange is about half the spar depth.

The strut is assumed to be perfectly flexible in bending, but has a finite extensional stiffness EA_w, and thus can change its length in response to extensional loads applied to it by the beam. Hence, it most closely represents a bracing wire, or a bracing strut with pinned endpoints. Note that such a strut could also be simulated by a fuselage-type beam with negligible bending stiffnesses, joined to the surface at one end, and grounded at the other end. However, the strut is far cheaper computationally, since it does not introduce additional structural variables. The strut is also assumed to be uniform, and hence is simpler to specify in an input file.

Following the notation used earlier to describe the pylon supporting a point mass, the strut length vector $\vec{L}_w$ is defined as follows.

$$\vec{L}_w\ =\ \vec{r}_w - \vec{r}_p \qquad (140)$$

The strut anchor $\vec{r}_w$ is assumed to be at a fixed location in airplane axes, while $\vec{r}_p$ changes as the beam deforms, as with the point mass case. The point load and moment applied to the beam by the tensile force of the strut is related to its change in length by

$$
\begin{aligned}
\Delta\vec{F}_{\mathrm{strut}} &= EA_w \left(\frac{|\vec{L}_w|}{|\vec{L}_w|_0} - 1\right) \frac{|\vec{L}_w|}{|\vec{L}_w|_0} && (141)\\
\Delta\vec{M}_{\mathrm{strut}} &= \Delta\vec{r}_p \times \Delta\vec{F}_{\mathrm{strut}} && (142)
\end{aligned}
$$

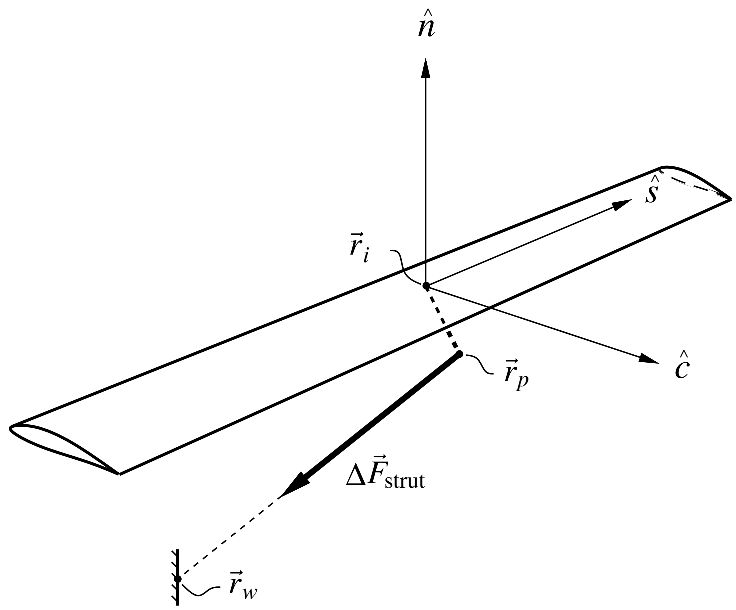

Figure 12: External bracing strut or wire attached to wing by rigid pylon, and anchored at fixed location $\vec{r}_w$.

where $|\vec{L}_w|_0$ is the length of the strut or wire in its unloaded state, and $\Delta\vec{r}_p$ is the pylon length vector as before. The above expression for $\Delta\vec{F}_{\text{strut}}$ would of course need to be limited if the length change is negative, and the resulting compressive load exceeds the buckling load of the strut.

3.6 Joint loads

Another type of concentrated load on a beam is due to a *joint* to another beam. Such a joint is implemented as a rigid pylon connecting the joint locations $\vec{r}_1$ and $\vec{r}_2$ on the two beams, as shown in Figure 13. Joint locations which nearly cooincide thus represent a direct structural joint, while joint locations which are relatively distant are in effect connected by a perfectly rigid massless beam (this beam can be given mass by superimposing one or more point masses on it). However, the formulation is the same for any joint distance.

Figure 13 also shows the auxilliary variables $\Delta\vec{r}_J$, $\Delta\vec{\theta}_J$, $\vec{F}_J$, $\vec{M}_J$, which define the state of the imaginary link forming the joint, and are used to define loads and kinematic constraints on the joined beams. The load resultants of the joint are applied as concentrated loads to the beam containing joint point #1.

$$\Delta\vec{F}_{\text{joint}} = \vec{F}_J \qquad\qquad \Delta\vec{M}_{\text{joint}} = \vec{M}_J \qquad\qquad \text{(at point \#1)} \tag{143}$$

The joint position change and Euler angle change vectors are imposed on the beam at joint point #2 as kinematic constraints in lieu of the moment and force balance equations (55,56) across the structural interval containing joint point #2.

$$\vec{r}_i = \vec{r}_{0_i} + \Delta\vec{r}_J \qquad\qquad \vec{\theta}_i = \vec{\theta}_{0_i} + \Delta\vec{\theta}_J \qquad\qquad \text{(at point \#2)} \tag{144}$$

The "lost" equations (55,56) for the interval containing point #2 will be imposed as global constraints, as described later.

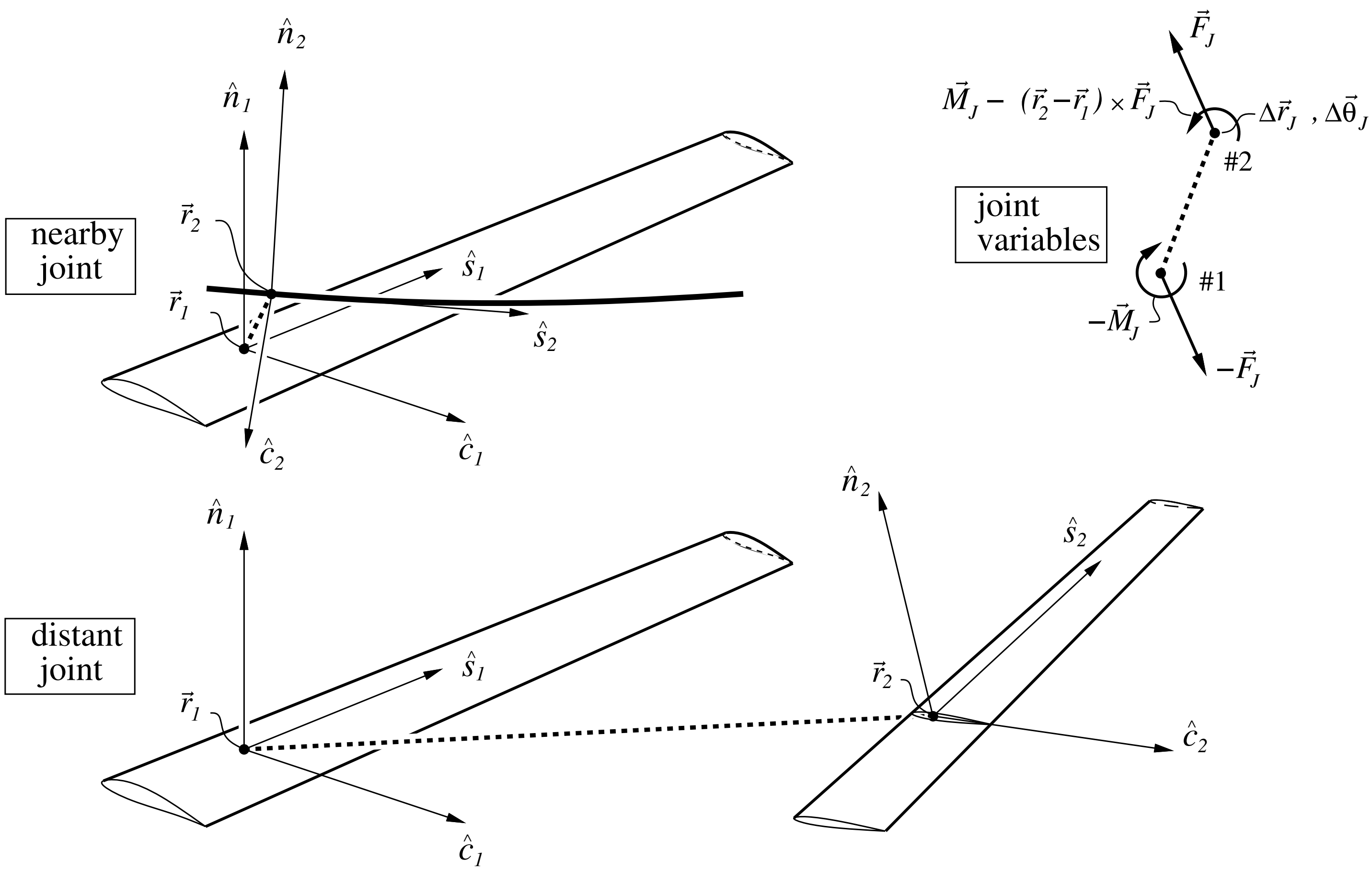

Figure 13: Nearby joint simulating a direct structural connection, and a distant joint simulating a rigid connecting beam. No distinction is made in the formulation. Variables $\vec{F}_J$, $\vec{M}_J$, ...are load resultants on the imaginary joint pylon (dashed).

3.7 Ground-point loads

A *ground* is a joint between a location on a beam and a fixed point in the x, y, z axes. A ground must be present in each beam which has no joints pointing to it, so that the ground serves to restrain the beam's rigid-body translation and rotation modes. As mentioned earlier, a ground is not necessary (and should *not* be used, in fact) if the beam in question already has a joint pointing to it, since the joint kinematic constraints (144) then act as the necessary kinematic constraints.

The ground is implemented very simply by replacing the moment and force equilibrium equations (55,56) at the interval containing the grounding point with simple kinematic constraints on the displacements and Euler angles.

$$\vec{r}_i \;=\; \vec{r}_{0_i} \qquad , \qquad \vec{\theta}_i \;=\; \vec{\theta}_{0_i} \qquad \text{(at ground)} \qquad (145)$$

Note that these are the same as the kinematic joint constraints (144) but without the joint degrees of freedom $\Delta\vec{r}_J$, $\Delta\vec{\theta}_J$.

Unlike the joint #2 point, the ground does not have its "lost" equations (55,56) enforced later — they are omitted altogether. The computed reaction loads against the ground point will simply be the overall force and moment applied to the configuration, and will produce a discontinuity in $\vec{F}$ and $\vec{M}$. If equilibrium is specified, as it should be in a physically correct representation of an actual flight condition, these reaction loads and the discontinuities will be computed to be zero.

3.8 Beam Groups

A *beam group* is a set of beams connected by joints, each joint having #1 and #2 points. Which joint point is labeled #1 or #2 is not physically significant and does not theoretically influence the solution, but it does affect the well-posedness of the numerical problem. The sub-matrix for each beam is partially solved independently of the other beams, and the individual partial solutions are appropriately combined via the joint variables and other global variables such as $\vec{\Omega}$, A_k, etc. Despite appearances, this approach does not make any approximations to the full Newton method, but it does give computational economy compared to using a single matrix for the entire configuration. A ground point and a #2 joint point each receive kinematic constraints during the factorization of the sub-matrix for that beam. If these constraints are absent, the beam's rigid body modes are unconstrained, which will produce a singular sub-matrix and numerical solution failure. Every beam must therefore have at least one such kinematically-constrained point. Figure 14 shows instances of such a "proper" beam group, and an "improper" beam group where this rule is violated. In the latter, the middle fuselage beam has no ground point or #2 joint point, and hence no kinematic constraints.

If the beam has finite bending and extensional stiffness, it is permissible to have more than one #2 joint point per beam, but this can give numerical difficulties and should be avoided if at all possible. In contrast, a beam can have an arbitrary number of #1 joint points with no ill effects, since these merely receive applied forces (143) rather than kinematic constraints (144) or (145).

4 Velocity Influence Coefficients

4.1 Prandtl-Glauert Transformation

The induced velocity has contributions from the bound and trailing vorticity on the lifting surface beams, and source and doublet distributions along the beams with significant volume. Figure 15 shows the quantities involved in the relevant summation integrals. The integration is performed in the wind-aligned and streamwise-stretched Prandtl-Glauert $\xi\eta\zeta$ axes to account for compressibility.

$$\begin{Bmatrix} \xi \\ \eta \\ \zeta \end{Bmatrix} = \begin{bmatrix} & \bar{\bar{P}} & \end{bmatrix} \begin{Bmatrix} x \\ y \\ z \end{Bmatrix} \tag{146}$$

$$\text{or} \qquad \vec{r}_P = \bar{\bar{P}}\,\vec{r} \tag{147}$$

$$\bar{\bar{P}} = \begin{bmatrix} \cdots \ \hat{\xi}^T \ \cdots \\ \cdots \ \hat{\eta}^T \ \cdots \\ \cdots \ \hat{\zeta}^T \ \cdots \end{bmatrix} = \begin{bmatrix} \frac{1}{\lambda}\cos\alpha\,\cos\beta & -\frac{1}{\lambda}\sin\beta & \frac{1}{\lambda}\sin\alpha\,\cos\beta \\ \cos\alpha\,\sin\beta & \cos\beta & \sin\alpha\,\sin\beta \\ -\sin\alpha & 0 & \cos\alpha \end{bmatrix}_{\text{wind}}$$

The $\vec{\xi}$ vector is aligned with the "wind direction"

$$\lambda\,\vec{\xi} = \frac{\vec{V}_\infty}{V_\infty} = \begin{Bmatrix} \cos\alpha\,\cos\beta \\ -\sin\beta \\ \sin\alpha\,\cos\beta \end{Bmatrix}_{\text{wind}} \quad , \quad \lambda = \sqrt{1 - M_{\text{PG}}^2} \tag{148}$$

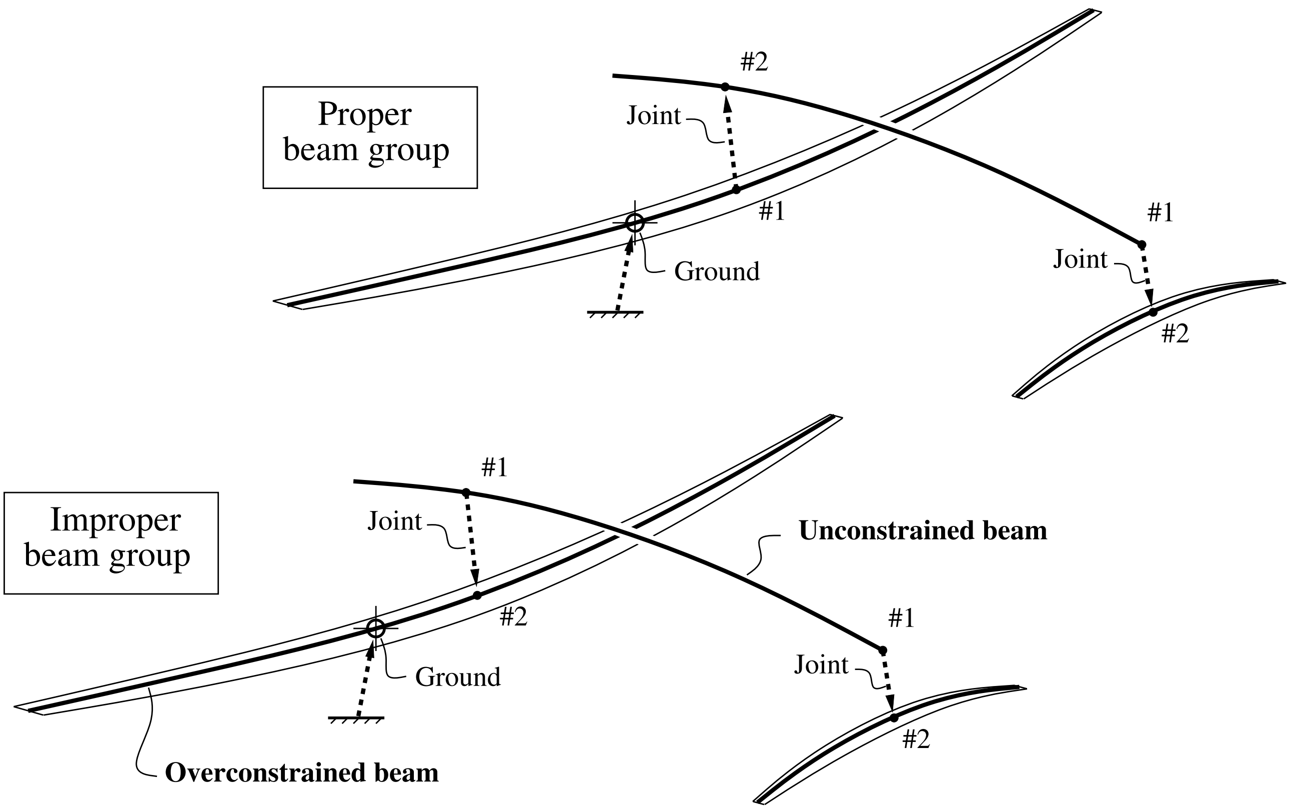

Figure 14: Proper and improper beam groups. Improper group has unconstrained fuselage beam with no kinematic constraints, which is not allowed. Overconstrained surface beam is allowed but not recommended.

as can be seen by comparing with equation (1). The $\hat{\zeta}$ vector is in the xz plane and perpendicular to $\vec{V}_\infty$, and hence is antiparallel to the $\hat{z}$ vector of standard stability axes. The remaining $\hat{\eta}$ vector is perpendicular to both $\vec{\xi}$ and $\hat{\zeta}$, and is not in general parallel to y axis, except in the zero-sideslip $\beta = 0$ case.

As indicated by the subscripts, the implementation actually defines $\bar{\bar{P}}$ and $\vec{\xi}$ in terms of the "wind angles" α_{wind}, β_{wind}, which can be set either to the true α, β, or to any other values deemed suitable for the case at hand. Likewise, the "Prandtl-Glauert" Mach number M_{PG} used to define the stretching factor λ above can be either the actual Mach number M_∞, or set to some suitable nominal value. Setting $M_{\text{PG}} = 0$ is acceptable for low-speed cases, for which $M_\infty^2 \ll 1$.

The Prandtl-Glauert equation for the perturbation potential $\phi(x, y, z)$ transforms to the Laplace equation in ξ, η, ζ space

$$\lambda^2 \frac{\partial^2 \phi}{\partial x^2} + \frac{\partial^2 \phi}{\partial y^2} + \frac{\partial^2 \phi}{\partial z^2} = 0 \qquad \rightarrow \qquad \frac{\partial^2 \phi}{\partial \xi^2} + \frac{\partial^2 \phi}{\partial \eta^2} + \frac{\partial^2 \phi}{\partial \zeta^2} = 0$$

whose solution for unit A_k and V_∞ gives the respective influence functions $\vec{v}_k$ and $\vec{w}_{\text{vol}}$ in terms of appropriate integrals over the singularities. The integrals effectively give the velocities $\partial\phi/\partial\xi$, $\partial\phi/\partial\eta$, $\partial\phi/\partial\zeta$ in transformed space. The velocities in physical space are then obtained via the chain rule, which amounts to multiplication by the transpose of the transformation matrix $\bar{\bar{P}}$ (not

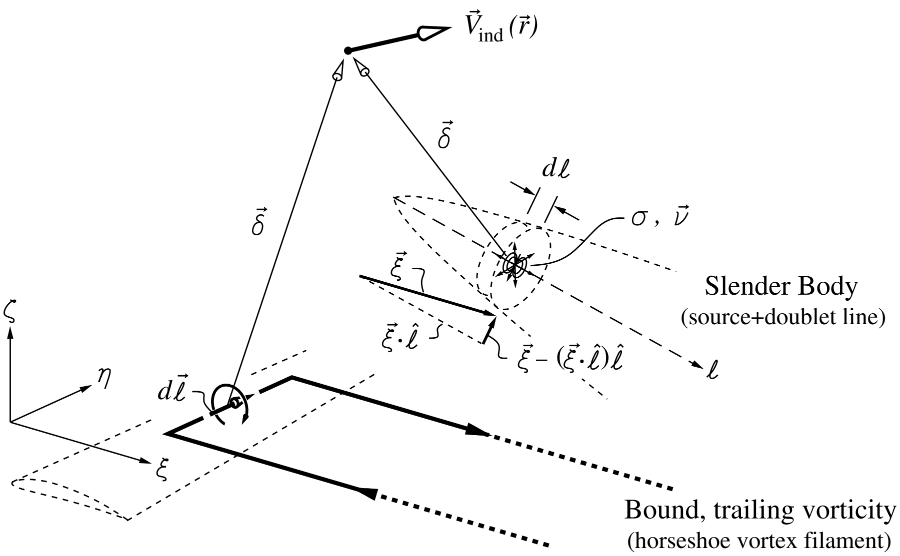

Figure 15: Induced velocity contributions from bound vortices and source and doublet distributions.

its inverse).

$$\left\{ \begin{array}{c} \partial\phi/\partial x \\ \partial\phi/\partial y \\ \partial\phi/\partial z \end{array} \right\} = \left[\begin{array}{ccc} \xi_x & \eta_x & \zeta_x \\ \xi_y & \eta_y & \zeta_y \\ \xi_z & \eta_z & \zeta_z \end{array} \right] \left\{ \begin{array}{c} \partial\phi/\partial \xi \\ \partial\phi/\partial \eta \\ \partial\phi/\partial \zeta \end{array} \right\} = \left[\quad \bar{\bar{P}}^T \quad \right] \left\{ \begin{array}{c} \partial\phi/\partial \xi \\ \partial\phi/\partial \eta \\ \partial\phi/\partial \zeta \end{array} \right\} \tag{149}$$

4.2 Vortex influence function

The vortex influence function $\vec{v}_k(\vec{r})$ is given by the Biot-Savart integral over the circulation distributions on all the beams. For the Fourier-mode representation (63) on a flat unswept wing, a simple approach would be to use the analytical result from Prandtl wing theory

$$\vec{v}_k = -\left[\frac{\lambda}{\pi\bar{c}} + \frac{k}{2b}\frac{1}{\sin(\theta)}\right]\sin(k\theta)\,\hat{z} \qquad \text{(flat unswept wing)}$$

where the two terms are from the bound and the trailing vorticity. For the general wing geometries and flow conditions considered here, a numerical approach must be taken, employing a discrete bound/trailing vortex system typically used in vortex-lattice methods. Such a vortex system is shown in Figure 16, with the bound vortices being placed at the quarter-chord point in the local c, n plane, and the trailing vortices being aligned with the relative freestream in the $\vec{\xi}$ direction. The modal contribution Γ_k to each bound vortex segment, which extends over the structural interval $s_i \ldots s_{i+1}$, is simply the weighted mode sampled at the Glauert-angle midpoint value.

$$\Gamma_k = A_k \sin(k\theta_a) \tag{150}$$

$$\text{where} \quad \theta_a = \frac{1}{2}(\theta_i + \theta_{i+1}) \tag{151}$$

$$\text{and also} \quad s_a = s_{\max}\cos\theta_a \tag{152}$$

The alternative "pointwise" circulation discretization (62) assumes a simple piecewise-constant circulation over each $s_i \ldots s_{i+1}$ interval.

$$\Gamma(s_a) = \left\{ \begin{array}{ll} A_i \ , & s_i < s_a < s_{i+1} \\ 0 \ , & \text{otherwise} \end{array} \right. \tag{153}$$

In this section, the subscript "a" denotes a midpoint average in θ rather than in physical space. The θ-averaged position vectors are obtained via a weighted interpolation using s_a,

$$\vec{r}_a \;=\; \vec{r}_i \,+\, (\vec{r}_{i+1} \,-\, \vec{r}_i)\,\frac{s_a - s_i}{\Delta s} \tag{154}$$

where $\vec{r}_i$ is simply the beam node position x_i, y_i, z_i. Interpolating in θ gives more accurate results for the predicted aerodynamic properties.

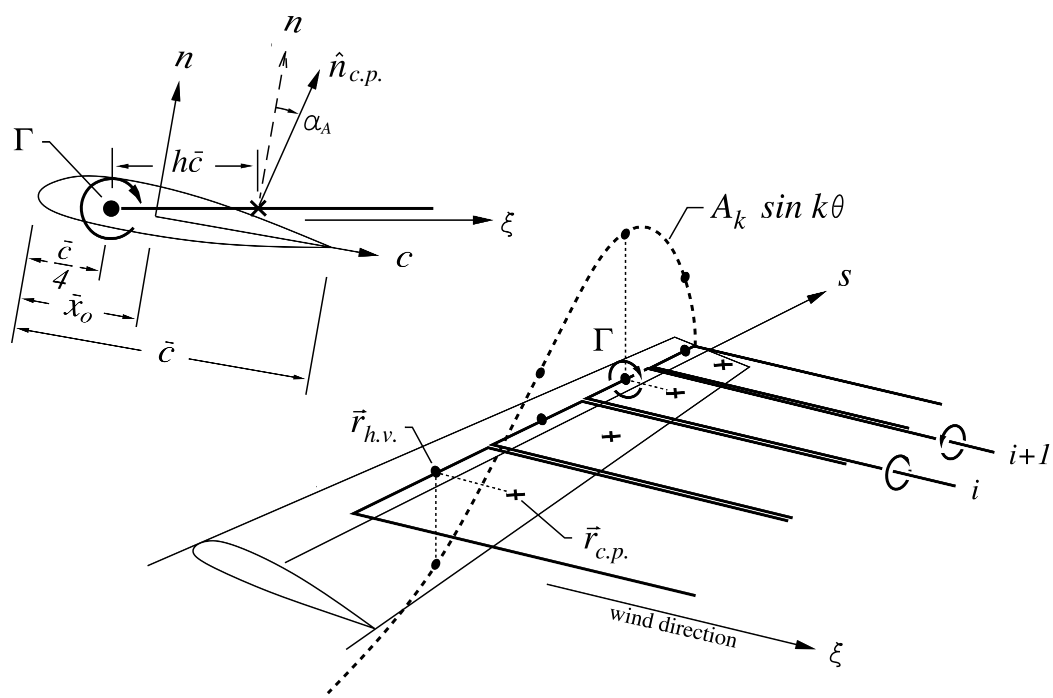

Figure 16: Airfoil-plane dimensions, and circulation mode represented by horseshoe vortices.

The location of the bound vortex segment midpoint $\vec{r}_{h.v.}$, where the lift force is defined to be located, is at the quarter-chord point along the ξ axis,

$$\vec{r}_{h.v.} \;=\; \vec{r}_a \,+\, \frac{\bar{c}/4 - \bar{x}_o}{|\vec{\xi}\times\hat{s}|}\,\vec{\xi} \tag{155}$$

The location of the control point $\vec{r}_{c.p.}$ is then directly "downstream" along the same $\vec{\xi}$ direction,

$$\vec{r}_{c.p.} \;=\; \vec{r}_{h.v.} \,+\, \frac{h\,\bar{c}_a}{|\vec{\xi}\times\hat{s}|}\,\vec{\xi} \tag{156}$$

where h is chosen so that the local incompressible 2-D section lift-curve slope is reproduced.

$$h \;=\; \frac{1}{4\pi}\frac{dc_\ell}{d\alpha} \tag{157}$$

For a thin airfoil, $h = 1/2$, which is also the value used by the standard vortex-lattice method.

The formulation used here differs from most standard vortex-lattice methods in that the trailing vorticity is always aligned with the freestream velocity direction $\vec{\xi}$, as opposed to being predefined to lie along $\hat{x}$, say. The control points at $\vec{r}_{c.p.}$ also "slosh around" as the freestream direction changes, but always remain at the local 3/4 chord line, or slightly farther aft if $h > 1/2$.

Aligning with the freestream naturally gives better accuracy for large angles of attack and large sideslip angles, since this is what the trailing vorticity actually does. On the other hand, it will fail if any part of the beam/wing aligns with the freestream, in which case $|\vec{\xi} \times \hat{s}| = 0$ in the equations above. Of course, the physical lifting-line model itself fails in this extreme and rather unlikely situation, so this may be a moot point.

The quasi-normal vector $\hat{n}_{c.p.}$ at the control point is rotated away from the local normal vector $\hat{n}$ by the local 2-D section aerodynamic angle of attack α_A relative to the local c axis.

$$\hat{n}_{c.p.} = \bar{\bar{T}}^T \begin{Bmatrix} \sin \alpha_A \\ 0 \\ \cos \alpha_A \end{Bmatrix} \tag{158}$$

This local angle of attack is defined as a constant part, plus contributions from control-surface or flap deflections δ_F.

$$\alpha_A = \alpha_{A\,o} + \frac{dc_\ell/d\delta_{F\,1}}{dc_\ell/d\alpha}\,\delta_{F\,1} + \frac{dc_\ell/d\delta_{F\,2}}{dc_\ell/d\alpha}\,\delta_{F\,2}\ldots \tag{159}$$

The control-surface derivatives $dc_\ell/d\delta_F$ are specified properties of the local 2-D section, as are $dc_m/d\delta_F$ and $dc_\ell/d\alpha$.

The overall influence coefficient function for the $k'th$ circulation mode is then obtained from the Biot-Savart law applied to all the horseshoe vortices with strengths corresponding to unit A_k.

$$\vec{v}_k = \begin{bmatrix} & \bar{\bar{P}}^T & \end{bmatrix} \begin{Bmatrix} \partial\phi/\partial\xi \\ \partial\phi/\partial\eta \\ \partial\phi/\partial\zeta \end{Bmatrix}_k (\vec{r}) = \begin{bmatrix} & \bar{\bar{P}}^T & \end{bmatrix} \left\{ \frac{1}{4\pi} \sum_{i=1}^{I-1} \sin(k\theta_a) \int \frac{d\vec{\ell} \times \vec{\delta}}{\delta^3} \right\} \tag{160}$$

The vortex element $d\vec{\ell}$ belongs to the horseshoe vortex spanning the $i...i+1$ stations, and $\vec{\delta}$ extends from the vortex element to the field point, as shown in Figure 15. Both are defined in the transformed Prandtl-Glauert space.

$$d\vec{\ell} = d\vec{r}_P = \bar{\bar{P}}\, d\vec{r} \qquad\qquad \vec{\delta} = \vec{r}_P - \vec{r}_{P(\ell)} = \bar{\bar{P}}\{\vec{r} - \vec{r}_{(\ell)}\}$$

For evaluating the righthand side integrals for surfaces which do not contain the control point in question, the induced velocity expression for $\vec{v}_k$ is modified by incorporation of a finite vortex core size ε.

$$\vec{v}_k = \begin{bmatrix} & \bar{\bar{P}}^T & \end{bmatrix} \left\{ \frac{1}{4\pi} \sum_{i=1}^{I-1} \sin(k\theta_a) \int \frac{d\vec{\ell} \times \vec{\delta}}{(\delta^2 + \varepsilon^2)^{3/2}} \right\} \tag{161}$$

Choosing $\varepsilon = \max(\bar{c}_a/4\,,\,\Delta s)$ results in the singular velocity field of the trailing vortex filaments being smeared into a continuous vortex sheet whose thickness is some reasonable fraction of the chord. This is essential to produce well-behaved lift forces on any surface immersed in the vortex wake of another upstream surface. It also weakens the dependence of the local wake velocity field on its geometry, justifying the lagging of the wake geometry in the Newton iteration cycle.

4.3 Volume influence functions

The volume contribution to the induced velocity is determined via the beam source/length density σ and doublet/length density $\vec{\nu}$. Both are set to give flow tangency on the circular beam of cross-sectional area πR^2, immersed in the local unit-V_∞ freestream velocity vector $\vec{\xi} = \bar{\bar{P}}\vec{V}_\infty/V_\infty$, as shown in Figure 15.

$$\sigma(\ell) = \frac{d(\pi R^2)}{d\ell}\left(\vec{\xi}\cdot\hat{\ell}\right) \qquad\qquad \vec{\nu}(\ell) = 2\pi R^2\left(\vec{\xi} - (\vec{\xi}\cdot\hat{\ell})\hat{\ell}\right) \tag{162}$$

These are most conveniently defined in transformed space which then automatically corrects for compressibility.

$$\vec{\xi} = \left\{\frac{1}{\lambda}\,,\,0\,,\,0\right\}^T \quad , \qquad \hat{\ell} = \frac{\bar{\bar{P}}\hat{s}}{|\bar{\bar{P}}\hat{s}|} \quad , \qquad d\ell^2 = d\xi^2 + d\eta^2 + d\zeta^2$$

The integrated effects of the densities then gives the volume influence function in physical space.

$$\vec{w}_{\mathrm{vol}}(\vec{r}) = \left[\ \bar{\bar{P}}^T\ \right]\left\{\frac{1}{4\pi}\int\left[\frac{\sigma\vec{\delta}}{(\delta^2+\varepsilon^2)^{3/2}} + \frac{\vec{\nu}\delta^2 - 3(\vec{\nu}\cdot\vec{\delta})\,\vec{\delta}}{(\delta^2+\varepsilon^2)^{5/2}}\right]d\ell\right\} \tag{163}$$

A suitable desingularizing "core size" is $\varepsilon = R/2$.

The above expressions for the beam volume influence function $\vec{w}_{\mathrm{vol}}$ can be used to approximate the volume influence of a thick wing. In this case, the circular beam area πR^2 is replaced by

$$\frac{d(\pi R^2)}{d\ell} \rightarrow \frac{d\mathcal{A}}{d\ell} \qquad\qquad 2\pi R^2 \rightarrow \left(1 + \frac{\mathcal{A}}{\bar{c}^2}\right)\mathcal{A}$$

where $\mathcal{A}$ is the airfoil cross-sectional area. The resulting volume influence coefficient is accurate at distances greater than the local chord $\bar{c}$.

4.4 Point-mass influence functions

A point mass with significant drag and volume contributes to the overall induced velocity in the flowfield. This velocity has the same form as equation (163), with the singularity strengths being given in terms of the drag area $(C_DA)_p$ and volume $\mathcal{V}_p$ of the point mass.

$$\int \sigma\, d\ell = (C_DA)_p \qquad\qquad \int \vec{\nu}\, d\ell = \mathcal{V}_p\,\vec{\xi} \tag{164}$$

A suitable core size is $\varepsilon = \max[(C_DA/\pi)^{1/2}, (\mathcal{V}/\pi)^{1/3}]$, which is typically comparable to the radius of the point-mass object.

4.5 Ground effect

Ground effect is modeled using images of the horseshoe vortices, sources, and doublets representing the lifting surfaces and fuselage beams. The ground plane is assumed to contain the origin of the inertial (Earth) XYZ coordinate system, and have a unit normal vector $\hat{n}_{G_E}$, specified in Earth axes, denoted by the $()_E$ subscript. In the case of level ground, this is simply $\hat{n}_{G_E} = \{\,0\;0\;1\,\}^T$.

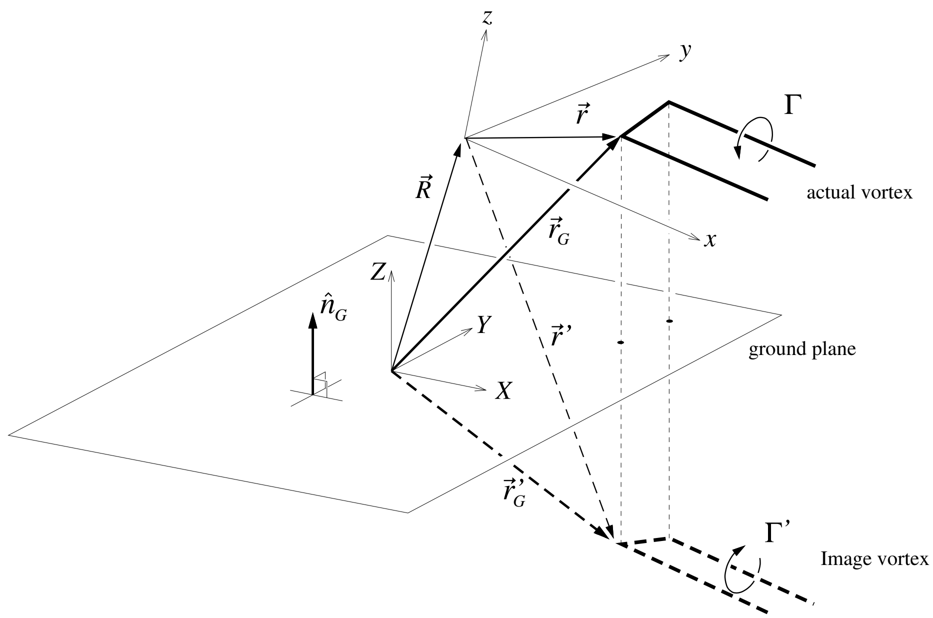

Figure 17: Ground effect image vortex and related geometry vectors.

Referring to Figure 17, the position of an aircraft vortex point $\vec{r}$ relative to the XYZ Earth origin is

$$\vec{r}_G = \vec{R} + \vec{r} \tag{165}$$

$$\text{where} \qquad \vec{R} = \bar{\bar{T}}_E^T \vec{R}_E \tag{166}$$

where the body/earth transformation tensor $\bar{\bar{T}}_E$ will be defined later in terms of the aircraft Euler angles Φ, Θ, Ψ. The $\vec{R}$ calculation is required since the aircraft position state is represented in the Earth axes as $\vec{R}_E$. We also define $\hat{n}_G$ as the ground unit normal vector in the aircraft axes.

$$\hat{n}_G = \bar{\bar{T}}_E^T \hat{n}_{G_E} \tag{167}$$

The corresponding image's position in the aircraft frame is finally computed as follows.

$$\vec{r}_G' = \vec{r}_G - 2 (\vec{r}_G \cdot \hat{n}_G) \hat{n}_G \tag{168}$$

$$\vec{r}' = \vec{r}_G' - \vec{R} = \vec{r} - 2 \left[\left(\vec{R} + \vec{r} \right) \cdot \hat{n}_G \right] \hat{n}_G \tag{169}$$

The image position $\vec{r}'$ is then used to compute the AIC matrices of the images in the same way as for the actual vortices, sources, and doublets. The image calculations above are actually performed in the wind axes $\xi\eta\zeta$, using the transformed vectors

$$\hat{n}_{G_P} = \bar{\bar{P}} \hat{n}_G \tag{170}$$

$$\vec{R}_P = \bar{\bar{P}} \vec{R} \tag{171}$$

$$\vec{r}_{G_P} = \bar{\bar{P}} \vec{r}_G \tag{172}$$

and the resulting $\vec{r}_P$ is used in the Biot-savart integrations (160) and (161). The image's circulation strengths are related to the real strengths as follows.

$$\Gamma' = \begin{cases} -\Gamma \ , & \text{solid ground plane} \\ \Gamma \ , & \text{free-surface ground plane} \end{cases} \tag{173}$$

The image's source and doublet strengths are given as follows.

$$\sigma' = \begin{cases} \sigma & , \text{ solid ground plane} \\ -\sigma & , \text{ free-surface ground plane} \end{cases} \tag{174}$$

$$\vec{\nu}\,' = \begin{cases} \vec{\nu} - 2\,(\vec{\nu}\cdot\hat{n}_G)\,\hat{n}_G & , \text{ solid ground plane} \\ -\vec{\nu} + 2\,(\vec{\nu}\cdot\hat{n}_G)\,\hat{n}_G & , \text{ free-surface ground plane} \end{cases} \tag{175}$$

4.6 Linearization

Using the wind-aligned Prandtl-Glauert transformation results in overall induced velocity having the following dependence:

$$\sum_{k=1}^{K} \vec{v}_k\,A_k \;+\; \vec{w}_{\rm vol}\,V_\infty \;=\; \vec{V}_{\rm ind}(\,\vec{r}\;;\;A_k\;\;V_\infty\;\;\alpha_{\rm wind}\;\;\beta_{\rm wind}\;\;M_{\rm PG}\;\;x_i\;\;y_i\;\;z_i\,) \tag{176}$$

In practice, only the dependence on A_k needs to be implicitly treated in the coupled structural/aerodynamic solution procedure for an isolated wing. This is because $\vec{v}_k$ hardly changes between Newton iterations, and so all variables besides A_k have a very weak influence. These other variables can then be safely lagged by one Newton iteration with little effect on the overall quadratic convergence. Without the implicit treatment the $12I \times 12I$ structural Jacobian matrix has a bandwidth of at most 24, and is very rapidly solved by a block-tridiagonal solver. With the exact implicit treatment the matrix would become 1/4 full (the 3 x_i, y_i, z_i variables out of 12 for each beam would have global influence on all beams), resulting in an enormous increase in computational cost. Hence, a full implicit treatment would be counterproductive.

For multiple-surface configurations, the dependence on $\vec{r}$, V_∞, $\alpha_{\rm wind}$, $\beta_{\rm wind}$, $M_{\rm PG}$, x_i, y_i, z_i can be considerably greater, since these quantities then have influence on the relative spacing between the vortex wake and the downstream surface which is immersed in the wake's velocity field. As a compromise, only the dependence on A_k and on the freestream V_∞, $\alpha_{\rm wind}$, $\beta_{\rm wind}$ is taken into account, which still retains near-quadratic convergence for typical cases. Only the effect of *relative* deflections between aerodynamically interacting surfaces is lagged in the iteration scheme. In the most-simplified case, the $\vec{v}_k$ and $\vec{w}_{\rm vol}$ influence functions can be precomputed using the jig geometry x_{0_i}, y_{0_i}, z_{0_i}, and $\alpha_{\rm wind} = \beta_{\rm wind} = 0$, which is equivalent to the standard prescribed-wake vortex lattice method, and is appropriate for benign flow conditions and small deformations.

In the presence of ground effect, the overall induced velocity dependence (176) expands to also include the aircraft position and Euler angles.

$$\sum_{k=1}^{K} \vec{v}_k\,A_k \;+\; \vec{w}_{\rm vol}\,V_\infty \;=\; \vec{V}_{\rm ind}(\,\vec{r}\;;\;A_k\;\;V_\infty\;\;\alpha_{\rm wind}\;\;\beta_{\rm wind}\;\;M_{\rm PG}\;\;x_i\;\;y_i\;\;z_i\;\;\vec{R}\;\;\Phi\;\;\Theta\;\;\Psi\,) \tag{177}$$

For near-ground cases the effect of $\vec{R}$ and the Euler angles can be quite strong. However, for steady cases these are generally prescribed explicitly, and hence can be considered as constants during linearization.

5 Global Variables and Constraints

In addition to the twelve structural nodal unknowns $x_i, y_i, \ldots$ listed earlier, the overall aero/structural problem also has the "global" variables

$$\Delta\vec{r}_J \quad \Delta\vec{\theta}_J \quad \vec{F}_J \quad \vec{M}_J \quad A_1 \;\; A_2 \;\ldots\; A_K \qquad \vec{U} \quad \vec{\Omega} \quad \vec{a}_o \quad \vec{\alpha}_o \qquad \delta_{F_1} \quad \delta_{F_2} \;\ldots$$

which require the same number of constraints for a well-posed problem. The surface deflections are included as unknowns only to allow calculation of control derivatives, developed later.

5.1 Acceleration constraints

The coordinate-origin acceleration $\vec{a}_o$ can be constrained in a number of ways. The simplest approach is the specify an acceleration directly at some convenient reference point $\vec{r}_{\mathrm{ref}}$.

$$\vec{a}_{\mathrm{ref}} \;\equiv\; \vec{a}_o \,+\, \vec{\alpha}_o \times \vec{r}_{\mathrm{ref}} \,+\, \vec{\Omega} \times \left(\vec{\Omega} \times \vec{r}_{\mathrm{ref}}\right) \;=\; \vec{a}_{\mathrm{spec}} \tag{178}$$

This is appropriate for simulating a wing clamped to a tunnel wall at $\vec{r}_{\mathrm{ref}}$, in which case $\vec{a}_{\mathrm{spec}} = 0$ would be chosen. For simulating an aircraft in flight, it is appropriate to impose a constraint on the overall force instead.

$$\vec{\mathcal{F}} \;\equiv\; \int \left(\vec{f}_{\mathrm{lift}} + \vec{f}_{\mathrm{drag}} + \vec{f}_{\mathrm{acc}} + \vec{f}_{\mathrm{am}}\right) ds \;+\; \sum \left(\Delta\vec{F}_{\mathrm{pmass}} + \Delta\vec{F}_{\mathrm{joint}}\right) \;=\; \vec{\mathcal{F}}_{\mathrm{spec}} \tag{179}$$

Concentrated strut loads $\Delta\vec{F}_{\mathrm{strut}}$ have been excluded from the summation, since each such load is cancelled by the opposite load $-\Delta\vec{F}_{\mathrm{strut}}$ on the strut anchor at $\vec{r}_w$ which is obviously attached to the aircraft somwhere. Note that $\Delta\vec{F}_{\mathrm{joint}}$ similarly cancel among all the beams, and could also be left out of the summation with no effect. Because the overall force $\vec{\mathcal{F}}$ includes the inertial-reaction loads, $\vec{\mathcal{F}}_{\mathrm{spec}}$ must be chosen to be zero for an aircraft in flight.

Algebraic summation of all the discrete structural force equations (56) on all the beams, which is tantamount to performing the integrations and summations in (179), produces the very simple statement

$$\vec{F}_{i+1} - \vec{F}_i \;=\; \vec{\mathcal{F}}_{\mathrm{spec}} \qquad\qquad \text{(ground interval } i \ldots i{+}1\text{)} \tag{180}$$

which simply states that the net applied load shows up as an opposite reaction load at the ground interval. Because of its simplicity, constraint (180) is actually implemented in lieu of its formal equivalent (179). Note that in the free-flight case the ground interval has no load discontinuity. This is reassuring, since the ground interval in this case is entirely fictitious.

5.2 Lift-related constraints

The components of the aircraft velocity $\vec{U}$ can be constrained directly, most conveniently via a specified velocity magnitude $V_{\infty\mathrm{spec}}$ and specified flow angles α_{spec}, β_{spec}. For greatest flexibility, these are imposed at some arbitrary reference location $\vec{r}_{\mathrm{ref}}$ (e.g. air data port location) fixed in the body axes. The apparent air velocity components at this location are

$$\{\, u_{\mathrm{ref}} \;\; v_{\mathrm{ref}} \;\; w_{\mathrm{ref}} \,\}^T \;\;=\;\; -\vec{U} \,-\, \vec{\Omega} \times \vec{r}_{\mathrm{ref}} \,+\, \vec{V}_{\mathrm{gust}}(\vec{r}_{\mathrm{ref}}) \tag{181}$$

which then allow the specified velocity and flow angles to be imposed by the following equations.

$$\sqrt{u_{\text{ref}}^2 + v_{\text{ref}}^2 + w_{\text{ref}}^2} \;=\; V_{\infty\,\text{spec}} \tag{182}$$

$$\arctan\left(w_{\text{ref}}/u_{\text{ref}}\right) \;=\; \alpha_{\text{spec}} \tag{183}$$

$$\arctan\left(-v_{\text{ref}}/\sqrt{u_{\text{ref}}^2 + w_{\text{ref}}^2}\right) \;=\; \beta_{\text{spec}} \tag{184}$$

An alternative constraint is to specify the total aerodynamic lift normal to the freestream, with a convenient load factor N included.

$$\mathcal{L} \;\equiv\; \int \left(\vec{f}_{\text{lift}} + \vec{f}_{\text{drag}}\right) ds \;\cdot\; \{-\sin\alpha \quad 0 \quad \cos\alpha\}^T \;=\; N\,\mathcal{L}_{\text{spec}} \tag{185}$$

This can replace either the $V_{\infty\,\text{spec}}$ or the α_{spec} constraint (but not both, obviously). As indicated, the total aero lift force $\mathcal{L}$ is simply the integral of the distributed aero loading normal to the freestream along all the lifting surfaces. In most situations, only the contribution of $\vec{f}_{\text{lift}}$ is significant.

5.3 Moment-related constraints

The angular rates $\vec{\Omega}$ and angular accelerations $\vec{\alpha}_o$ can be constrained directly, e.g.

$$\vec{\Omega} \;=\; \vec{\Omega}_{\text{spec}} \qquad\qquad \vec{\alpha}_o \;=\; \vec{\alpha}_{\text{spec}} \tag{186}$$

or indirectly by specifying moments about the reference point $\vec{r}_{\text{ref}}$.

$$\vec{\mathcal{M}}_{\text{ref}} \;\equiv\; \vec{\mathcal{M}} \;+\; \vec{\mathcal{F}} \times \vec{r}_{\text{ref}} \;=\; \vec{\mathcal{M}}_{\text{spec}} \tag{187}$$

The total moment vector about the origin is obtained like the force vector, with the inertial loads included.

$$\begin{aligned}\vec{\mathcal{M}} \;&=\; \int \left[\vec{m}_{\text{lift}} + \vec{m}_{\text{drag}} + \vec{m}_{\text{acc}} + \vec{m}_{\text{am}} \;+\; \vec{r}\times\left(\vec{f}_{\text{lift}} + \vec{f}_{\text{drag}} + \vec{f}_{\text{acc}} + \vec{f}_{\text{am}}\right)\right] ds \\ &+\; \sum \left[\Delta\vec{M}_{\text{pmass}} \;+\; \Delta\vec{M}_{\text{joint}} \;+\; \vec{r}\times\left(\Delta\vec{F}_{\text{pmass}} \;+\; \Delta\vec{F}_{\text{joint}}\right)\right]\end{aligned} \tag{188}$$

As in the case of the total force constraint, the total moment constraint is actually implemented via the equivalent ground-reaction moment load.

$$\vec{M}_{i+1} - \vec{M}_i \;=\; \vec{\mathcal{M}}_{\text{spec}} \qquad\qquad \text{(ground interval } i \ldots i{+}1) \tag{189}$$

Since the inertial reaction loads are also included, all three components of $\vec{\mathcal{M}}_{\text{spec}}$ must be chosen to be zero if the ASWING model includes all the pieces actually present on the aircraft (i.e. the ground is fictitious and must carry no load). In this case $\vec{\mathcal{F}}$ would be zero as well, and so the moment-reference location $\vec{r}_{\text{ref}}$ in equation (187) is arbitrary.

If the configuration includes a horizontal stabilizer or equivalent surface which has a pitch response, the vertical velocity U_z, which is nearly equivalent to α, can be indirectly constrained by specifying a zero reference pitching moment $(\mathcal{M}_y)_{\text{spec}} = 0$. This allows the trim state to be easily computed without manual iteration. The sideslip velocity U_y, nearly equivalent to the sideslip angle β, can likewise be indirectly constrained via $(\mathcal{M}_z)_{\rm spec}$ if the model includes a rudder, or via $(\mathcal{M}_x)_{\rm spec}$ if some dihedral and/or sweep are present.

If the model is incomplete, then $-\vec{\mathcal{F}}_{\rm spec}$ and $-\vec{\mathcal{M}}_{\rm spec}$ would be chosen as the force and moment imparted by any "missing" surfaces or point masses. This force and moment would then appear as applied loads at the ground interval, as can be seen from the ground-reaction constraints (180,189). For example, if only the wing is being modeled, $-(\mathcal{M}_z)_{\rm spec}$ would typically be equal to the moment applied by the rudder, and $-(\mathcal{M}_y)_{\rm spec}$ would be the moment imparted by the elevator. In the computed solution, these moments would be reacted at the ground of the beam group representing the partial configuration, so that the ground should be placed at the location where the "missing" surfaces would normally be attached.

5.4 Beam joint constraints

Twelve constraints are required for the twelve variables $\Delta\vec{r}_J, \Delta\vec{\theta}_J, \vec{M}_J, \vec{F}_J$ defined for each beam joint. Six of these constraints are

$$
\begin{aligned}
\vec{r}_2 - \vec{r}_1 &= \bar{\bar{T}}_1^T \, \bar{\bar{T}}_{1_0} \, (\vec{r}_{2_0} - \vec{r}_{1_0}) && (190) \\
\left[\bar{\bar{T}}_1^T \, \bar{\bar{T}}_{1_0}\right] \times\!\cdot \left[\bar{\bar{T}}_2^T \, \bar{\bar{T}}_{2_0}\right] &= 0 && (191)
\end{aligned}
$$

where $(\,)_1$ and $(\,)_2$ denote the beam variables at the two #1 and #2 joint locations, and $(\,)_0$ denotes the unloaded state. Equation (190) constrains the joint pylon (shown dashed in Figure 13) to remain at its original length. The tensor cross-dot product in equation (191), defined earlier by equation (7), constrains the two joined beams at their joint locations to maintain the same relative orientation which they have in the unloaded state.

The remaining six constraints are the force and moment-balance equations (55,56) at joint point #2 which were removed to allow the six kinematic constraints (144) to be imposed.

$$
\vec{M}_{i+1} - \vec{M}_i + \vec{m}_a \, \Delta s + \Delta\vec{M} + \Delta\vec{r}\times\vec{F}_a = \vec{M}_J - (\vec{r}_{i_2} - \vec{r}_{i_1})\times\vec{F}_J \qquad (192)
$$

$$
\vec{F}_{i+1} - \vec{F}_i + \vec{f}_a \, \Delta s + \Delta\vec{F} = \vec{F}_J \qquad (193)
$$

These also include the joint loads added to the righthand side. All variables except $\vec{r}_{i_1}$ correspond to joint point #2, which is contained in the interval $i \ldots i+1$. Normally this interval would be chosen to have zero length, in which case the Δs and $\Delta\vec{r}$ terms would vanish.

5.5 Compliant beam joint constraints

The rigid joint constraints (191) are generalized by the addition of a compliance, where a joint deflection angle is made a function of the joint structural moment. This function can be nonlinear, and simulate phenomena such as joint slop, or structural failure possibly with some residual strength.

The simplest case of such a generalized joint is a specified compliance only about one axis, given by the hinge unit vector $\hat{h}_0$ specified for the unloaded geometry. The hinge moment M_h then gives the hinge deflection angle α_h. Using the point #1 rotation tensors and moment, this is computed as follows.

$$
\begin{aligned}
\hat{h} &= \bar{\bar{T}}_1^T \bar{\bar{T}}_{1_0} \, \hat{h}_0 && (194) \\
M_h &= \vec{M}_1 \cdot \hat{h} && (195) \\
\alpha_h &= \alpha_h(M_h) && (196)
\end{aligned}
$$

The hinge compliance function $\alpha_h(M_h)$ is assumed given.

The modification to the angle constraints (191) is to first define a modified $\widetilde{T}_{2_0}$ axis matrix, which is $\bar{\bar{T}}_{2_0}$ rotated by α_h about $\hat{h}_0$ We first note that

$$\bar{\bar{T}}^T \;=\; \left[\begin{array}{ccc} | & | & | \\ \hat{c} & \hat{s} & \hat{n} \\ | & | & | \end{array} \right]_{xyz} \tag{197}$$

so the rotation operation about $\hat{h}_0$, which is specified in xyz axes, must be performed on the columns of $\bar{\bar{T}}^T_{2_0}$ rather than its rows.

$$\widetilde{T}^T_{2_0} \;=\; \bar{\bar{T}}^T_{2_0} \cos\alpha_h \;+\; \hat{h}_0\,\hat{h}_0^T \cdot \bar{\bar{T}}^T_{2_0}(1-\cos\alpha_h) \;+\; \hat{h}_0 \times \bar{\bar{T}}^T_{2_0} \sin\alpha_h \tag{198}$$

This new matrix in effect defines a modified unloaded orientation of the #2 joint point, due to the hinge-rotation angle α_h. The same angle-constraint relations (191) can then be employed, except that the rotated $\widetilde{T}_{2_0}$ is used instead of $\bar{\bar{T}}_{2_0}$.

$$\left[\bar{\bar{T}}^T_1\,\bar{\bar{T}}_{1_0}\right] \times\!\cdot \left[\bar{\bar{T}}^T_2\,\widetilde{T}_{2_0}\right] \;=\; 0 \tag{199}$$

5.6 Circulation coefficient constraints

The circulation coefficients A_k for each surface require constraints which enforce flow tangency on that surface. The flow tangency requirement at a control point on each $i ... i\!+\!1$ interval is

$$\vec{V}(\vec{r}_{c.p.}) \cdot \hat{n}_{c.p.} \;=\; 0 \tag{200}$$

which cannot be satisfied exactly if the number of circulation coefficients A_k, $k = 1 ... K$, is less than the number of structural intervals $I-1$. A weighted-residual approach is taken to generate the correct number of constraints.

$$\sum_{i=1}^{I-1} \left(\vec{V}(\vec{r}_{c.p.}) \cdot \hat{n}_{c.p.}\right)_a \sin(k\theta_a)\,\Delta\theta \;=\; 0 \qquad ; \qquad k = 1 \ldots K \tag{201}$$

In effect, a discrete Fourier analysis of the flow tangency residual is performed for each surface, with the K lowest residual wavenumbers being required to vanish.

5.7 Separation and stall modeling

The local flow tangency requirement (200) must be modified if local stall occurs. An appropriate modification is to introduce a flow tangency "leakage" velocity $\vec{V}_{c.p.} \cdot \hat{n}_{c.p.} \neq 0$ which models the suction-side displacement effect of the separating boundary layer, as illustrated in Figure 18.

In accordance with infinite swept-wing theory, the leakage velocity is made a function of the local section lift coefficient

$$c_\ell \;=\; \frac{2\Gamma}{\bar{c}V_\perp} \tag{202}$$

based on the section-normal relative speed $\bar{c}V_\perp$. The modification occurs only outside the specified $c_{\ell\min}$ and $c_{\ell\max}$ limits. A suitable form for the modified equation which replaces (200) is

$$\vec{V}(\vec{r}_{c.p.}) \cdot \hat{n}_{c.p.} \;-\; \frac{V_\perp}{4\pi h}\,K_{\mathrm{s}}\,f_{\mathrm{stall}}(c_\ell) \;=\; 0 \tag{203}$$

$$f_{\mathrm{stall}} \;=\; \Delta c_\ell\,\log\frac{1+\exp[(c_\ell - c_{\ell\max})/\Delta c_\ell]}{1+\exp[(c_{\ell\min} - c_\ell)/\Delta c_\ell]} \tag{204}$$

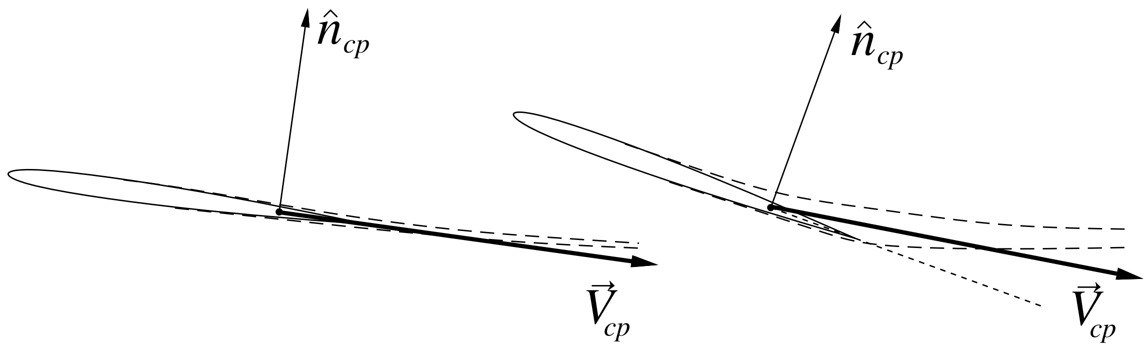

Figure 18: Flow-tangency "leakage" mimics effect of flow separation.

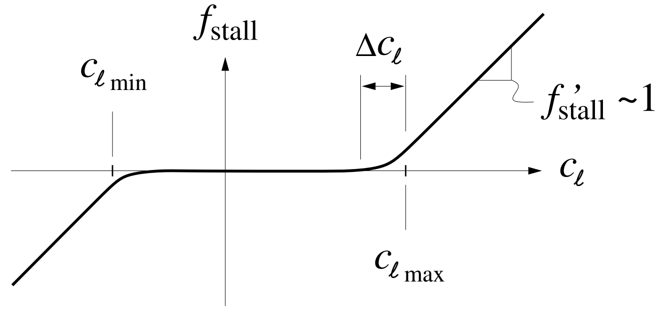

Figure 19: Flow-tangency "leakage" function active outside stall limits.

where the f_{stall} function shown in Figure 19.

This function is constructed so that its derivative is zero inside the stall limits, and unity outside the stall limits.

$$f'_{\text{stall}}(c_\ell) \;\simeq\; \begin{cases} 0 \quad , & c_{\ell_{\min}} < c_\ell < c_{\ell_{\max}} \\ 1 \quad , & c_\ell < c_{\ell_{\min}} \quad , \quad c_{\ell_{\max}} < c_\ell \end{cases}$$

In the 2D case this has the effect of giving a section lift curve slope of

$$\frac{dc_\ell}{d\alpha} \;\simeq\; \begin{cases} 4\pi h \quad , & c_{\ell_{\min}} < c_\ell < c_{\ell_{\max}} \\ 4\pi h/(1+K_{\text{s}}) \quad , & c_\ell < c_{\ell_{\min}} \quad , \quad c_{\ell_{\max}} < c_\ell \end{cases}$$

inside and outside the stall limits, as sketched in Figure 20. The width of the unstall/stall transition region at either end is proportional to the Δc_ℓ parameter, which therefore controls the sharpness of the lift reduction. The choices $K_{\text{s}} \simeq 40$ and $\Delta c_\ell \simeq 0.05$ give a realistic 2D $c_\ell(\alpha)$ lift curve. The nonzero post-stall $\vec{V} \cdot \hat{n}$ implied by equation (203) results in a profile pressure-drag contribution via equation (70). In the 2D case, the profile drag coefficient which results is

$$c_d \;=\; 4\left(\frac{\vec{V}\cdot\hat{n}}{V}\right)^2 \;\simeq\; 4\left(\frac{K_{\text{s}}}{1+K_{\text{s}}}\right)^2 \left(\sin\alpha \,-\, \frac{c_{\ell_{\max}}}{4\pi h}\right)^2 \qquad , \qquad c_\ell > c_{\ell_{\max}}$$

with the same expression occurring at the negative-stall end. This reaches approximately $c_d \simeq 2.0$ at $\alpha = 90°$.

It must be pointed out that the circulation and hence the c_ℓ do not decrease past stall, but are merely greatly reduced by the small factor $1/(1+K_{\text{s}})$. This may not be entirely physical, but it has the advantage of being very robust, since $\alpha(c_\ell)$ is then unique, and the possibility of hysteresis-loop cycling of Γ and c_ℓ during convergence is essentially ruled out.

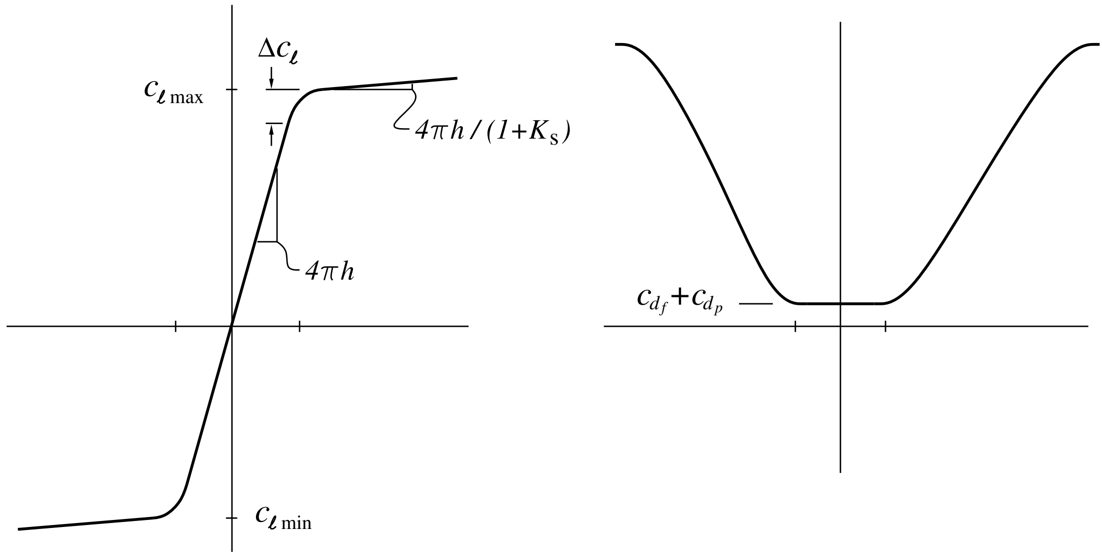

Figure 20: Effective section $c_\ell(\alpha)$ and $c_d(\alpha)$ resulting from stall model.

6 Wing/Beam Description

The following quantities are required to fully define the structural and aerodynamic properties of a beam. All are specified as functions of some arbitrary spanwise coordinate t. The second column is the input-file keyword for that variable.

t	`t`	t parameter along beam
x_0	`x`	x-location of reference s-axis of unloaded beam
y_0	`y`	y-location of reference s-axis of unloaded beam
z_0	`z`	z-location of reference s-axis of unloaded beam
ϑ_0	`twist`	twist angle of unloaded beam
EI_{cc}	`EIcc`	bending stiffness moment of inertia
EI_{nn}	`EInn`	bending stiffness moment of inertia
EI_{cn}	`EIcn`	bending stiffness product of inertia
EI_{cs}	`EIcs`	n-bending/torsion coupling stiffness
EI_{sn}	`EIsn`	c-bending/torsion coupling stiffness
GJ	`GJ`	torsional stiffness
EA	`EA`	extensional stiffness
GK_c	`GKc`	c-shear stiffness
GK_n	`GKn`	n-shear stiffness
t_ϵ	`tdeps`	extensional-strain damping time
t_γ	`tdgam`	shear-strain damping time
$\mu_1 g,$	`mg`	1st section weight/length
$\mu_2 g,$	`Dmg`	2nd section weight/length
$\iota_{cc_1} g$	`mgcc`	1st section rotational weight-inertia/length about its mass centroid
$\iota_{cc_2} g$	`Dmgcc`	2nd section rotational weight-inertia/length about its mass centroid
$\iota_{nn_1} g$	`mgnn`	1st section rotational weight-inertia/length about its mass centroid
$\iota_{nn_2} g$	`Dmgnn`	2nd section rotational weight-inertia/length about its mass centroid
c_{cg_1}	`Ccg`	c-distance from s-axis to μ_1 centroid
n_{cg_1}	`Ncg`	n-distance from s-axis to μ_1 centroid
c_{cg_2}	`DCcg`	c-distance from s-axis to μ_2 centroid
n_{cg_2}	`DNcg`	n-distance from s-axis to μ_2 centroid
c_{ta}	`Cta`	c-distance from s-axis to tension axis
n_{ta}	`Nta`	n-distance from s-axis to tension axis
c_{ea}	`Cea`	c-distance from s-axis to elastic axis
n_{ea}	`Nta`	n-distance from s-axis to elastic axis
$c_{\rm sh}$	`Cshell`	chordwise distance from tension axis to bending shell
$n_{\rm sh}$	`Nshell`	normal distance from tension axis to bending shell
$A_{\rm sh} t_{\rm sh}$	`Atshell`	enclosed area $\times$ thickness of torsion shell
R	`radius`	cylinder radius (for cross-sectional area πR^2)
c_{d_f}	`Cdf`	section profile friction drag coefficient
c_{d_p}	`Cdp`	section profile pressure drag coefficient

The overall mass distribution μ is composed of the two independent contributions μ_1, μ_2, in order to allow the mass of a wet wing to be more easily specified via separate structural and consumable mass distributions. Note that these each have their own mass centroid locations, defined as follows.

$$\begin{aligned}
c_{cg_1} &= \frac{1}{\mu_1}\int c\, d\mu_1 \\
n_{cg_1} &= \frac{1}{\mu_1}\int n\, d\mu_1 \\
\iota_{nn_1} &= \int (c - c_{cg_1})^2\, d\mu_1 \\
\iota_{cc_1} &= \int (n - n_{cg_1})^2\, d\mu_1
\end{aligned}$$

Corresponding definitions are used for the $(\,)_2$ quantities. The *net* mass distribution, centroid, and moments of inertia are then given by the following relations.

$$\begin{aligned}
\mu &= \int d\mu_1 \;+\; \int d\mu_2 \;=\; \mu_1 \;+\; \mu_2 \\
c_{cg} &= \frac{1}{\mu}\left[\int c\, d\mu_1 \;+\; \int c\, d\mu_2\right] \;=\; \frac{c_{cg_1}\mu_1 + c_{cg_2}\mu_2}{\mu_1 + \mu_2} \\
n_{cg} &= \frac{1}{\mu}\left[\int n\, d\mu_1 \;+\; \int n\, d\mu_2\right] \;=\; \frac{n_{cg_1}\mu_1 + n_{cg_2}\mu_2}{\mu_1 + \mu_2} \\
\iota_{nn} &= \int (c - c_{cg})^2\,(d\mu_1 \;+\; d\mu_2) \;=\; \iota_{nn_1} \;+\; \iota_{nn_2} \;+\; \frac{\mu_1\,\mu_2}{\mu_1 + \mu_2}\,(c_{cg_1} - c_{cg_2})^2 \\
\iota_{cc} &= \int (n - n_{cg})^2\,(d\mu_1 \;+\; d\mu_2) \;=\; \iota_{cc_1} \;+\; \iota_{cc_2} \;+\; \frac{\mu_1\,\mu_2}{\mu_1 + \mu_2}\,(n_{cg_1} - n_{cg_2})^2
\end{aligned}$$

The structural shell parameters $c_{\rm sh}$, $n_{\rm sh}$, $A_{\rm sh}t_{\rm sh}$ are used only for a posteriori calculation of the material extensional strain and shear stress via relations (28) and (29). They do not participate in the computation of the solution.

In addition to the above structural and drag-coefficient parameters, a surface beam also requires the following parameters to define its aerodynamic lift properties.

$\bar{c}$	`chord`	wing chord
$\bar{x}_o/\bar{c}$	`Xax`	distance/chord from leading edge to s axis (c, n origin)
α_{Ao}	`alpha`	angle of section zero-lift line above c-axis
c_{mo}	`Cm`	section pitching moment coefficient
$c_{\ell\max}$	`CLmax`	section c_ℓ limit
$c_{\ell\min}$	`CLmin`	section c_ℓ limit
$dc_\ell/d\alpha$	`dCLda`	section lift-curve slope
$dc_\ell/d\delta_{F_1}$	`dCLdF1`	section control-surface derivative
$dc_\ell/d\delta_{F_2}$	`dCLdF2`	section control-surface derivative
$dc_m/d\delta_{F_1}$	`dCMdF1`	section control-surface derivative
$dc_m/d\delta_{F_2}$	`dCMdF2`	section control-surface derivative
$dc_d/d\delta_{F_1}$	`dCDdF1`	section control-surface derivative
$dc_d/d\delta_{F_2}$	`dCDdF2`	section control-surface derivative

The surface section aerodynamic parameters c_{mo}, $dc_\ell/d\alpha$, $dc_\ell/d\delta_{F1\ldots}$, $dc_m/d\delta_{F1\ldots}$, correspond to incompressible flow, and are effectively increased at higher Mach numbers by the Prandtl-Glauert transformation. The remaining aerodynamic parameters are used without correction.

The beam arc length coordinate is derived directly from the input cartesian coordinates.

$$s_0 \;=\; \int^t \sqrt{dx_0^2 + dy_0^2 + dz_0^2}$$

The unloaded-state Euler angles are computed by inverting the transformation tensor (4) or (11).

$$\left.\begin{aligned} \varphi_0 &= \arctan\left(\frac{dz_0/dt}{dy_0/dt}\right) \\ \psi_0 &= \arctan\left(\frac{-dx_0/dt}{dy_0/dt\,\cos\varphi_0 \;+\; dz_0/dt\,\sin\varphi_0}\right) \end{aligned}\right\} \quad \text{(surface beam)}$$

$$\left.\begin{aligned} \psi_0 &= \arctan\left(\frac{-dx_0/dt}{dy_0/dt}\right) \\ \varphi_0 &= \arctan\left(\frac{dz_0/dt}{dy_0/dt\,\cos\psi_0 \;-\; dx_0/dt\,\sin\psi_0}\right) \end{aligned}\right\} \quad \text{(fuselage beam)}$$

6.1 Point mass description

Point masses are defined by the following parameters.

k_A	index of beam to which point mass is attached
t_A	t-location of pylon anchor point $\vec{r}_i$ on beam k_A
x_{p_0}	x-location of pylon endpoint $\vec{r}_p$ where mass is located in the undeformed state
y_{p_0}	y-location of pylon endpoint
z_{p_0}	z-location of pylon endpoint
m_p	point mass (currently specified as the *weight* $m_p g$)
$(C_D A)_p$	drag area
$\mathcal{V}_p$	volume
$\vec{H}_{p_0}$	angular momentum in undeformed state

6.2 Engine description

An engine is treated like a point mass, but with the applied force and moment being the sole loads. The unit vectors $\hat{F}_e, \hat{M}_e$ each have x, y, z components.

k_A	index of beam to which engine is attached
type	type of engine model (proportional, actuator disk, etc)
t_A	t-location of pylon anchor point $\vec{r}_i$ on beam k_A
x_{p_0}	x-location of pylon endpoint $\vec{r}_p$ where engine is located in the undeformed state
y_{p_0}	y-location of pylon endpoint
z_{p_0}	z-location of pylon endpoint
$T_{x_{\rm spec}}$	engine-axis vector jig-shape x component
$T_{y_{\rm spec}}$	engine-axis vector jig-shape y component
$T_{z_{\rm spec}}$	engine-axis vector jig-shape z component
$\hat{F}_e$	applied engine force per unit "power setting", $(= d\vec{F}_{\rm eng}/d\Delta_e)$
$\hat{M}_e$	applied engine moment per unit power setting, $(= d\vec{M}_{\rm eng}/d\Delta_e)$
$R_{\rm eng}$	prop radius for actuator-disk model
$\Omega_{\rm eng}$	prop rotation rate for actuator-disk model
$(C_D A)_{\rm eng}$	prop blade drag area

6.3 Strut description

Struts are defined by the following parameters.

k_A	index of beam to which strut is attached
t_A	t-location of strut-mounting pylon attachment point $\vec{r}_i$ on beam k_A
x_{p_0}	x-location of strut pylon endpoint $\vec{r}_{p_0}$ where strut end is located in the undeformed state
y_{p_0}	y-location of strut pylon endpoint
z_{p_0}	z-location of strut pylon endpoint
x_w	x-location of strut grounding point $\vec{r}_w$
y_w	y-location of strut grounding point
z_w	z-location of strut grounding point
ΔL_0	slack length added to strut
EA_w	strut extensional stiffness

The effective unloaded length of the strut which appears in equation (142) is calculated as follows.

$$\left|\vec{L}_w\right|_0 \;=\; |\vec{r}_{p_0} - \vec{r}_w| \;+\; \Delta L_0$$

The strut grounding point $\vec{r}_w$ is fixed in the body x, y, z system, so that this point is in effect connected to a beam ground point described below.

6.4 Ground point description

A beam ground point is defined very simply.

k_G	index of beam containing ground point.
t_G	t-location of ground point on beam k_G.

6.5 Beam joint description

A joint between two beams is specified by the following parameters.

k_{J_1}	index of beam containing joint endpoint #1.
k_{J_2}	index of beam containing joint endpoint #2.
t_{J_1}	t-location of joint endpoint #1 on beam k_{J_1}.
t_{J_2}	t-location of joint endpoint #2 on beam k_{J_2}.
$\alpha_h(M_h)$	moment/angle compliance function (optional)
$\hat{h}_0$	hinge axis vector (needed only if the compliance function is specified)

7 Operating Parameters

The following parameters, must be explicitly specified to fully define the operating state of the wing. These are treated as constants in the quasi-steady calculation.

M_∞	freestream Mach number (for Prandtl-Glauert)
ρ	air density (or Standard-Atmosphere altitude)
N	load factor (needed only if lift constraint is imposed)
g	gravity magnitude

It is also necessary to specify the parameters in the following list.

$\vec{U}_{\text{ref}}$	velocity vector at $\vec{r}_{\text{ref}}$
$\vec{\Omega}$	overall rotation rate vector
$\vec{a}_{\text{ref}}$	linear acceleration vector at $\vec{r}_{\text{ref}}$
$\vec{\alpha}_o$	overall rotational acceleration vector
Ψ	heading angle
Θ	elevation angle
Φ	bank angle
δ_{Fk}	control surface deflections
Δ_{ek}	engine-power settings

These differ from the preceding list in that they can be specified explicitly, or determined indirectly by specifying a suitable combination of the following dependent quantities.

V_{ref}	freestream speed at reference location
α_{ref}	angle of attack at reference location
β_{ref}	sideslip angle at reference location
$\mathcal{L}$	aerodynamic lift
γ	flight path angle
$\vec{\mathcal{F}}$	total force
$\vec{\mathcal{M}}_{\text{ref}}$	total moment about reference location
$\vec{U}_E$	velocity vector in Earth axes
$\vec{\Omega}_E$	rotation rate vector in Earth axes
$\vec{a}_{o_E}$	acceleration vector in Earth axes
$\vec{\alpha}_{o_E}$	rotational acceleration vector in Earth axes

The Euler angles Ψ, Θ, Φ define the transformation tensor $\bar{\bar{T}}_E$

$$\bar{\bar{T}}_E = \begin{bmatrix} \cos\Psi & \sin\Psi & 0 \\ -\sin\Psi & \cos\Psi & 0 \\ 0 & 0 & 1 \end{bmatrix} \begin{bmatrix} \cos\Theta & 0 & \sin\Theta \\ 0 & 1 & 0 \\ -\sin\Theta & 0 & \cos\Theta \end{bmatrix} \begin{bmatrix} 1 & 0 & 0 \\ 0 & \cos\Phi & \sin\Phi \\ 0 & -\sin\Phi & \cos\Phi \end{bmatrix} \tag{205}$$

This is used to relate the body-axes and Earth-axes vectors, e.g.

$$\vec{\Omega}_E = \bar{\bar{T}}_E \vec{\Omega}$$

In particular, it also defines the gravity vector $\vec{g}$ in body axes.

$$\vec{g} = \bar{\bar{T}}_E^T \{0 \quad 0 \quad -g\}^T \tag{206}$$

7.1 Constraint Well-Posedness

Specification of the dependent quantities listed earlier may or may not be suitable for specific situations. For example, specifying the lift $\mathcal{L}$ to constrain α is ill-posed if most of the wing is stalled. Similarly, specifying a pitching moment $\mathcal{M}_y$ to constrain α is not appropriate if the ASWING model does not include the horizonal stabilizer. In these examples, the relevant stability derivatives such as $\partial\mathcal{L}/\partial\alpha$, $\partial\mathcal{M}/\partial\alpha$, etc. are nearly zero, which will produce a nearly singular global Newton matrix and solution failure.

The well-posedness of other combinations requires that the associated stability derivatives also be non-negligible, which in turn requires that the ASWING model has certain aerodynamic properties. For example, specifying the roll moment $(\mathcal{M}_x)_{\text{ref}}$ to constrain the sideslip β relies on the presence of sufficient dihedral effect so that $\partial\mathcal{M}_x/\partial\beta$ is significant.

Any parameter which is not prescribed explicitly (e.g. α if $\mathcal{L}$ is prescribed), is a result of the calculation. A typical use of the constraint options is to determine aileron reversal speed, for example. Some small aileron deflection δ_F is specified, and the roll moment $(\mathcal{M}_x)_{\text{ref}}$ is prescribed to be zero in lieu of specifying the roll rate Ω_x. The resulting solution produces an Ω_x value which is the steady-state roll rate of the wing. As the speed V_∞ is increased, the computed roll rate will initially increase linearly, but then gradually level off and eventually decrease and go back to zero at the reversal speed. Of course, this will occur only if $(dc_m/d\delta_F)/(dc_\ell/d\delta_F)$ is negative, and the wing is sufficiently compliant in torsion.

A dependent quantity must not be prescribed more than once. For example, $\mathcal{M}_y$ cannot be specified to determine α and then specified again to determine Ω_y. Such redundant equations in the Newton system will make it singular and will give an arithetic fault. This can only occur because of an incorrect problem specification, since a physically relevant flight situation will not result in such redundant constraints.

8 Computed Parameters

8.1 Aerodynamic parameters

Parameters which are results of the calculation include any quantity from the parameter list above, such as α or Ω_x, which is not specified directly. For a trimmed complete configuration, the total moments $\vec{\mathcal{M}}_{\rm ref}$, which include inertial reactions, should be zero and so do not convey any information. For wing-alone configurations they *are* relevant, since they correspond to the moments imposed by the missing pieces of the configuration like the tail surfaces. In this case they may be of interest in tail sizing for various flight conditions.

It is useful to compute the total induced drag, lift, side force, and rolling moment coefficients in the η-ζ Trefftz Plane oriented perpendicular to the wind direction $\hat{\xi}$.

$$C_{Li} = \frac{2}{\rho V_\infty^2 S_{\rm ref}} \int \rho\Gamma\, V_\infty\, \hat{\zeta}\cdot d\vec{A} \tag{207}$$

$$C_{Yi} = \frac{2}{\rho V_\infty^2 S_{\rm ref}} \int \rho\Gamma\, V_\infty\, \hat{\eta}\cdot d\vec{A} \tag{208}$$

$$C_{Di} = \frac{2}{\rho V_\infty^2 S_{\rm ref}} \int \rho\Gamma\, \vec{V}_{\rm ind}\cdot d\vec{A} \tag{209}$$

$$C_{Mi} = \frac{2}{\rho V_\infty^2 S_{\rm ref}} \int \rho\Gamma\, \hat{\xi}\cdot \{0\ \ \eta\ \ \zeta\}^T \times d\vec{A} \tag{210}$$

with $d\vec{A}$ being the wake trace area element with η and ζ components. In general, C_{Yi} and C_{Li} will be quite close to the force coefficients obtained via integration of $\vec{f}_{\rm lift}$ on the configuration. However, the total force also includes $\vec{f}_{\rm drag}$ contributions if these are not aligned with $\vec{V}_\infty$, such as in the case of a fuselage beam at an angle of attack. The latter will in reality deposit a vortex wake in the Trefftz Plane, but representing this is beyond the scope of the ASWING formulation, so that its contribution does not appear in the Trefftz Plane calculation.

The span efficiency e is defined from the Trefftz Plane forces using the same reference area $S_{\rm ref}$ and some reference span $b_{\rm ref}$. Inclusion of the side force C_Y makes e independent of coordinate orientation.

$$e = \frac{1}{\pi}\frac{S_{\rm ref}}{b_{\rm ref}^2}\frac{C_{Li}^2 + C_{Yi}^2}{C_{Di}} \tag{211}$$

Since these reference quantities are arbitrary and not "obvious" for a highly flexible wing in extreme flight situations, the span efficiency e must be interpreted simply as a measure of C_{Di}/C_{Li}^2 rather than whether or not the loading is elliptical. For example, if $b_{\rm ref}$ is chosen to be the geometric span, a significant sideslip angle β will typically cause a significant reduction in e even if the loading remains elliptical, since the span of a wing's trace in the Trefftz-Plane varies like $\cos\beta$.

In addition to all the overall force coefficient parameters, the following local aerodynamic parameters are typically of interest.

$c_\ell\,(s)$	section lift coefficient distribution	$= 2\,\Gamma\,/\,\bar{c}\,V_\perp$
$\Delta\alpha_{\rm eff}\,(s)$	effective-incidence angle change	$= \vec{V}(\vec{r}_{c.p.})\cdot(\hat{n}-\hat{n}_0)_{c.p.}\;/\;V_\perp$

The effective-incidence change $\Delta\alpha$ summarizes the influence of all structural deflections and twists on the local airfoil section aerodynamics, and hence is useful for monitoring the importance of aeroelastic effects. Note that $\Delta\alpha$ is zero for a perfectly-rigid aircraft.

8.2 Structural parameters

The following local structural parameters along the span convey most of the significant information for monitoring the structural state of the aircraft, although other parameters may also be of interest in special cases.

$\Delta z\,(s)$	vertical displacement	$= z - z_0$
$\Delta\vartheta\,(s)$	net twist	$= \vartheta - \vartheta_0$
$F_n\,(s)$	"up-down" shear	$= \vec{F}\cdot\hat{n}$
$M'_c\,(s)$	"up-down" bending moment about tension axis	$= \vec{M}\cdot\hat{c} + n_{ta}\vec{F}\cdot\hat{s}$
$M'_n\,(s)$	"fore-aft" bending moment about tension axis	$= \vec{M}\cdot\hat{n} - c_{ta}\vec{F}\cdot\hat{s}$
$M'_s\,(s)$	torsion moment about elastic axis	$= \vec{M}\cdot\hat{s} - n_{ea}\vec{F}\cdot\hat{c} + c_{ea}\vec{F}\cdot\hat{n}$
$\epsilon\,(s)$	maximum axial strain	$= \left\lvert c_{\rm sh}\kappa_n\right\rvert + \left\lvert n_{\rm sh}\kappa_c\right\rvert + \left\lvert F_s/EA\right\rvert$
$\tau\,(s)$	torsional shear stress	$= \left\lvert M'_s\,/\,2\,A_{\rm sh}\,t_{\rm sh}\right\rvert$

8.3 Structural, aerodynamic stability and control derivatives

Flexible-aircraft derivatives are readily taken about any flight condition and aeroelastic state by constructing linear-response solutions to unit parameter changes. These response solutions are generated with the same Newton system that was used to solve for the nonlinear state itself. For calculation of the derivatives, the Newton system variables are grouped as follows.

$$
\begin{aligned}
\mathbf{x} &= \left(\, \vec{r}_i \;\; \vec{\theta}_i \;\; \vec{M}_i \;\; \vec{F}_i \quad \vec{r}_J \;\; \vec{\theta}_J \;\; \vec{M}_J \;\; \vec{F}_J \quad A_1 \ldots A_K \,\right) \\
\mathbf{a} &= \left(\, \vec{a}_o \;\; \vec{\alpha}_o \,\right) \\
\mathbf{v} &= \left(\, \vec{U} \;\; \vec{\Omega} \,\right) \\
\mathbf{d} &= \left(\, \delta_{F1} \;\; \delta_{F2} \;\ldots\; \Delta_{e1} \;\; \Delta_{e2} \;\ldots \,\right)
\end{aligned}
$$

Treating $\mathbf{v}$ as the independent aircraft state variables, the structural-response matrix is defined as

$$
\left[\frac{d\mathbf{x}}{d\mathbf{v}}\right] = \begin{bmatrix}
\frac{\partial \vec{r}_i}{\partial U_x} & \frac{\partial \vec{r}_i}{\partial U_y} & \frac{\partial \vec{r}_i}{\partial U_z} & \frac{\partial \vec{r}_i}{\partial \Omega_x} & \frac{\partial \vec{r}_i}{\partial \Omega_y} & \frac{\partial \vec{r}_i}{\partial \Omega_z} \\
\frac{\partial \vec{\theta}_i}{\partial U_x} & \frac{\partial \vec{\theta}_i}{\partial U_y} & \frac{\partial \vec{\theta}_i}{\partial U_z} & \frac{\partial \vec{\theta}_i}{\partial \Omega_x} & \frac{\partial \vec{\theta}_i}{\partial \Omega_y} & \frac{\partial \vec{\theta}_i}{\partial \Omega_z} \\
\vdots & \vdots & \vdots & \vdots & \vdots & \vdots \\
\frac{\partial A_K}{\partial U_x} & \frac{\partial A_K}{\partial U_y} & \frac{\partial A_K}{\partial U_z} & \frac{\partial A_K}{\partial \Omega_x} & \frac{\partial A_K}{\partial \Omega_y} & \frac{\partial A_K}{\partial \Omega_z}
\end{bmatrix}
$$

and the acceleration-response matrix is defined similarly.

$$\left[\frac{d\mathbf{a}}{d\mathbf{v}}\right] = \begin{bmatrix} \frac{\partial \vec{\alpha}_o}{\partial U_x} & \frac{\partial \vec{\alpha}_o}{\partial U_y} & \frac{\partial \vec{\alpha}_o}{\partial U_z} & \frac{\partial \vec{\alpha}_o}{\partial \Omega_x} & \frac{\partial \vec{\alpha}_o}{\partial \Omega_y} & \frac{\partial \vec{\alpha}_o}{\partial \Omega_z} \\ \frac{\partial \vec{a}_o}{\partial U_x} & \frac{\partial \vec{a}_o}{\partial U_y} & \frac{\partial \vec{a}_o}{\partial U_z} & \frac{\partial \vec{a}_o}{\partial \Omega_x} & \frac{\partial \vec{a}_o}{\partial \Omega_y} & \frac{\partial \vec{a}_o}{\partial \Omega_z} \end{bmatrix}$$

Structural and acceleration response matrices are also defined for the control vector $\mathbf{d}$.

$$\left[\frac{d\mathbf{x}}{d\mathbf{d}}\right] = \begin{bmatrix} \frac{\partial \vec{r}_i}{\partial \delta_{F_1}} & \frac{\partial \vec{r}_i}{\partial \delta_{F_2}} & \cdots \\ \vdots & \vdots & \end{bmatrix} \qquad \left[\frac{d\mathbf{a}}{d\mathbf{d}}\right] = \begin{bmatrix} \frac{\partial \vec{\alpha}_o}{\partial \delta_{F_1}} & \frac{\partial \vec{\alpha}_o}{\partial \delta_{F_2}} & \cdots \\ \frac{\partial \vec{a}_o}{\partial \delta_{F_1}} & \frac{\partial \vec{a}_o}{\partial \delta_{F_2}} & \cdots \end{bmatrix}$$

These matrices are formulated in terms of the Newton system residuals, which are grouped like the variables as follows.

$$\begin{aligned} \mathbf{r}\left(\mathbf{x},\mathbf{a},\mathbf{v},\mathbf{d}\right) &= 0 && \text{structural equations, joint-variable constraints, circulation constraints} \\ \mathbf{f}\left(\mathbf{x},\mathbf{a},\mathbf{v},\mathbf{d}\right) &= 0 && \text{total force and moment constraints:} \quad \vec{\mathcal{F}} = 0\ , \quad \vec{\mathcal{M}}_{\text{ref}} = 0 \\ \mathbf{p}\left(\mathbf{v}\right) &= 0 && \text{direct constraint relations, e.g.} \quad V_\infty - (V_\infty)_{\text{spec}} = 0\ , \quad \text{etc.} \\ \mathbf{q}\left(\mathbf{d}\right) &= 0 && \text{direct constraint relations, e.g.} \quad \delta_{F_1} - (\delta_{F_1})_{\text{spec}} = 0\ , \quad \text{etc.} \end{aligned}$$

All the residuals are expressed in linearized form in terms of the overall system Jacobian matrix.

$$\begin{Bmatrix} \delta\mathbf{r} \\ \delta\mathbf{f} \\ \delta\mathbf{p} \\ \delta\mathbf{q} \end{Bmatrix} = \begin{bmatrix} \frac{\partial \mathbf{r}}{\partial \mathbf{x}} & \frac{\partial \mathbf{r}}{\partial \mathbf{a}} & \frac{\partial \mathbf{r}}{\partial \mathbf{v}} & \frac{\partial \mathbf{r}}{\partial \mathbf{d}} \\ \frac{\partial \mathbf{f}}{\partial \mathbf{x}} & \frac{\partial \mathbf{f}}{\partial \mathbf{a}} & \frac{\partial \mathbf{f}}{\partial \mathbf{v}} & \frac{\partial \mathbf{f}}{\partial \mathbf{d}} \\ \mathbf{0} & \mathbf{0} & \mathbf{I} & \mathbf{0} \\ \mathbf{0} & \mathbf{0} & \mathbf{0} & \mathbf{I} \end{bmatrix} \begin{Bmatrix} \delta\mathbf{x} \\ \delta\mathbf{a} \\ \delta\mathbf{v} \\ \delta\mathbf{d} \end{Bmatrix} \tag{212}$$

Implicitly differentiating this system with respect to $\mathbf{v}$ and to $\mathbf{d}$, and requiring that $\delta\mathbf{r} = 0$ and $\delta\mathbf{f} = 0$ (since the $\mathbf{r} = 0$ and $\mathbf{f} = 0$ equations are inviolable), gives an implicit system for the structural-response and acceleration-response matrices for the state and control variables. The Jacobian matrix is evaluated at the operating and aeroelastic states at which the derivatives are defined.

$$\begin{bmatrix} \frac{\partial \mathbf{r}}{\partial \mathbf{x}} & \frac{\partial \mathbf{r}}{\partial \mathbf{a}} & \frac{\partial \mathbf{r}}{\partial \mathbf{v}} & \frac{\partial \mathbf{r}}{\partial \mathbf{d}} \\ \frac{\partial \mathbf{f}}{\partial \mathbf{x}} & \frac{\partial \mathbf{f}}{\partial \mathbf{a}} & \frac{\partial \mathbf{f}}{\partial \mathbf{v}} & \frac{\partial \mathbf{f}}{\partial \mathbf{d}} \\ \mathbf{0} & \mathbf{0} & \mathbf{I} & \mathbf{0} \\ \mathbf{0} & \mathbf{0} & \mathbf{0} & \mathbf{I} \end{bmatrix} \begin{Bmatrix} \frac{d\mathbf{x}}{d\mathbf{v}} & \frac{d\mathbf{x}}{d\mathbf{d}} \\ \frac{d\mathbf{a}}{d\mathbf{v}} & \frac{d\mathbf{a}}{d\mathbf{d}} \\ \frac{d\mathbf{v}}{d\mathbf{v}} & \frac{d\mathbf{v}}{d\mathbf{d}} \\ \frac{d\mathbf{d}}{d\mathbf{v}} & \frac{d\mathbf{d}}{d\mathbf{d}} \end{Bmatrix} = \begin{Bmatrix} \mathbf{0} & \mathbf{0} \\ \mathbf{0} & \mathbf{0} \\ \mathbf{1} & \mathbf{0} \\ \mathbf{0} & \mathbf{1} \end{Bmatrix} \tag{213}$$

The upper Jacobian block $\partial\mathbf{r}/\partial\mathbf{x}$, which constitutes the bulk of this matrix, is already available in factored form from the Newton solution procedure, and so inverting this system has almost negligible additional cost. The necessary operations involve only a number of back-substitutions and dot products to eliminate the off-diagonal blocks, and factorization of the typically small modified diagonal block $\partial\mathbf{f}/\partial\mathbf{a}$.

8.4 Interpretation of Stability Derivatives

Solution of system (213) produces the stability and control derivative matrices $\frac{d\mathbf{x}}{d\mathbf{v}}$, $\frac{d\mathbf{x}}{d\mathbf{d}}$, etc. The traditional interpretation of these derivatives is that they quantify the first-order response of the state $\mathbf{x}$ of the aircraft as a result of small imposed deviations $\Delta\mathbf{v}, \Delta\mathbf{d}$ from a given trimmed operating state $\mathbf{v}_0, \mathbf{d}_0$.

$$\mathbf{v} = \mathbf{v}_0 + \Delta\mathbf{v} \tag{214}$$

$$\mathbf{d} = \mathbf{d}_0 + \Delta\mathbf{d} \tag{215}$$

$$\mathbf{x} = \mathbf{x}_0 + \frac{d\mathbf{x}}{d\mathbf{v}}\Delta\mathbf{v} + \frac{d\mathbf{x}}{d\mathbf{d}}\Delta\mathbf{d} \tag{216}$$

$$\mathbf{a} = \mathbf{a}_0 + \frac{d\mathbf{a}}{d\mathbf{v}}\Delta\mathbf{v} + \frac{d\mathbf{a}}{d\mathbf{d}}\Delta\mathbf{d} \tag{217}$$

The perturbed accelerations $\mathbf{a} = \dot{\mathbf{v}}$ are simply the result of net force and moment imbalances due to the state perturbations.

For a flexible aircraft, these relations require careful interpretation. The perturbation relations above make the key assumption that $\dot{\mathbf{x}}$ is assumed to be negligible. Specifically, the geometry deformation rates $\dot{\vec{r}}_i$ and $\dot{\vec{\theta}}_i$ are assumed to be zero, even though $\Delta\vec{r}_i$ and $\Delta\vec{\theta}_i$ are not zero. In other words, any structural deformations $\Delta\vec{r}$, $\Delta\vec{\theta}$ resulting from the $\Delta\vec{U}$, $\Delta\vec{\Omega}$, $\Delta\delta_F$ perturbations are assumed to be fast and well-damped, so the deformations follow the changing aircraft loads in a quasi-static manner. For example, if the aircraft is suddenly subjected to an increased angle of attack, with $\Delta\vec{U} \simeq \{0, 0, -V_\infty\Delta\alpha\}$, there will be a response in the vertical wing bending $\Delta\vec{r}_i \simeq \{0, 0, \Delta z_i\}$. For the purpose of computing $dz_i/d\alpha$, it is necessary to assume that the wing bend instantaneously reaches its new value after $\Delta\alpha$ is imposed. Any wing bending oscillation is ignored, by the assumption of $\dot{z}_i = 0$.

The consequence of the quasi-steady assumption in computing the derivatives is that they strictly apply only to quasi-steady (e.g. relatively slow) aircraft motions. Fast aircraft motions which involve significant structural dynamics will not be properly captured by stability and control derivatives.

8.5 Axis transformation

Forces, moments, and stability derivatives are traditionally expressed in stability axes $\bar{x}, \bar{y}, \bar{z}$, which are aligned with the velocity vector in α but not in β, and the directions of the x and z axes are also reversed. It is also convenient to sometimes employ "reverse stability axes" $-\bar{x}, \bar{y}, -\bar{z}$, which cooincide with the body axes for $\alpha = 0$. Figure 21 shows the three systems, along with the rotational rates p, q, r associated with the stability axes. The transformation for any vector from x, y, z to $\bar{x}, \bar{y}, \bar{z}$ is then given by the tensor $\bar{\bar{S}}$ which depends only on α.

$$\left\{ \begin{array}{c} \bar{x} \\ \bar{y} \\ \bar{z} \end{array} \right\} = \left[\quad \bar{\bar{S}} \quad \right] \left\{ \begin{array}{c} x \\ y \\ z \end{array} \right\} \quad , \qquad \bar{\bar{S}} = \left[\begin{array}{ccc} -\cos\alpha & 0 & -\sin\alpha \\ 0 & 1 & 0 \\ \sin\alpha & 0 & -\cos\alpha \end{array} \right] \tag{218}$$

The non-dimensional rates $\tilde{p}, \tilde{q}, \tilde{r}$ in the stability axes are by convention defined as follows.

$$2V_\infty \left\{ \begin{array}{c} \tilde{p}/b_{\mathrm{ref}} \\ \tilde{q}/c_{\mathrm{ref}} \\ \tilde{r}/b_{\mathrm{ref}} \end{array} \right\} \equiv \left\{ \begin{array}{c} p \\ q \\ r \end{array} \right\} = \left\{ \begin{array}{c} \Omega_{\bar{x}} \\ \Omega_{\bar{y}} \\ \Omega_{\bar{z}} \end{array} \right\} = \left[\quad \bar{\bar{S}} \quad \right] \left\{ \begin{array}{c} \Omega_x \\ \Omega_y \\ \Omega_z \end{array} \right\} \tag{219}$$

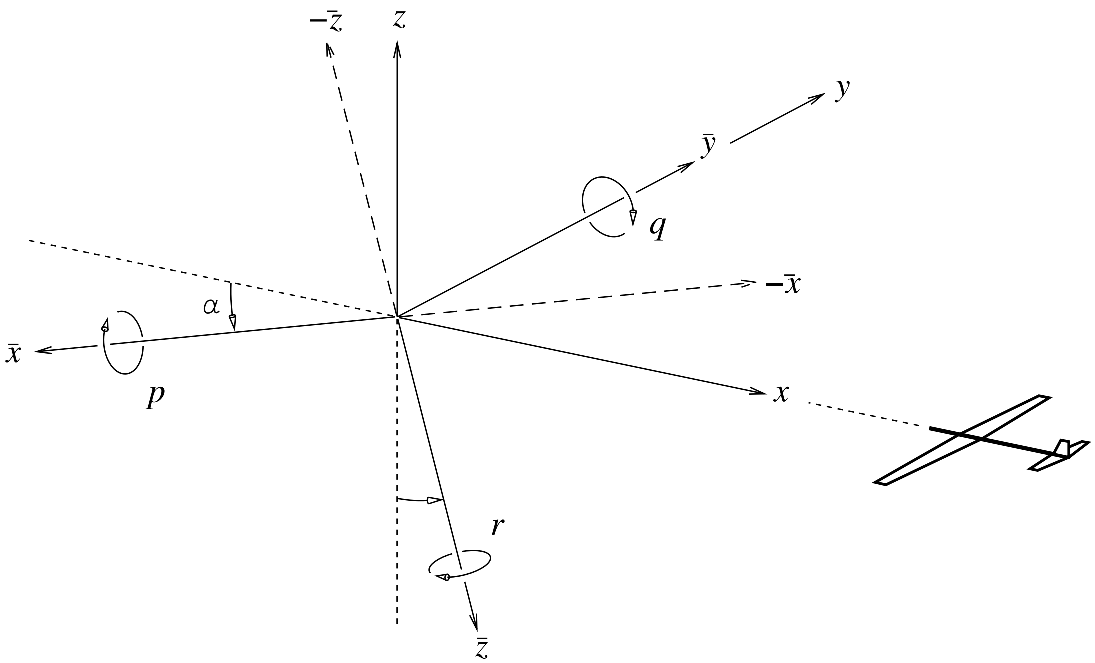

Figure 21: Body axes x, y, z, stability axes $\bar{x}, \bar{y}, \bar{z}$, and reverse stability axes $-\bar{x}, \bar{y}, -\bar{z}$.

8.6 Force and moment derivatives

The aerodynamic force and moment are defined in terms of the integrated applied aero loads.

$$\vec{\mathcal{F}}_{\text{aero}} = \int \left(\vec{f}_{\text{lift}} + \vec{f}_{\text{drag}} \right) ds \tag{220}$$

$$\vec{\mathcal{M}}_{\text{aero}} = \int \left(\vec{m}_{\text{lift}} + \vec{m}_{\text{drag}} \right) ds \; + \; \int \vec{r} \times \left(\vec{f}_{\text{lift}} + \vec{f}_{\text{drag}} \right) ds \tag{221}$$

The traditional stability-derivative matrices, which relate $\vec{\mathcal{F}}_{\text{aero}}$, $\vec{\mathcal{M}}_{\text{aero}}$ to $\mathbf{v}$, are obtained from the acceleration-response matrix by differentiating the above relations.

$$\frac{d\vec{\mathcal{F}}_{\text{aero}}}{d\mathbf{v}} = \int \left(\frac{d\vec{f}_{\text{lift}}}{d\mathbf{v}} + \frac{d\vec{f}_{\text{drag}}}{d\mathbf{v}} \right) ds \tag{222}$$

$$\frac{d\vec{\mathcal{M}}_{\text{aero}}}{d\mathbf{v}} = \int \left(\frac{d\vec{m}_{\text{lift}}}{d\mathbf{v}} + \frac{d\vec{m}_{\text{drag}}}{d\mathbf{v}} \right) ds \; + \int \frac{d\vec{r}}{d\mathbf{v}} \times \left(\vec{f}_{\text{lift}} + \vec{f}_{\text{drag}} \right) ds \; + \int \vec{r} \times \left(\frac{d\vec{f}_{\text{lift}}}{d\mathbf{v}} + \frac{d\vec{f}_{\text{drag}}}{d\mathbf{v}} \right) ds \tag{223}$$

The derivatives $d\vec{f}/d\mathbf{v}$ etc., are obtained by differentiating the definitions of $\vec{f}$ given by equations (67,69,70,71) and using the various components of the derivative matrices $d\mathbf{x}/d\mathbf{v}$ and $d\mathbf{a}/d\mathbf{v}$ in chain-rule fashion. The derivatives of $\vec{f}$ and $\vec{m}$ are already available from the construction of the overall Newton system, so calculation of these derivatives amounts to merely multiplying already-existing matrices. The standard force and moment coefficients in stability axes are then determined as follows.

$$\frac{1}{2}\rho V_\infty^2 \, S_{\text{ref}} \begin{Bmatrix} C_{\bar{x}} \\ C_{\bar{y}} \\ -C_L \end{Bmatrix} \equiv \begin{Bmatrix} \mathcal{F}_{\bar{x}} \\ \mathcal{F}_{\bar{y}} \\ \mathcal{F}_{\bar{z}} \end{Bmatrix}_{\text{aero}} = \left[\quad \bar{\bar{S}} \quad \right] \begin{Bmatrix} \mathcal{F}_x \\ \mathcal{F}_y \\ \mathcal{F}_z \end{Bmatrix}_{\text{aero}} \tag{224}$$

$$\frac{1}{2}\rho V_\infty^2\, S_{\mathrm{ref}} \left\{ \begin{array}{c} b_{\mathrm{ref}}\, C_\ell \\ c_{\mathrm{ref}}\, C_m \\ b_{\mathrm{ref}}\, C_n \end{array} \right\} \;\equiv\; \left\{ \begin{array}{c} \mathcal{M}_{\bar{x}} \\ \mathcal{M}_{\bar{y}} \\ \mathcal{M}_{\bar{z}} \end{array} \right\}_{\mathrm{aero}} \;=\; \left[\begin{array}{ccc} & & \\ & \bar{\bar{S}} & \\ & & \end{array} \right] \left\{ \begin{array}{c} \mathcal{M}_x \\ \mathcal{M}_y \\ \mathcal{M}_z \end{array} \right\}_{\mathrm{aero}} \tag{225}$$

Using the known $\vec{\mathcal{F}}_{\mathrm{aero}}$ and $\vec{\mathcal{M}}_{\mathrm{aero}}$ derivatives (222,223) in body axes, the standard nondimensional derivatives in stability axes are then determined as follows. The righthand sides contain only body-axes quantities.

$$\left[\begin{array}{ccc} C_{\bar{x}_u} & C_{\bar{x}_\alpha} & \\ & & C_{\bar{y}_\beta} \\ C_{L_u} & C_{L_\alpha} & \end{array} \right] = \frac{1}{\frac{1}{2}\rho V_\infty^2 S_{\mathrm{ref}}} \left[\begin{array}{ccc} 1 & & \\ & 1 & \\ & & -1 \end{array} \right] \left[\begin{array}{ccc} & & \\ & \bar{\bar{S}} & \\ & & \end{array} \right] \left[\frac{\partial \vec{\mathcal{F}}_{\mathrm{aero}}}{\partial (V_\infty, \alpha, \beta)} \right] \left[\begin{array}{ccc} V_\infty & & \\ & 1 & \\ & & 1 \end{array} \right] \tag{226}$$

$$\left[\begin{array}{ccc} & & C_{\ell_\beta} \\ C_{m_u} & C_{m_\alpha} & \\ & & C_{n_\beta} \end{array} \right] = \frac{1}{\frac{1}{2}\rho V_\infty^2 S_{\mathrm{ref}}} \left[\begin{array}{ccc} \frac{1}{b_{\mathrm{ref}}} & & \\ & \frac{1}{c_{\mathrm{ref}}} & \\ & & \frac{1}{b_{\mathrm{ref}}} \end{array} \right] \left[\begin{array}{ccc} & & \\ & \bar{\bar{S}} & \\ & & \end{array} \right] \left[\frac{\partial \vec{\mathcal{M}}_{\mathrm{aero}}}{\partial (V_\infty, \alpha, \beta)} \right] \left[\begin{array}{ccc} V_\infty & & \\ & 1 & \\ & & 1 \end{array} \right] \tag{227}$$

$$\left[\begin{array}{ccc} & C_{\bar{x}_q} & \\ C_{\bar{y}_p} & & C_{\bar{y}_r} \\ & C_{L_q} & \end{array} \right] = \frac{1}{\frac{1}{2}\rho V_\infty^2 S_{\mathrm{ref}}} \left[\begin{array}{ccc} 1 & & \\ & 1 & \\ & & -1 \end{array} \right] \left[\begin{array}{ccc} & & \\ & \bar{\bar{S}} & \\ & & \end{array} \right] \left[\frac{\partial \vec{\mathcal{F}}_{\mathrm{aero}}}{\partial \vec{\Omega}} \right] \left[\begin{array}{ccc} & & \\ & \bar{\bar{S}}^T & \\ & & \end{array} \right] \left[\begin{array}{ccc} \frac{2V_\infty}{b_{\mathrm{ref}}} & & \\ & \frac{2V_\infty}{c_{\mathrm{ref}}} & \\ & & \frac{2V_\infty}{b_{\mathrm{ref}}} \end{array} \right] \tag{228}$$

$$\left[\begin{array}{ccc} C_{\ell_p} & & C_{\ell_r} \\ & C_{m_q} & \\ C_{n_p} & & C_{n_r} \end{array} \right] = \frac{1}{\frac{1}{2}\rho V_\infty^2 S_{\mathrm{ref}}} \left[\begin{array}{ccc} \frac{1}{b_{\mathrm{ref}}} & & \\ & \frac{1}{c_{\mathrm{ref}}} & \\ & & \frac{1}{b_{\mathrm{ref}}} \end{array} \right] \left[\begin{array}{ccc} & & \\ & \bar{\bar{S}} & \\ & & \end{array} \right] \left[\frac{\partial \vec{\mathcal{M}}_{\mathrm{aero}}}{\partial \vec{\Omega}} \right] \left[\begin{array}{ccc} & & \\ & \bar{\bar{S}}^T & \\ & & \end{array} \right] \left[\begin{array}{ccc} \frac{2V_\infty}{b_{\mathrm{ref}}} & & \\ & \frac{2V_\infty}{c_{\mathrm{ref}}} & \\ & & \frac{2V_\infty}{b_{\mathrm{ref}}} \end{array} \right] \tag{229}$$

The derivatives with respect to V_∞, α, β, are computed from the $\vec{U}$ derivatives, using the relating Jacobian.

$$\frac{\partial[\;]}{\partial(V_\infty, \alpha, \beta)} = \frac{\partial[\;]}{\partial \vec{U}} \frac{\partial \vec{U}}{\partial(V_\infty, \alpha, \beta)}$$

$$\frac{\partial \vec{U}}{\partial(V_\infty, \alpha, \beta)} = \left[\begin{array}{ccc} -\cos\beta\cos\alpha & V_\infty\cos\beta\sin\alpha & V_\infty\sin\beta\cos\alpha \\ \sin\beta & 0 & V_\infty\cos\beta \\ -\cos\beta\sin\alpha & -V_\infty\cos\beta\cos\alpha & V_\infty\sin\beta\sin\alpha \end{array} \right]$$

8.7 Real and Apparent Masses and Inertias

Although the total mass and inertias are not required to compute a solution in ASWING, knowing these quantities is of considerable interest in applications. These are computed as described below. The inertias will be derived from the fundamentals, which will clarify the somewhat unusual form of the apparent inertia. The real mass and inertia quantities will be denoted by $(\,)_{\mathrm{rm}}$, and the apparent mass and inertia quantities will be denoted by $(\,)_{\mathrm{am}}$.

For the purpose of deriving the moment-of-inertia tensors, it's convenient to first define an antisymmetric tensor $\bar{\bar{r}}$ which is formed from the three components of the corresponding vector $\vec{r}$,

$$\vec{r} \;=\; x\hat{\imath} + y\hat{\jmath} + z\hat{k} \tag{230}$$

$$\bar{\bar{r}} \;\equiv\; \vec{r} \times \bar{\bar{1}} = \left[\begin{array}{ccc} 0 & -z & y \\ z & 0 & -x \\ -y & x & 0 \end{array} \right] \tag{231}$$

where $\bar{\bar{1}}$ is the identity matrix. This allows a cross product of $\vec{r}$ with any vector $\vec{A}$ to be expressed as a matrix-vector product which is easier to manipulate.

$$\vec{r}\times\vec{A} \;=\; \bar{\bar{r}}\vec{A} \tag{232}$$

$$\vec{A}\times\vec{r} \;=\; -\vec{r}\times\vec{A} \;=\; -\bar{\bar{r}}\vec{A} \tag{233}$$

The mass centroids and moments of inertia will be determined for the purpose of computing the overall linear and angular momenta of the configuration. The inertial-frame velocity $\vec{v}$ of any point at location $\vec{r}$ measured from some origin is given by

$$\vec{v} \;=\; \vec{U} + \vec{\Omega}\times\vec{r} \tag{234}$$

where $\vec{U}$ is the velocity of the origin and Ω is the rotation rate. The corresponding inertial-frame acceleration $\vec{a}$ is

$$\vec{a} = \dot{\vec{v}} \;=\; \vec{a}_o + \vec{\alpha}\times\vec{r} + \vec{\Omega}\times\left(\vec{\Omega}\times\vec{r}\right) \tag{235}$$

$$\vec{a}_o \;=\; \dot{\vec{U}} + \vec{\Omega}\times\vec{U} \tag{236}$$

where $\vec{a}_o$ is the acceleration of the origin, and $\vec{\alpha}$ is the angular acceleration.

8.7.1 Real mass

The total real mass is simply the integrated mass distribution over all the beams, plus the summed masses of all the point weights.

$$m_{\rm rm} \;=\; \sum_i \Delta m_i \;+\; \sum_p m_p \tag{237}$$

$$\Delta m_i \;=\; \mu_i \, \Delta s_{0_i} \tag{238}$$

The beam-interval mass Δm_i is defined using the local mass/length density μ_i, which is the sum of the local individual constributions μ_1 and μ_2, as defined by (205).

8.7.2 Real-mass moment and mass centroid

Using relations (232) and (233), the linear momentum of a mass element is

$$\Delta\vec{P} \;=\; \Delta m\,\vec{v} \;=\; \Delta m\left(\vec{U}+\vec{\Omega}\times\vec{r}\right) \;=\; \Delta m\left(\vec{U}-\bar{\bar{r}}\,\vec{\Omega}\right) \tag{239}$$

so that the total real-mass momentum is obtained concisely by summing over all the beam mass distributions and point masses.

$$\vec{P}_{\rm rm} \;=\; \sum\Delta\vec{P} \;=\; m_{\rm rm}\left(\vec{U} + \vec{\Omega}\times\vec{r}_{\rm rm}\right) \;=\; m_{\rm rm}\left(\vec{U} - \bar{\bar{r}}_{\rm rm}\vec{\Omega}\right) \tag{240}$$

where

$$\vec{r}_{\rm rm} \;=\; \frac{1}{m_{\rm rm}}\left(\sum_i \Delta m_i\,\vec{r}_{cg_i} \;+\; \sum_p m_p\,\vec{r}_p\right) \tag{241}$$

$$\vec{r}_{cg_i} \;=\; \vec{r}_i + c_{cg_i}\hat{c}_i + n_{cg_i}\hat{n}_i \tag{242}$$

The various quantities used to define the effective local-section moment arm $\vec{r}_{cg_i}$ were treated in previous sections.

8.7.3 Real-mass moment of inertia

The angular momentum $\Delta\vec{H}$ of the mass element is

$$\Delta\vec{H} \;=\; \vec{r}\times\Delta\vec{P} \;=\; \bar{\bar{r}}\,\Delta\vec{P} \;=\; \Delta m\,\bar{\bar{r}}\left(\vec{U} - \bar{\bar{r}}\,\vec{\Omega}\right) \tag{243}$$

which can then be summed over all the mass elements.

$$\vec{H}_{\rm rm} \;=\; \sum \Delta\vec{H} \;=\; m_{\rm rm}\,\bar{\bar{r}}_{\rm rm}\,\vec{U} \;+\; \bar{\bar{I}}_{\rm rm}\,\vec{\Omega} \tag{244}$$

$$\text{where} \qquad \bar{\bar{I}}_{\rm rm} \;=\; \sum_i \Delta m_i\;(-\bar{\bar{r}}_{cg_i}\,\bar{\bar{r}}_{cg_i}) \;+\; \sum m_p\;(-\bar{\bar{r}}_p\,\bar{\bar{r}}_p) \;+\; \sum_i \left(\bar{\bar{T}}^T\,\bar{\bar{\imath}}\,\bar{\bar{T}}\right)_i \Delta s_{0_i} \tag{245}$$

The third sum in (245) is over the beam elements' self-inertias, as defined by (80). The double-tensor products above evaluate to the familiar inertia tensors, e.g.

$$-\bar{\bar{r}}\,\bar{\bar{r}} \;=\; \begin{bmatrix} y^2+z^2 & -xy & -xz \\ -yx & x^2+z^2 & -yz \\ -zx & -zy & x^2+y^2 \end{bmatrix} \tag{246}$$

8.7.4 Apparent mass

In accordance with thin-airfoil theory, the apparent mass of a surface beam is assumed to correspond to the mass of a circular cylinder of air, with local diameter equal to the local chord. However, this apparent mass reacts only to linear acceleration components normal to the surface. In effect, the apparent mass is a tensor rather than a scalar.

$$\bar{\bar{m}}_{\rm am} \;=\; \sum_i \Delta m_{{\rm am}_i}\;\hat{n}_i\,\hat{n}_i^T \tag{247}$$

$$\Delta m_{{\rm am}_i} \;=\; \rho\frac{\pi}{4}\bar{c}_i^2\;\Delta s_i \tag{248}$$

8.7.5 Apparent-mass moment

The apparent-mass linear momentum of a surface beam element is

$$\Delta\vec{P} \;=\; \Delta m\,\hat{n}\,\hat{n}^T\,\vec{v} \;=\; = \;\Delta m\,\hat{n}\,\hat{n}^T\left(\vec{U}+\vec{\Omega}\times\vec{r}\right) \;=\; \Delta m\,\hat{n}\,\hat{n}^T\left(\vec{U} - \bar{\bar{r}}\,\vec{\Omega}\right) \tag{249}$$

so that the total apparent-mass momentum is obtained concisely by summing over all the beam section elements.

$$\vec{P}_{\rm am} \;=\; \sum \Delta\vec{P} \;=\; \bar{\bar{m}}_{\rm am}\,\vec{U} \;-\; (\bar{\bar{m}}_{\rm am}\bar{\bar{r}}_{\rm am})\,\vec{\Omega} \tag{250}$$

$$\text{where} \qquad \bar{\bar{m}}_{\rm am}\bar{\bar{r}}_{\rm am} \;=\; \sum_i \Delta m_{{\rm am}_i}\;\hat{n}_i\,\hat{n}_i^T\,\bar{\bar{r}}_{c/2_i} \tag{251}$$

$$\vec{r}_{c/2} \;=\; \vec{r}_i + c_{c/2_i}\hat{c}_i \tag{252}$$

Two essential differences of this apparent-mass momentum (250), when compared with the real-mass momentum (240), are
1) The apparent mass is a tensor rather than a simple scalar multiplying $\vec{U}$, and
2) The mass-moment product cannot in general be separated into an apparent mass $\bar{\bar{m}}_{\rm am}$ and an apparent-mass centroid $\bar{\bar{r}}_{\rm am}$, since $\bar{\bar{m}}_{\rm am}$ may not have full rank. For example, $\bar{\bar{m}}_{\rm am}$ for a flat wing has a rank of only 1.

8.7.6 Apparent-mass inertia

The apparent-mass angular momentum of a surface beam element is

$$\Delta\vec{H} \;=\; \vec{r}\times\Delta\vec{P} \;=\; \bar{\bar{r}}\,\Delta\vec{P} \;=\; \Delta m\,\bar{\bar{r}}\,\hat{n}\,\hat{n}^T\left(\vec{U}-\bar{\bar{r}}\,\vec{\Omega}\right) \tag{253}$$

so that the total apparent-mass angular momentum is obtained concisely by summing over all the beam section elements.

$$\vec{H}_{\rm am} \;=\; \sum\Delta\vec{H} \;=\; (-\bar{\bar{m}}_{\rm am}\,\bar{\bar{r}}_{\rm am})\,\vec{U} \;+\; \bar{\bar{I}}_{\rm am}\,\vec{\Omega} \tag{254}$$

where

$$\bar{\bar{I}}_{\rm am} \;=\; \sum_i \Delta m_{{\rm am}_i}\,\bar{\bar{r}}_i\,\hat{n}_i\,\hat{n}_i^T\,\bar{\bar{r}}_i \;+\; \sum_i {\rm I}_{ss_i}\;\hat{s}_i\,\hat{s}_i^T \tag{255}$$

$${\rm I}_{ss_i} \;=\; \rho\frac{\pi}{128}\,c_i^4\,\Delta s_i \tag{256}$$

The second term accounts for the local apparent inertia I_s of the air surrounding the surface, which reacts to only the angular acceleration components along the spanwise axis $\hat{s}$.

References

[1] P.J. Minguet. *Static and dynamic behavior of composite helicopter rotor blades under large deflections.* PhD thesis, MIT, June 1989.

[2] F.M. White. *Viscous Fluid Flow.* McGraw-Hill, New York, 1974.